

BIO-ALGORITHMS AND MED-SYSTEMS



Vol. 4, No. 7

2008

MEDICAL
SCIENCE

COMPUTER
SCIENCE

PHARMACOLOGY

COMMERCE

LAW

JOURNAL EDITED BY MEDICAL COLLEGE - JAGIELLONIAN UNIVERSITY - KRAKOW - POLAND

<http://www.bams.cm-uj.krakow.pl>

EDITORIAL BOARD

EDITOR-IN-CHIEF

Professor IRENA ROTERMAN-KONIECZNA
Medical College – Jagiellonian University, Krakow, st. Lazarza 16

HONORARY ADVISOR

Professor RYSZARD TADEUSIEWICZ
AGH – University of Science and Technology
Professor JAN TRĄBKA
Medical College – Jagiellonian University

MANAGING EDITORS

BIOCYBERNETICS – Professor PIOTR AUGUSTYNIAK
AGH – University of Science and Technology, Krakow, al. Mickiewicza 30

BIOLOGICAL DISCIPLINES – Professor LESZEK KONIECZNY
Medical College – Jagiellonian University, Krakow, Kopernika 7

MEDICINE – Professor KALINA KAWECKA-JASZCZ
Medical College – Jagiellonian University, Krakow, Pradnicka 80

PHARMACOLOGY – Professor STEFAN CHŁOPICKI
Medical College – Jagiellonian University, Krakow, Grzegórzecka 16

PHYSICS – Professor STANISŁAW MICEK
Faculty of Physics – Jagiellonian University, Krakow, Reymonta 4

MEDICAL INFORMATICS AND COMPUTER SCIENCE – Professor MAREK OGIELA
AGH – University of Science and Technology, Krakow, al. Mickiewicza 30

TELEMEDICINE – Professor ROBERT RUDOWSKI
Medical Academy, Warsaw, Banacha 1a

LAW – Dr SYBILLA STANISŁAWSKA-KLOC
Law Faculty – Jagiellonian University, Krakow, Kanoniczna 14, Institute of Intellectual Property Law

ASSOCIATE EDITORS

Medical College – Jagiellonian University, Krakow, Kopernika 7e

EDITOR-IN-CHARGE – PIOTR WALECKI
E-LEARNING (project-related) – ANDRZEJ KONONOWICZ
E-LEARNING (general) – WIESŁAW PYRCZAK
DISCUSSION FORUMS – WOJCIECH LASOŃ
ENCRYPTION – KRZYSZTOF SARAPATA

TECHNICAL SUPPORT

Medical College – Jagiellonian University, Krakow, st. Lazarza 16
ZDZISŁAW WIŚNIEWSKI – in charge
WOJCIECH ZIAJKA
ANNA ZAREMBA-ŚMIETAŃSKA

Polish Ministry of Science and Higher Education journal rating: 4.000

Sustaining institution: Ministry of Science and Higher Education

Edition: 300 copies

© COPYRIGHT BY INDIVIDUAL AUTHORS AND MEDICAL COLLEGE – JAGIELLONIAN UNIVERSITY

ISSN 1895-9091 (print version)
ISSN 1896-530X (electronic version)

<http://www.bams.cm-uj.krakow.pl>

OPENING PAPER

- 5 Use of Personal Data and Patients' Image in Scientific Publications
Paweł Markiewicz

BIOINFORMATICS

- 9 GenFoSS – java application for presentation of coding stretches of Never Born Proteins
Monika Piowar, Ewa Matczyńska, Piotr Ochlawski, Mateusz Kosibowicz, Damian Kość, Michał Swatowski,
Piotr Więcek, Tomasz Szepieniec

MODELING AND SIMULATION

- 19 Simulation of ratio of old to young people in countries like Poland
Dietrich Stauffer and Krzysztof Kułakowski

BIOMEDICAL ENGINEERING

- 25 Magnetocardiography – measurement conduction, data formats and diagnostic applications
Kamila Baron-Paľucka

PATTERN RECOGNITION

- 35 An algorithm for detecting lesions in CBF and CBV perfusion maps
Tomasz Hachaj
- 43 The registration and atlas construction of noisy brain computer tomography images based on free
form deformation technique
Tomasz Hachaj
- 51 Image processing application for enhancement of medical diagnostic features
Joanna Jaworek, Eliaz Kańtoch
- 57 Digital Skeletonization as a Probe of Correlation between Sutural Bones and Diffusion Limited
Aggregation Clusters
Janusz Skrzat, Jerzy Walocha

TELEMEDICINE

- 63 Learning-by-e-teaching: Experience from involving students in preparation of e-learning materials
Andrzej A. Kononowicz, Aleksandra J. Stachoń, Anna Romanowska-Pawliczek, Piotr Obtułowicz, Wiesław
Pyrzczak

USE OF PERSONAL DATA AND PATIENTS' IMAGE IN SCIENTIFIC PUBLICATIONS

PAWEŁ MARKIEWICZ

*Student of the Law Faculty of the Jagiellonian University, TBSP
(Association of Law Students Library of the Jagiellonian University), Bracka 12/302, 31-005 Krakow*

Doctors who present in scientific and medical publications clinical cases in which particular **patients are indicated** may face the problem of illegal disclosure of patients personal data and consequently the problem of civil and criminal liability. The purpose of this article is to present legal regulations limiting freedom of the authors of medical publications in respect of reference to examples from physician's practice in the eye of the regulations of the Civil Code¹, Act on the Protection of Personal Data² and Act on Copyright and Neighboring Rights³. Such information as: case history, photos showing pathological changes, information about the age, etc. may lead to violation of personal rights of the patients they relate to, or violation of rights of their relatives and friends. In the person's lifetime authors have to obtain his or her consent for such publication. The issue of consent takes a different angle after patient's death and further remarks are devoted to this problem.

Protection of personal data of the deceased patients

Act on the Protection of Personal Data constitutes fundamental legal act governing the use of other persons personal data. Pursuant to the wording of art. 6.1. of the Act, „... personal data shall mean any information relating to an identified or identifiable natural person.” Thus, in the eye of this act, in order to denote a medical publication presenting a particular case as inadmissible, there must be objective

possibility to identify a given patient by the reader. Thus the descriptions, photos, etc. published must make it possible to disclose the person's identity. It is sufficient that the person is recognized by a certain group of people, e.g. by his or her colleagues. The possibility of identification may obviously result from a direct disclosure of the name and surname of the person whose case has been described, yet naturally such situations are very rare. Much more common is the possibility of identification of a person through the photos attached to such a publication, where apart from pathological changes some other characteristic features of that person can be seen: for example a tattoo, a rare body deformation, physical appearance etc. The person can also be recognized through the description of the situation which lead to the injury mentioned in the text, especially if it was a rare incident and additional information indicating the place of the incident took place. The possibility of linking a theoretically anonymous patient presented in the publication with a specific person may also result from the unique nature of the disease or from the fact that this person is well known. However, the remarks concerning the elements of the publication which can lead to identification of a patient should be considered in the eye of Article 6.3 of the above mentioned Act, which states that: “A piece of information shall not be regarded as identifying where the identification requires an unreasonable amount of time, cost and manpower.”⁴ Thus, identification of a patient on the basis of data from a publication must be possible with the use of the means which are generally accessible and commensurate.

Here one should answer the question whether the Act under consideration is to be applied also in case of deceased people. The Act on Personal Data Protection contains two types of provisions:

¹ Act of 23rd April 1964: the Civil Code (Journal of Laws No. 16, item 93 as amended).

² Act of 29th August 1997 on the Protection of Personal Data (i.e. Journal of Laws of 2002, No. 101, item 926 as amended).

³ Act of 4th February 1994 on Copyright and Neighboring Rights (i.e. Journal of Laws of 2006, No. 90, item 631, as amended).

⁴ Act of 29th August 1997 on the Protection of Personal Data (i.e. Journal of Laws of 2002, No. 101, item 929 as amended).

those related to public law aspect and those related strictly to private law aspect. Private law aspect covers all regulations addressed to natural and legal persons, whereas public law aspect marks a certain standard concerning personal data processing and is addressed to database administrators.

It is undisputable that at the moment of a patient's death provisions of private law character cease to apply, for example the provisions requiring consent, as such consent obviously cannot be granted. Another question should be asked however: whether after a patient's death protection resulting from public law provision still applies, i.e. the duties subject to public authority control, regardless of the activity of the person directly involved.

In case of a patient's death, regulations imposing duties on third parties or requiring certain behavior standards from them theoretically still apply. For example article 26 paragraph 1 concerns database administrators, requiring from them all their possible diligence in data processing in order to protect interests of the people whose data is being processed. However, possibility to apply this act to deceased people should be assessed negatively. The letter of the Inspector General for the Protection of the Personal Data (this official is generally known in Poland under the acronym GIODO) of 12th February 2002 (symbol GI – DP – 024 /145/01/427), where he noted that the act does not concern deceased people, confirms that such an opinion is right. It is evident that the Act on the Protection of Personal Data in any case does not affect the limitations of the permitted publication of data in the situation of patient's death.⁵ It must be also added that the Act will be certainly applied in relation to data of deceased people when such data somehow also relates to the third parties, for example to the relatives. A situation may occur when, for instance, the publication contains the description of the course of a hereditary disease of the deceased patient. Then, it would be possible to consider such publication as law infringement pursuant to the Act on the Protection of Personal Data but only in relation to the issue (offspring) and not to the deceased patient.

To sum up: from the point of view of the Act on the Protection of Personal Data placing in a scientific publication information such as: the deceased patient's case history, his/her age, blood group, medicines taken, addictions etc. in no case infringes duties of data administrator.

Image protection of the deceased patients

Another legal institution determining the limits of permissible publication with regard to the rights of

the persons mentioned in the publication, is the image protection introduced in article 81 of the Act on Copyright and Neighboring Rights. Image means „a visual presentation of a person i.e. typical physical features of a person, which give the idea about the person's appearance”⁶. For example a photo of a patient printed in a publication can fall into this definition. It must be noted, however, that a photo, which makes it possible to identify a person, yet does not illustrate the likeness (i.e. does not give the idea of one's looks – pictures of particular parts of someone's body, pictures of tissues etc.) cannot be considered to constitute a person's image.

In such a case the subject of protection is the exclusiveness of image management – i.e. the right to decide about its publication. This right evidently does not refer to the deceased patient. Emotional sphere connected with publication of the image may be protected pursuant to Civil Code regulations on the protection of personal interest (article 23 and 24 of the Civil Code). Law infringement requires negative psychological experience of the patient caused by the publication of the image. Protection resulting from articles 23 and 24 of the Civil Code does not allow for creation of legal fiction, i.e. existence of personal interest of a subject who is no longer alive. Article 24 of the Civil Code, stating that the measures of personal rights protection may be used by „a person whose personal right is threatened...”, evidently denies the possibility to apply this protection in relation to the deceased. The foregoing opinion is absolutely undisputable in the eye of civil law.

Protection of the rights of third parties

From the hereto presented institutions protecting the rights of persons being „the subject” of publication one may draw a conclusion, that on the basis of Polish law there is a rule under which when a publication describes cases of the deceased people there are no limitations in respect of disclosure of information relating to these people and their image. However, this conclusion would be false. The scope of permissible data disclosure concerning a deceased patient is specified not by protection of a deceased patient's rights but by protection of third parties' rights (relatives of the deceased). Pursuant to the legal structure adopted in articles 23 and 24 of the Civil Code, at the moment of the patient's death his/her rights ensuring protection of non-pecuniary interest expire. One does not find an analogical institution to the one related to copyright, based on “transferring” author's moral rights from the deceased to a determined group of relatives, with the possibility to use them as own rights. As the wording of article 23, sentence 1 („personal interest

⁵ Compare J. Barta, P. Fajgielski, R. Markiewicz, *Ochrona Danych Osobowych – Komentarz*, Kraków 2004, p. 376.

⁶ J. Błęszyński, Glosa do wyroku SN z 27.02.2003 r., [Comment to the Decision of the Supreme Court of February 27, 2003] IV CKN 1819/00, OSP 2004, No. 6, item. 75, p. 320.

of a man in particular...") indisputably settles an exemplary nature of the list of personal interest subject to protection, both the doctrine and the jurisdiction distinguish personal right of the deceased person's relatives to protection of their feelings connected with the memory and respect of the deceased. Personal interest of those people is defined as „the cult of memory of the deceased person". Therefore the problem of publication of the information about the deceased person is looked at through the prism of the feelings of the deceased person's relatives and not through the prism of the feelings of the subject who is no longer alive.

The analysis of court decisions leads to the conclusion that the subject of protection is mental peace connected with the experience of going through the loss of a close person, thus the subject of protection is the emotional sphere related to the cult of memory of the deceased person. Keeping this in mind I shall try to present logical reasoning which should be adopted in the process of examination whether personal interest in question has been violated. The first step is to establish if the elements included in the publication enter into the sphere protected by the law. It is therefore necessary to answer the question whether publication of the deceased patient's case history leads to violation of the aforementioned mental peace of the relatives. It is obviously very difficult to determine it in an abstract manner, without reference to any specific case. It seems, however, that in the majority of cases the answer to this question will be positive, no matter whether the publication contains drastic descriptions, the history of a disease commonly considered as embarrassing or it is only a dry relation which does not arouse any emotions in the reader. It results from the fact that it is sufficient for violation of the cult of memory of a deceased person to infringe the aforementioned mental peace and that will occur at the moment of publication of the information evoking the memories of the deceased. In order to talk about the infringement of a personal right it is necessary that the discussed infringement of mental peace leads to negative mental experience in a subject of the right to the cult of memory of the deceased person, i.e. in a relative.

Determination of such negative experience cannot be made subjectively. It is not enough to rely only on a declaration of a person claiming protection of his/her rights as in case of hypersensitive persons the assigned protection would go absolutely too far. It is therefore necessary to determine the relation between the infringement and the mental experience, which would be commensurate to an average person, i.e. it would be objective.

Article 23 of the Civil Code determines that protection of personal interest is assigned in case of illegal infringement of these rights. Thus infringement of a personal interest takes place in the event of entering into the protected sphere and causing negative feelings of the subject of the right in re-

spect of the cult of memory of the deceased person. At the same time entering in this manner into the protected sphere will be illegal. In this context one should refer to the Doctor and Dentist Profession Act⁷, which specifies what is legal and illegal in the behavior of these professionals. Paragraph 1 of article 40 of this Act states that: „The physician is obliged to keep confidential any information relating to the patient obtained in connection with his practice". Paragraph 2 of the article 42 enumerates situations when despite disclosure of information no infringement of medical confidentiality occurs. For example the cases where disclosure of information is "necessary for practical teaching of medical profession" (item 6) or "it is necessary for medical research" (item 7). When a publication contains information concerning a deceased patient, and such information infringe personal rights of his/her relatives, the illegality of this infringement shall be excluded if a prerequisite of necessity of the publication occurs, in the eye of scientific purposes and the necessity of practical teaching of the profession. Of course the word „necessary" used in the act is not clear and determination of existence of such prerequisite will be possible only in a specific case, based on the knowledge of experts in a given field of medicine. It must be noted that the prerequisite of „necessity" also refers to the manner of publication of the information – not only there has to be the necessity to publish the information, justified by the aspects provided in article 42, items 6 and 7 of the Doctor and Dentist Profession Act⁸, but also the appropriate form and content of the publication should consider possibly slightest disturbance for the people whose personal interest are infringed. To sum up, article 42, items 6 and 7 of the aforementioned act specify circumstances excluding illegality of the actions taken by the author of publication in which a particular case is being presented. Publication of data necessary for scientific purposes and for acquiring practical knowledge does not always have to be combined with publication of data **allowing for the identification of the patient.**

There is also another occasion excluding illegality of physician's publication of information about a patient which was acquired in the course of medical practice. It is the situation when a patient or his statutory representative expresses his/her consent to the use of such information. Such consent may also be expressed by the deceased patient's relative after the patient's death but its effectiveness will be different. It will exclude illegality of physician's actions only in relation to persons who expressed

⁷ Ustawa z dnia 5 grudnia 1996 o zawodach lekarza i lekarza dentysty [Doctor and Dentist Profession Act of December 5, 1996], i.e. Journal of Laws 2008, No. 136, item. 857.

⁸ Ustawa z dnia 5 grudnia 1996 o zawodach lekarza i lekarza dentysty [Doctor and Dentist Profession Act of December 5, 1996], Journal of Laws 2005, No. 226, item. 1943.

such a consent. In consequence, so as the publication would not be considered illegal the author should obtain consent of all the people authorized to claim protection of their rights in connection with the protection of the cult of memory of the deceased person. Determining who actually belongs of the group of those people will be possible only within the context of a specific case. The discussed right is the personal interest assigned to the relatives of the deceased. Such determination of the subject of this right does not settle exactly who can enjoy its protection. It seems, however, that such right can be assigned not only to the relatives or members of the family of the deceased person but also to people emotionally attached to the deceased. The task of the court will be to determine in relation to whom it is possible the existence of a relation justifying examination whether the aforementioned personal interest has not been violated.

Obviously all reflections presented in this paper refer to the situation when in a scientific research medical publication a case of a deceased patient is presented and the publication infringes the rights of the patient's relatives in relation to protection of the worship of a deceased person, assuming that the **relatives can recognize a person to whom they are emotionally attached.**

Conclusions

To sum up the foregoing we may talk about impermissibility of a publication presenting clinical cases concerning deceased people only in the context of infringement of rights of the persons related to the deceased. In order to state that the personal interest has been violated and such violation justifies the use of measures provided in article 24 of the Civil Code (such as compensation, submission of an appropriate statement, forbidding infringement) it is necessary to establish that such activity, i.e. publication of any of the aforementioned elements such as: case history, photos of disease symptoms etc., lead to entering a sphere which is legally protected by this right and therefore it has disturbed mental peace of a relative. At the same time such an infringement must cause negative mental experience. The last prerequisite that needs to be established, in order to consider the publication as impermissible, is the illegality of the author's activity, assessed on the basis of the provisions of the Doctor and Dentist Profession Act⁹ obliging a physician to keep confidential any information relating to the patient which was obtained in connection with physician's medical practice.

⁹ Ustawa z dnia 5 grudnia 1996 o zawodach lekarza i lekarza dentysty [Doctor and Dentist Profession Act of December 5, 1996], Journal of Laws 2005, No. 226, item. 1943.

GENFOSS – JAVA APPLICATION FOR PRESENTATION OF CODING STRETCHES OF NEVER BORN PROTEINS

MONIKA PIWOWAR¹, EWA MATCZYŃSKA¹, PIOTR OCHLAWSKI², MATEUSZ KOSIBOWICZ²,
 DAMIAN KOŚC², MICHAŁ SWATOWSKI², PIOTR WIĘCEK², TOMASZ SZEPIENIEC³

¹ *Department of Bioinformatics and Telemedicine, Jagiellonian University, Collegium Medicum, Sw. Anny 12, 31-008 Krakow, Poland*

² *Astronomy and Applied Informatics, Jagiellonian University, Faculty of Physics, Reymonta 4, Krakow, Poland*

³ *Academic Computer Center CYFRONET, Nawojki 11, 30-950 Krakow, Poland*

Abstract: Application of genomes analysis results with respect to project of “never born protein” (NBP) is presented in this paper. GenFoSS application concerns visualisation of genomic sequence stretches that could encode proteins that are not observed in the Nature. The sequences of these proteins were generated randomly aimed to recognize the proteins of potential pharmacological activity. Identification of sequences similar to these of NBP can be viewed by GenFoSS application. GenFoSS gives information about sequence frequencies, percent identity, percent of similarity of alignments and E-value for aligned sequences. Comparison between two chromosomes in common organism and between different genomes as well can be done by these applications. There are also possibilities to check codon frequencies of nucleotide sequences that were found as a stretch of NBP.

Key words: never born proteins, genomes analysis, nucleotide sequences distribution

Introduction

The structure prediction of proteins of potential pharmacological application was one of the aims that EUChinaGrid project was focused on [3]. Materials to reach it were sequences of 70 amino acids in polypeptide (10^7 of them are classified as ‘never born protein’) which were used to produce their three dimensional structures [4]. Never born proteins were defined as proteins that were not identified in known protein (and genetic) databases [7,9]. Finding of traces of NBP among completely sequenced as well as in progress DNA sequences was of special interest [1]. It is expected to identify stretches of genomic sequences of potential biological function not identified (so far) in the Nature.

The genFoSS tool was generated to visualize the results of genomic analysis.

Identification of sequences similar to NBP in particular genomes gives information about dispersion sequences than could encode proteins that are not existing in nature currently but could have existed in nature as proteins formerly (in evolution time) and could have had a particular function in the past. Searching of traces of NBP was done on different level of accordance. There were accessed percent of similarity and per-

cent of identity in aligned sequences by using BLAST program with proper matrices (Fig. 1).

Identified stretches allow comparison of aligned sequences distribution in both compared chromosomes in one genome as well as between genomes of different level of evolutionary tree. The conclusions from such analysis may recognize the sequences composition (high or low probability to find random sequences in genomes can suggest less or more “planed” sequence composition). GenFoSS application allow check codon frequencies of nucleotide sequences that were found as stretch of NBP.

Material and Methods

Proteins data:

Never born proteins were obtained from Roma Tre University proteomic group [7]. Research material (besides DNA) was proteins written in Fasta format that were randomly generat-

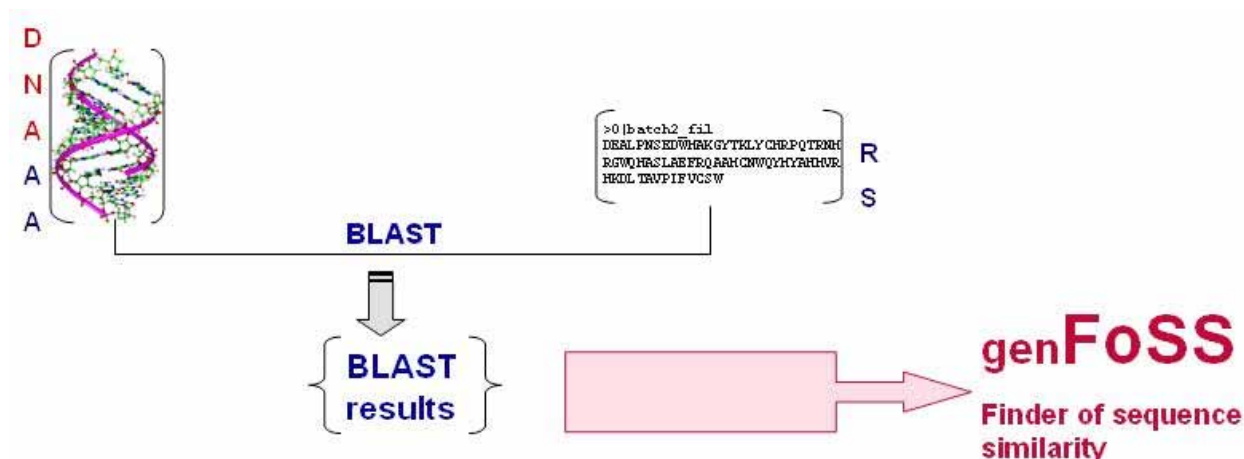


Fig. 1. genFoSS input. Data to genFoSS application come from BLAST results. DNA AA: DNA Amino Acids (DNA translated to amino acid sequences), RS: Random sequences

ed. Such generated database represented “NBP”. Number of polypeptides that was classified as proteins not existing in nature was 104. Selected NBPs that were found in genetic material are separated for further description and characterization.

Software that was used:

BAST – Basic Local Alignment Search Tool [5]

Technology used for creating application:

MySQL – data for genFoSS were collected in database created in MySQL technology.

Java – genFoSS is a tool created to research some of genetic parameters in known and already stored in databases genomes. The technology we used is simply Java Web Start, because of its portability and stability. This is why the only thing you have to have installed before running it is JRE – Java Runtime Environment. If you don't have it installed just go in your web browser to address: <http://www.java.com/en/download/manual.jsp> and download suitable version. All the information about installation of JRE can also be found there.

Genetic material

DNA sequences were taken for analysis from National Center of Biotechnology Information [8]. Most of them were represented by nucleotide sequences that have not been noticed information about stretches encoding known proteins.

Searching method

The first step in finding similarities was translating genome sequences to amino acids sequences. Tree reading frames were taken into consideration. The standard genetic code was

applied to translate human genetic information to amino acids sequences [6].

Next step was scanning translated genome sequence by BLAST – The Basic Local Alignment Search Tool for comparing gene and protein sequences against others [5] (fig. 2).

Results

GenFoSS is a 3-tier database application that used Java servlets and the Java Database Connection (JDBC). User interacts with the application by choosing the concrete values from the query form. Once the form is submitted then the Java servlet uses JDBC to find the information in a database. Afterwards, a Java object is created by the servlet and returned to the user application using object serialization.

The application is partitioned into three tiers: user interface layer(1), the business rules layer(2) and the data storage layer(3) (fig. 4):

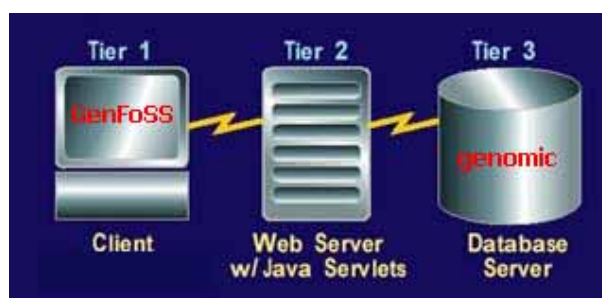


Fig. 3: Tiers of genFoSS application user interface layer(1), the business rules layer(2) and the data store layer(3):

- first tier is a stand alone application. In the first phase of the application, Swing components were used for user-input and displaying the database query results.
- second tier of the application is implemented with a Web server capable of executing Java servlets. The Java serv-

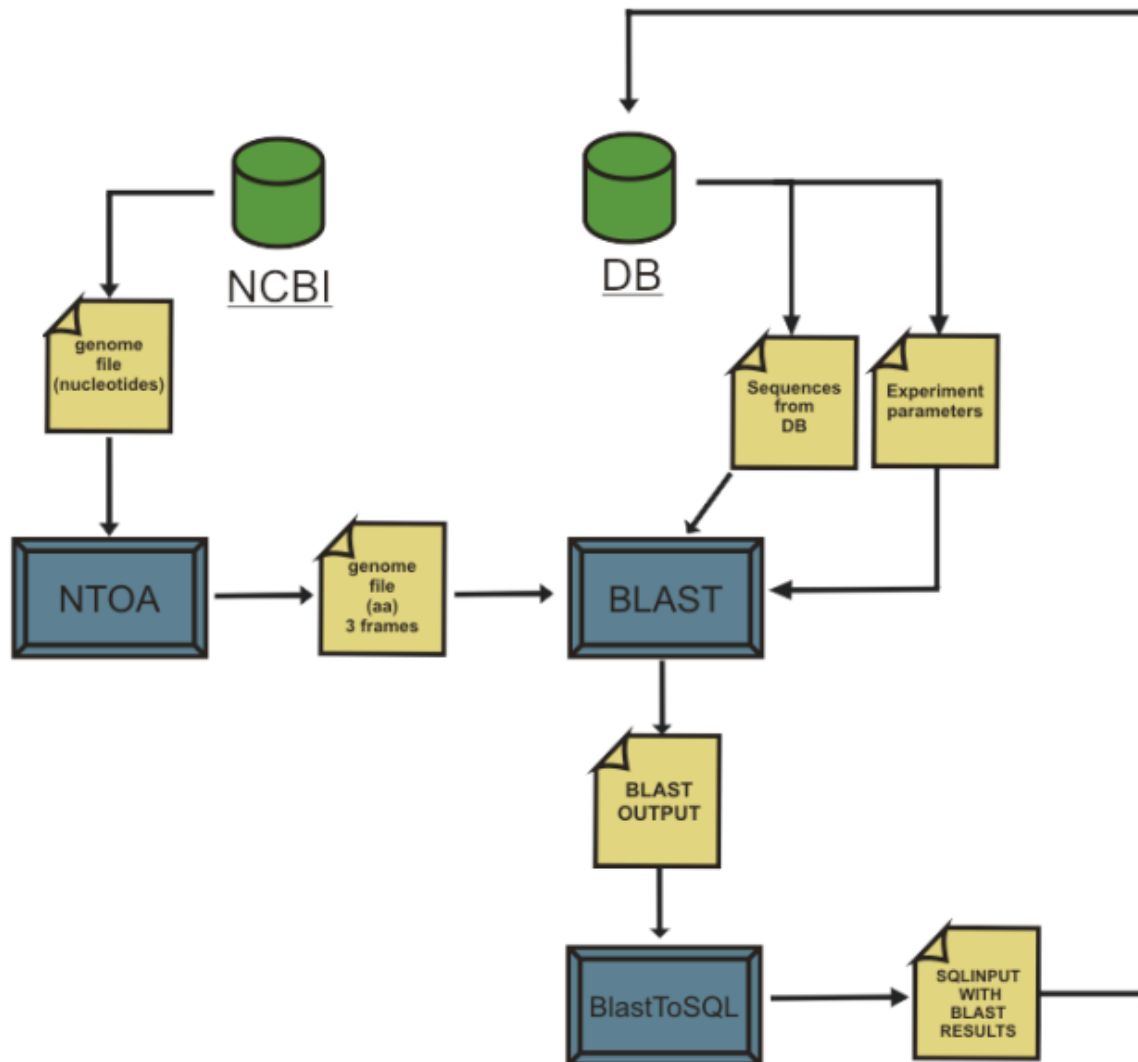


Fig. 2. Diagram of job execution.

let harnesses the power of JDBC to access the database to retrieve information as needed.

- third tier is composed of our database server. The database server stores the information that is used by the application. Thanks to the JDBC API, the servlet can access the database in a portable fashion by using the SQL call-level interface.

Database structure

Databases for storing data used by genFoSS application were created in a relational database management system MySQL because of its usefulness in storing and processing large amounts of data (fig. 3). BLAST output is parsed and stored in this database. genFoSS connects with the database through Java Servlet (described below). All needed data is quickly gathered and calculated thanks to SQL queries. Obtained re-

sults are sent back to genFoSS, which presents them in a simple and accessible way.

Stand alone application – servlet communication

Since servlets support the HTTP interface, there can be communication with the servlet over HTTP socket connections. The application simply has to open a connection to the specified servlet URL. Once this connection is made, then the application can get an output stream or input stream on the servlet. The application can send data to the servlet by sending a POST method. To send a POST method to a servlet, the application can use the *java.net.URLConnection* class. It must also inform the URL connection that data will send over the output stream. The POST method is powerful because it's possible to send any form of data (plain text, binary, serialized object, etc) using it. All that must be done is set the content type

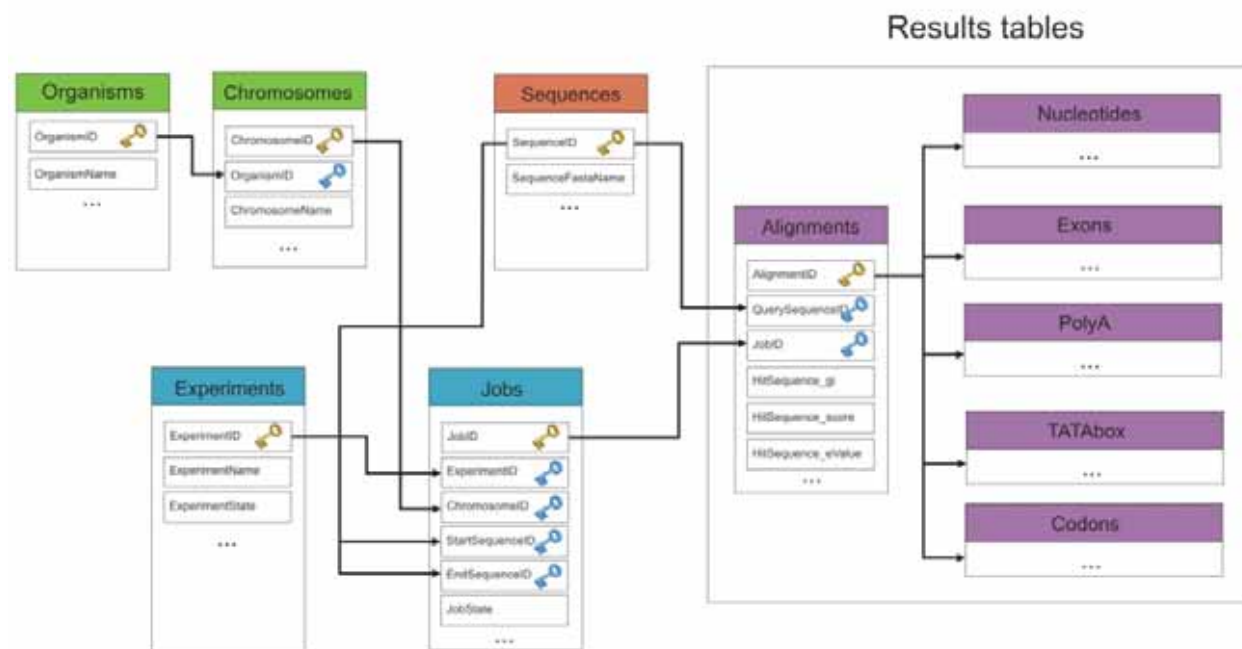


Fig. 4. MySQL database (GENOMIC database) schema.

in the HTTP request header – in this case it will be the serialized object “*application/x-java-serialized-object*”.

The code fragment:

```
// connect to the servlet
URL testServlet = new URL("http://www.sample.com/servlet/Serv-
let");
URLConnection servletConnection = testServlet.openConnection();

// inform the connection that it will send output and accept input
servletConnection.setDoInput(true);
servletConnection.setDoOutput(true);

// There can not be used a cached version of URL connection.
servletConnection.setUseCaches (false);
servletConnection.setDefaultUseCaches (false);

// Specify the content type that it will send binary data
servletConnection.setRequestProperty("Content-Type", "<insert fa-
vorite mime type>");

// get input and output streams on servlet
...

// send data to the servlet
...
```

Passing an object between the application and the servlet is done by Java object serialization. Java 1.1 introduced object serialization, which allows an object to be flattened and saved as a binary file. The values of the data members are saved so in fact, the state of the object is persisted or serialized. At a later time, the object can be loaded or deserialized from the binary file with the values of its data members intact. Object serialization is fascinating in that it frees the developer from low-level details of saving and restoring the object.

Objects can also be serialized to any output stream. This even includes an output stream based on a socket connection. It can serialize an object over a socket output stream. In order for a Java object to be serializable, its class must implement the *java.io.Serializable* interface. The *java.io.Serializable* interface is simply a tag for the Java Virtual Machine. It can be created a custom class as follows:

```
class Example implements java.io.Serializable
{
    // normal declaration of data members,
    // constructors and methods
}
```

There were four classes created: Experiments, Organisms, Chromosomes and Codons. Each of them implements the *java.io.Serializable* interface and has two constructors – one for creating object that stores information from query form and one for creating object that will be passed to client application with data from database.

Options selection in genFoSS

When genFoSS starts, welcome screen disappears (Fig. 5). A second screen (by Query Form) makes possible to choose the experiment of interest.

By defining it you can select the type of organism specified by that experiment. To select the organism simply click on the picture at context menu. It shows all available organisms in the selected experiment. The next step is selecting required parameter of organism's genome (%identity, similarity, E-value or Length) and its range (From and To) with its interval (how many 'boxes' creates specified range). When everything is selected – press Submit button (fig. 6).

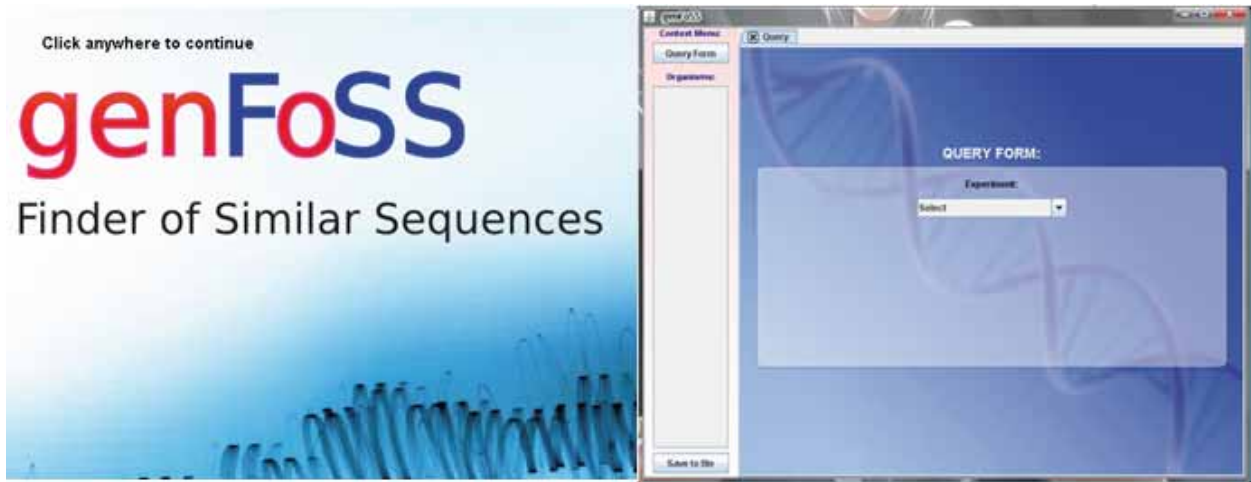


Fig. 5. Welcome and Query Form screen of genFoSS

After selecting parameters under consideration the results are available. There are two buttons at the top of context menu: Histograms and Comparison. It allows few aspects of results available.

– Histograms

Histograms show distribution of parameters for complete set of organism's chromosomes. There is also a summary distribution of theme (fig. 7).

New buttons on context menu allow specification of selected chromosomes. Buttons in 'Chromosomes' are named according to chromosomes names. To show/hide histogram the appropriate button should be pressed. "+" Button shows all chromosomes, "-" button hides them all. "S" button shows/hides summary histogram. Interested details of single chart appear after clicking on it (fig. 8).

Clicking the required bar (number of them is defined by interval size) allows detailed view. It shows how many cases are included inside this sub-range.

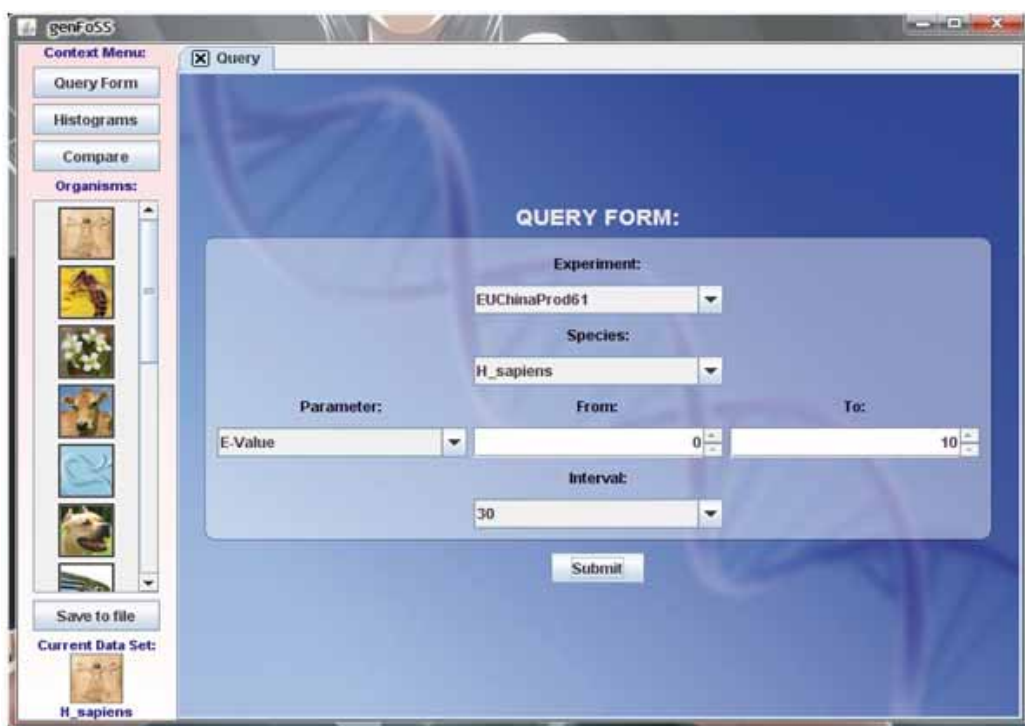


Fig. 6. Filled form with Homo Sapiens organism selected

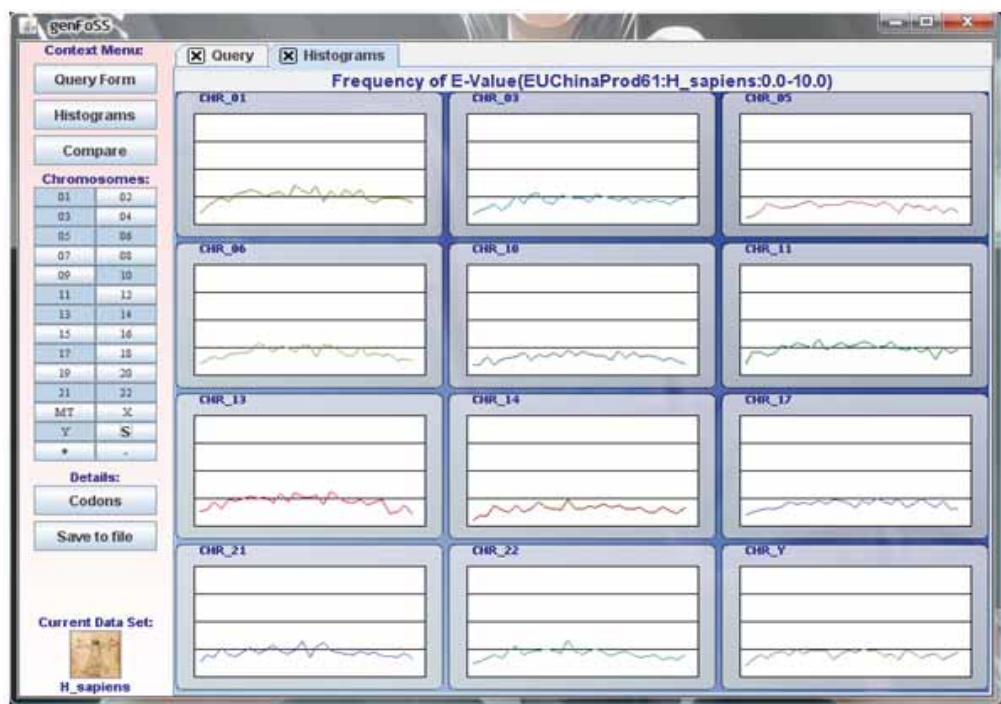


Fig. 7. Histograms of E-Value for all selected Homo Sapiens chromosomes

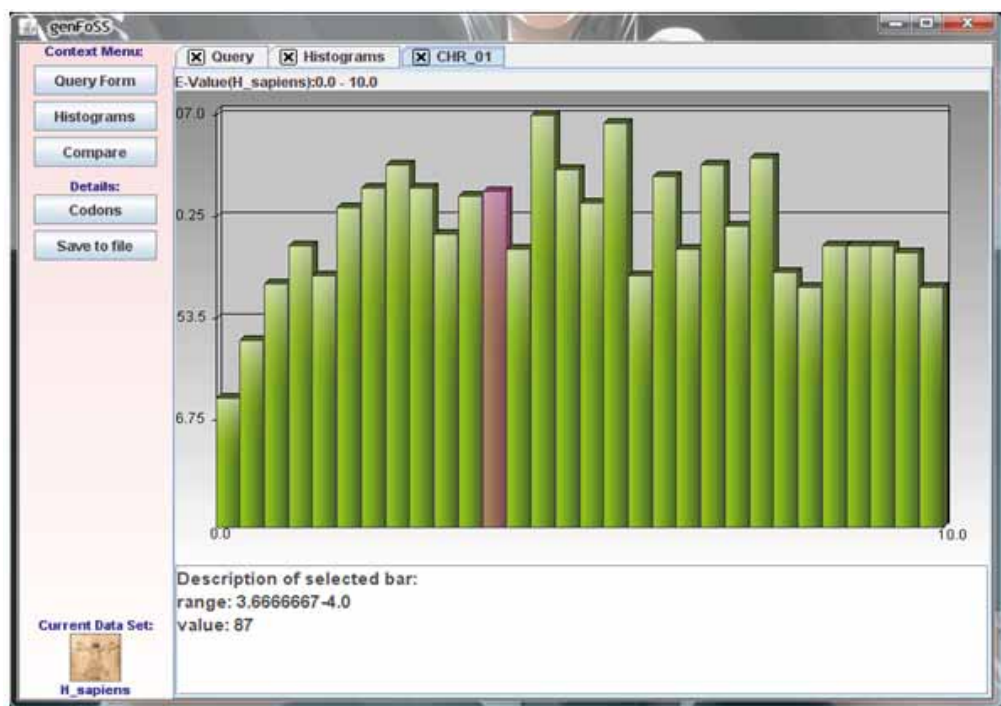


Fig. 8. Detailed E-value (in range 0-10 and with interval 30) histogram of *Homo Sapiens* chromosome 1

– Comparison

Comparing a few distributions of defined parameter at one chart is possible by clicking “Compare” button at the context menu followed by the appearance of one, big and empty histogram. To add/remove data set to it just use chromosomes-like

named buttons in chromosomes section at context menu bar (fig. 9).

To change colors on the chart click on the legend box at the bottom of the tab and select other color from palette. Boxes have the same colors as corresponding lines at chart and they have names of the chromosomes.

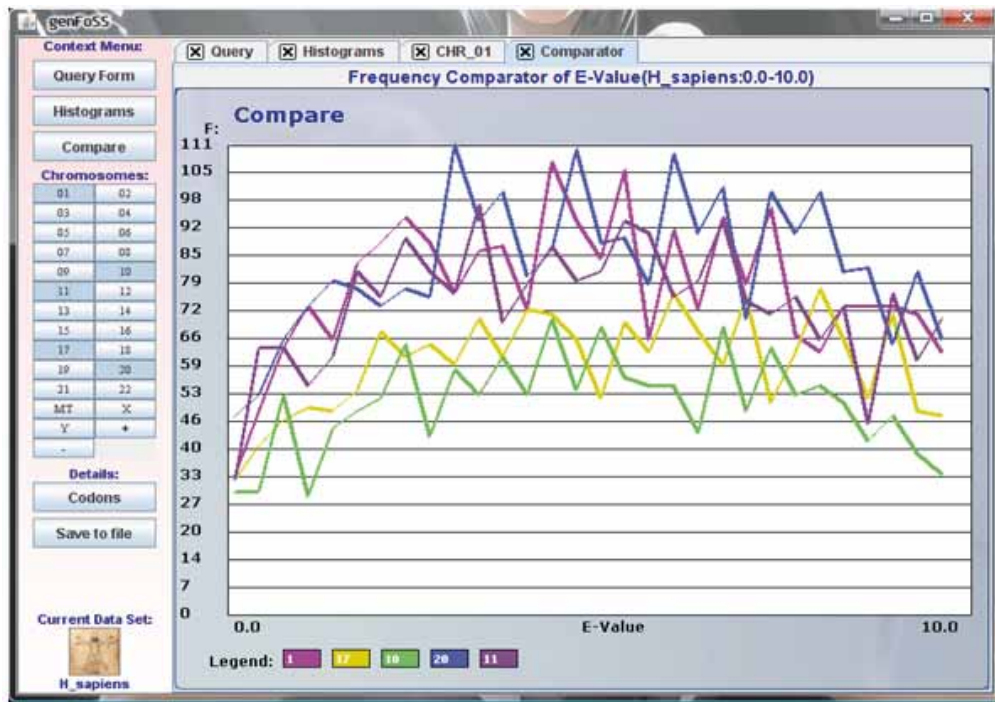
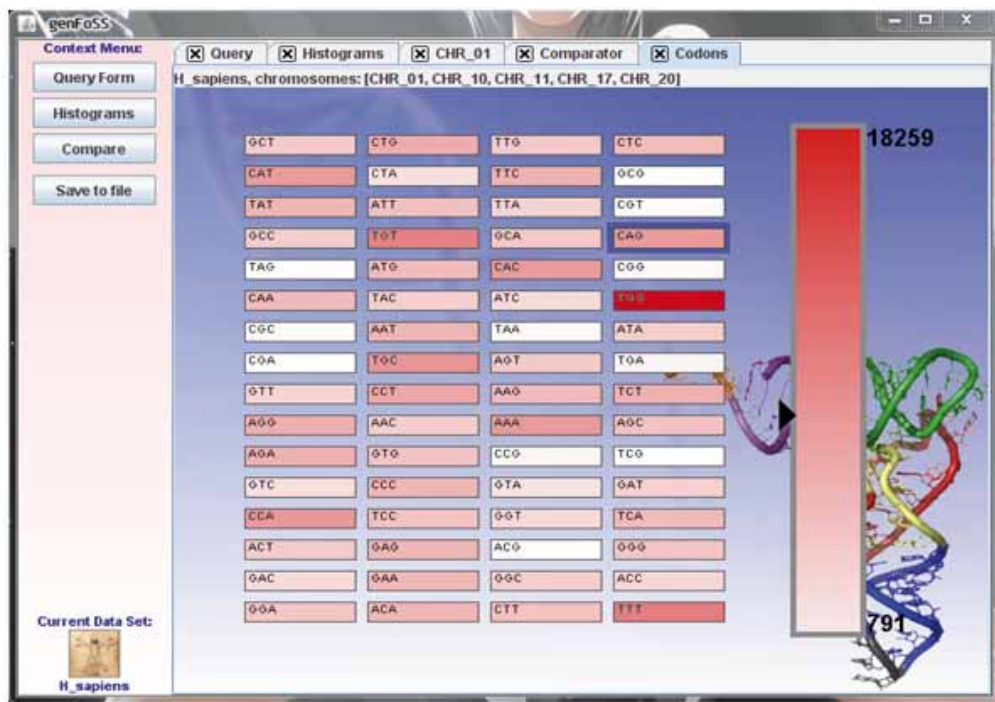


Fig. 9. Comparator of selected chromosomes

Fig. 10. Codons for *Homo Sapiens* chromosomes 1,10,11,17 and 20

– Codon statistics

At histograms, or comparator, there is a “Codons” button available at the context menu bar. It shows new tab with quantity information about selected chromosomes codons. There is possibility to obtain codon statistics by pressing on active de-

tailed chart tab. To see summary codons information just use histograms or comparator. To have all required chromosomes visible just press Codons button and result for them will appear (fig. 10).

The darker color of codon, the bigger number of its type found in selected chromosomes. Additional options are avail-

able by using right mouse button on the Codons tab. Colors of codons can be changed to grayscale. A set minimal value of shown codons (all of codons with lower value are hidden) can be marked. Details about codon quantities in codon's boxes can also be viewed. The vertical bar at the right side of codons map shows the scale and maximum value. When you click the codon's box, the black arrow will show where selected quantity is situated on axis.

– Saving Results

To save results for later purpose press “Save” button (on the bottom of context menu bar). All entries have ‘more’ hyperlink, which can help to decide if the tab is necessary or not (fig. 11).

When all tabs to export are selected, choose the format from combo box pressing Save to file button. Then information about file destination will appear.

Conclusion and Perspectives

GenFoSS application helps to analyse and visualise stretches of genomic regions that can encode NBP. Application is easy to use with standard and context menu. GenFoSS is still con-

nected with and data stored in database so everyone can check results. Application gives information about parameters like: sequence frequencies, percent identity, percent similarity of alignments and E-value. Application allows comparing different portion of genomes and checking codon frequencies of nucleotide sequences that were found as stretch of NBP. What is very important about genFoSS is it's available for free. There is a plan of creating web service by which particular tasks will have to be sent on grid infrastructure or local clusters structure. Resources in size of about 300 CPU enabled us to complete all computations in a couple of hours or days depending on amount of genomic data (Having the framework prepared, we were able to carry out the whole experiment in 38 hours. Average usage of resources was 126 CPUs). Additionally, the results of our work was a framework, that would be used easily for any further computations in which BLAST package and selection of gather DNA material used.

References

- [1]. Piwowar M., Szepienie T., Roterman-Konieczna I.: Massive identification of similarities in DNA materials organized in Grid environment. BAMS, 5, (2007).
- [2]. Malawski M., Szepienie T., Kochanczyk M., Piwowar M., Roterman-Konieczna I.: An approach to protein folding on the grid EUChinaGrid experience. BAMS, 5, (2007).
- [3]. Roterman-Konieczna I., Kochanczyk M., Malawski M., Piwowar M., Szepienie T.: The Quest for Pharmacology Active ‘Never Born Proteins’ within EUChinaGRID Project, Grid Workshop; Kraków; October 15-18 2006.
- [4]. Brylinski M., Konieczny L., Roterman I.: Fuzzy-oil-drop hydrophobic force field – a model to represent late-stage folding (in silico) of lysozyme. J Biomol Struct Dyn., 23, 519-528, (2006).
- [5]. Altschul S.F., Gish W., Miller W., Myers E.W. & Lipman D.J.: Basic local alignment search tool. J. Mol. Biol. 215: 403-410, (1990).
- [6]. The Genetic Codes: <http://www.ncbi.nlm.nih.gov/Taxonomy/Utils/wprintgc.cgi?mode=c>
- [7]. Chiarabelli C., Vrijbloed J.W., De Lucrezia D., Thomas R.M., Stano P., Polticelli F., Ottone T., Papa E., Luisi P.L.: Investigation of de novo Totally Random Biosequences. Part II. On the Folding Frequency in a Totally Random Library of de novo Proteins Obtained by Phage Display. Chemistry & Biodiversity, 3, 840-859, (2006).
- [8]. National Center of Biotechnology Information (<ftp.ncbi.nih.gov>).
- [9]. Chiarabelli C., Vrijbloed J. W., Thomas R. M., Luisi P. L.: Investigation of de novo totally random biosequences, part I: A general method for in vitro selection of folded domains from a random polypeptide library displayed on phage. Chem Biodivers 3, 827-839, (2006).

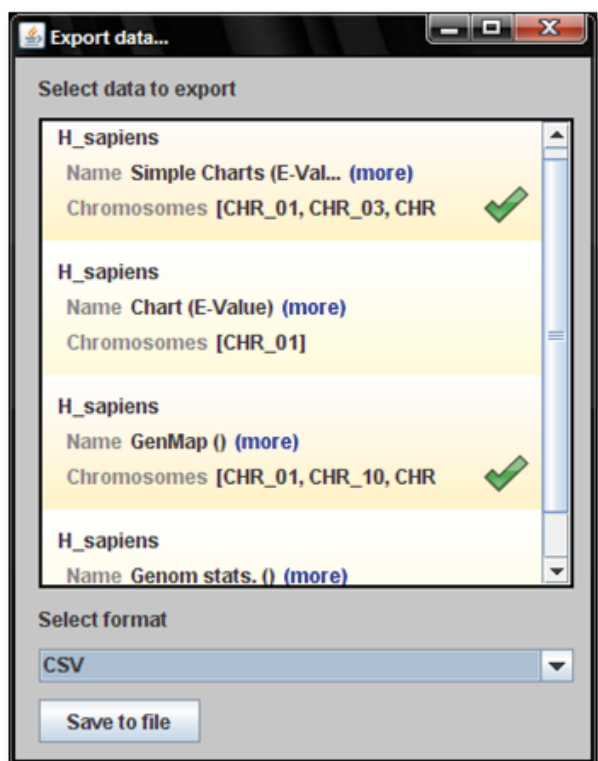
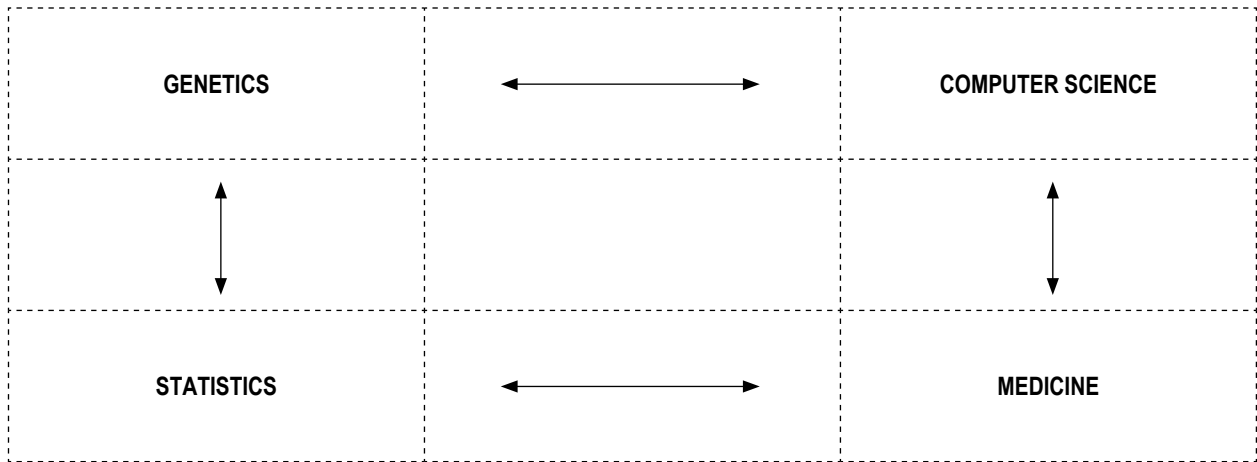


Fig. 11. Export results from first and third tab



SIMULATION OF RATIO OF OLD TO YOUNG PEOPLE IN COUNTRIES LIKE POLAND

DIETRICH STAUFFER¹ AND KRZYSZTOF KUŁAKOWSKI²

*Faculty of Physics and Applied Computer Science, AGH University of Science and Technology,
Mickiewicza 30, PL-30059 Krakow, Poland*

¹ *On leave from Institute of Theoretical Physics, Cologne University, D-50923 Köln, Germany.
Visit supported by COST P10. E-mail: dstauff@thp.uni-koeln.de*

² *E-mail: kulakowski@novell.ftj.agh.edu.pl*

Abstract: Countries like Poland with a recent sharp drop in birth rates still have some time to prepare for the problems of an ageing society. After the year 2030 they can become increasingly serious.

Retirement gets difficult to support if everybody lives longer, the birth rates go down, and retirement age and immigration/emigration remain constant. This demographic change [1] influences the ratio of people in retirement age to those of working age. These effects have been simulated by statistical offices in many countries, but also with detailed assumptions in journals and a book [2-6]; the latter two references give a complete Fortran program.

These methods, with minor adjustments, were used to predict the future growth of this ratio for countries with low birth rates like Germany [2,3,7], intermediate birth rates like Algeria, [4] and high birth rates like the Palestinian territories [6], always ignoring special historical events which are particular for these countries. Now we apply this method to a country like Poland where massive immigration may be less realistic; instead we simulate increases of birth rate and retirement age. Simulation details are shifted to an appendix.

The decay of the birth rate (more precisely, the average number of children per woman, unfortunately called the total fertility rate) came in Poland later but sharper than in Germany and is approximated by $2.3-0.55 [1+\tanh(0.15\cdot\text{year}-1993)]$. The total simulated population, normalized by the actual Polish population in 2002, agrees well with what the official Polish authority, www.stat.gov.pl, predicted: Fig.2. Fig.3 shows the ratio of people above retirement age of 63 to the people between 20 and retirement age (lower curve). (Our time units are years throughout.)

The future looks less problematic if the number of people up to age 20 is added to those above 63, both groups needing public support. Then the ratio is approaching a minimum: middle curve in Fig.3. Thus for some time, according to Fig.3 until about 2030, the fraction of people needing support from

the working population will not be much higher than it was in the past. Thus one has some years time to think, discuss and agree on how to solve the future problems of demographic change. The upper curve there shows the effects of a net emigration of 0.1 percent per year, starting in 2010 (e.g. from Poland to Western Europe; some statistical data give higher values already now). In the past this emigration was negligibly small, about 0.04 percent per year. The lowest curve in Fig.4 shows the resulting decay of the total population.

To get more optimistic curves, the retirement age was assumed to increase from 63 by one year and the births by 0.2 in the years 2020, 2025, 2030 and 2035; increase in retirement age alone did not help much. These assumptions give the x symbols in Fig. 4. The two lines on both sides of the x curve correspond to changes 0.25 (higher line) and 0.15 (lower line) in the births and indicate the order of magnitude of the extrapolation errors. Fig.5 shows the ratios of people in retirement age to people in working age, corresponding to the same simulations as in Fig.4.

In the above simulations the Gompertz slope was taken as $b=0.093$, with the mortality function increasing for adults as $\exp(bx)$ with increasing age x , as in [1,2], including the possible change around the year 1972 [8-11] (see in particular Fig. 6 in [10]). The actual Polish value is near 0.08 similar to Algeria [4]. Using $b = 0.08$ instead of 0.093 we get Figs. 6 and 7, which overlap with the results of Figs. 4 and 5.

Thus enhanced birth rates as simulated here and massive immigration as simulated for countries like Germany [2,5] could reduce the shrinking of the population and the burden of the working population to support the retired people. That burden would also be alleviated by increasing retirement age; German parliament adopted in 2006 a law regulating these future in-



Fig. 1. Real and assumed births. The + come from the official Polish statistics, the line is the *tanh* approximation used in the present simulations.

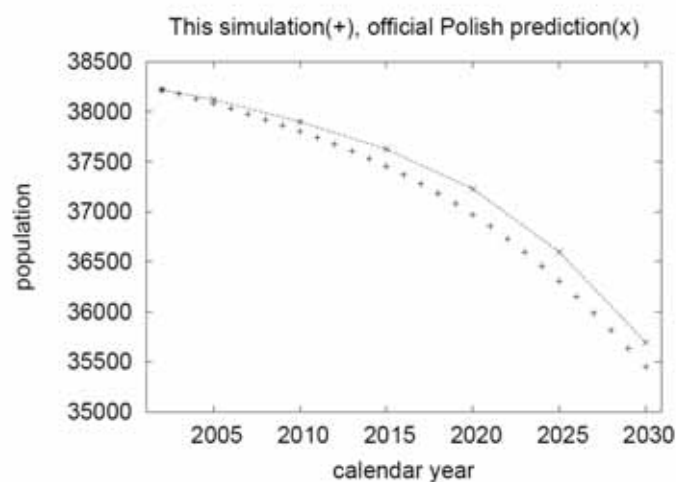


Fig. 2. Official (line) and present (+ symbols) extrapolations of Polish population.

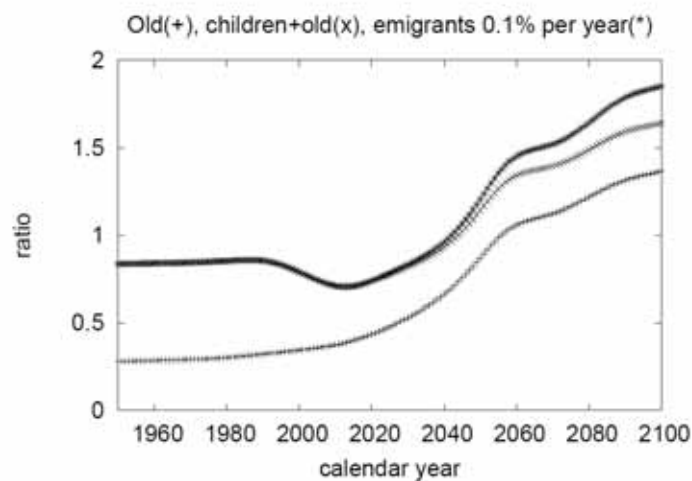


Fig. 3. Ratio of old to working-age people. For the two upper curves the young people were added to the old ones. Border ages are 20 and 63.

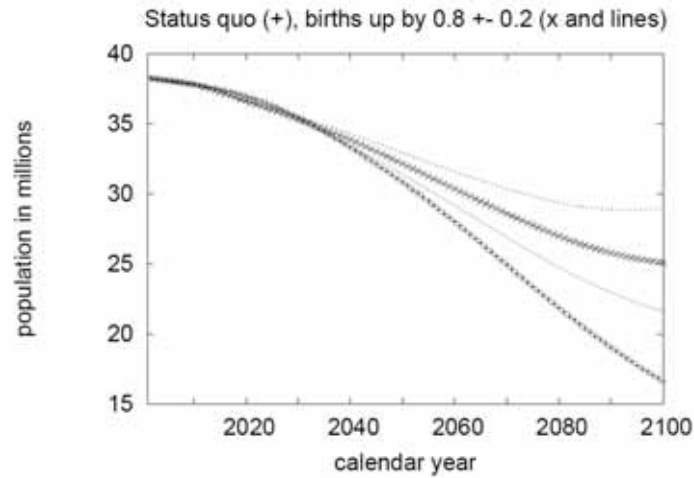


Fig. 4. Help from increased births. The lowest curve uses the present birth rate, the higher curves assume more or less strong increases of births in the future.

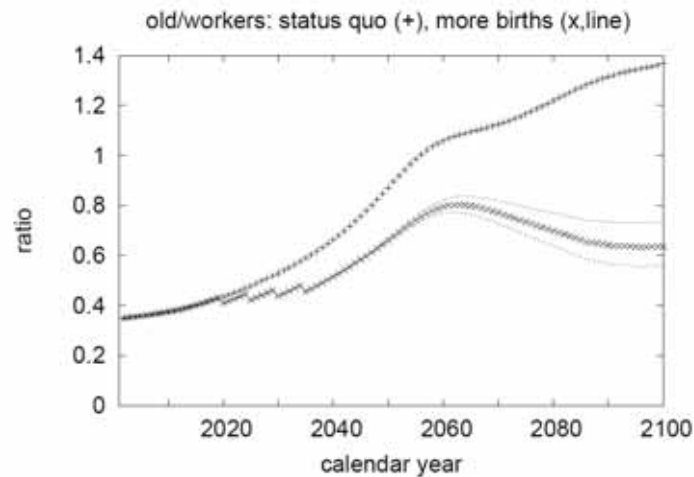


Fig. 5. Help from increased births and increased retirement age. Same simulation as in the previous figure; the rise of retirement age from 63 to 67 does not affect the total population shown in the previous figure.

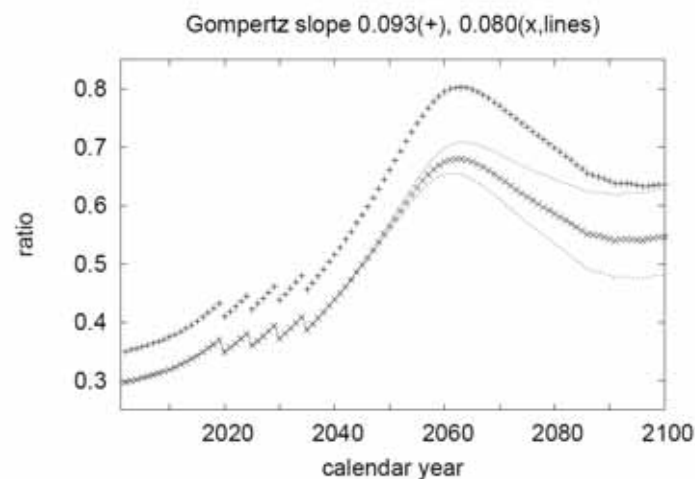


Fig. 6. Ratio of old to working-age people for different Gompertz slopes 0.093 (plus signs, Germany) and 0.08 (other curves, Polish men).

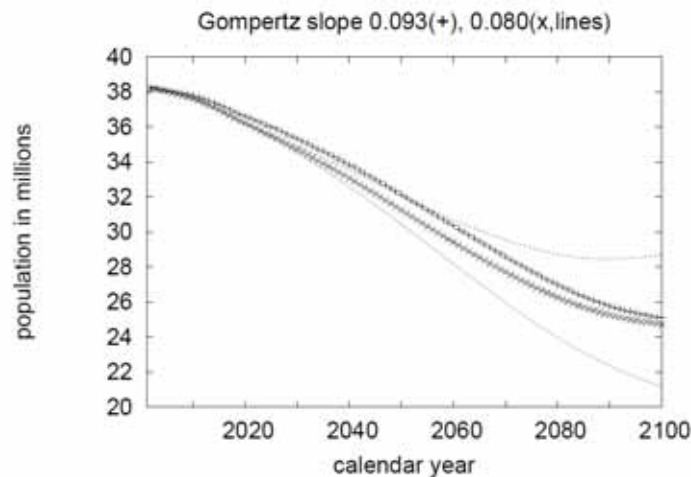


Fig. 7. Populations for different Gompertz slopes, same simulations as in previous figure.

creases. France recently increased the births from 1.7 to 1.9 within a decade. Other countries in the European Union, like Bulgaria, Romania or the three Baltic states, may be in a situation similar to Poland.

Simulations like these took less than a second each, in contrast to more sophisticated methods [12], and readers can change parameters to check for the effects of different assumptions. Countries corresponding to these simulations still have time to adjust to the future problems of the demographic change. The ageing problems seem to become very serious after the year 2050.

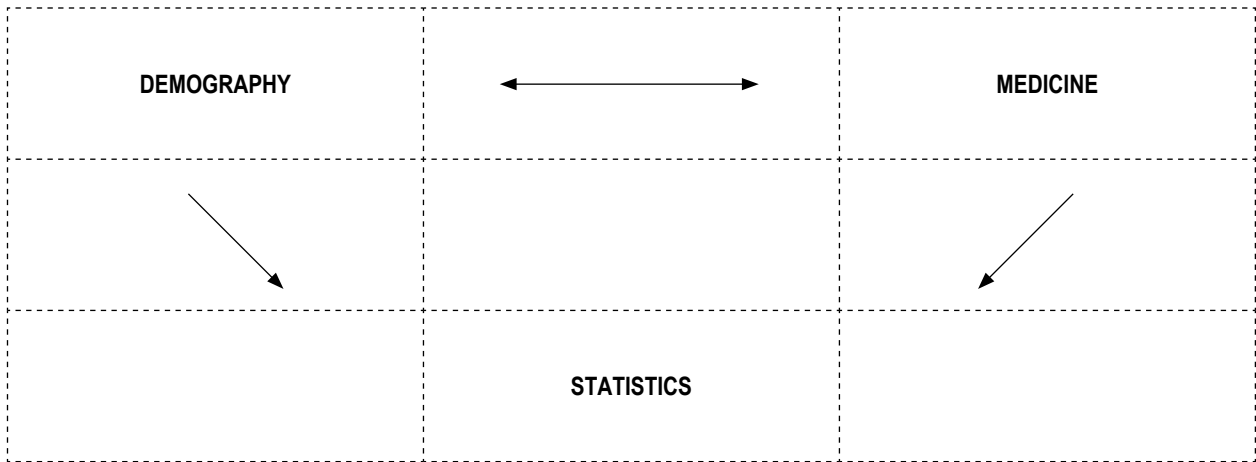
Appendix

The simulations calculate the age distribution of the population in one year from that in the preceding year, neglecting possible correlations between a mother and her daughters. Fathers and sons are neglected. For extrapolations over a few generations this approximation should be good enough. A complete Fortran program is given in [5,6], and it is available in the electronic version of this journal.

Women give birth from ages 21 to 40, of daughters with half of the birth number given in the text, spread evenly over these 20 years. Sons represent the other half and can be neglected. The population increases by immigration or decreases by emigration, affecting equally all ages from 6 to 40. The mortality is assumed as $7b \exp[b(x-X)]$, giving a survival probability $S(x)$ from birth to age x as $S = \exp[-7 \exp(-bX)(\exp(bx)-1)]$. Thus after births and migration have been dealt with, the population $P(x)$ at age x is calculated from $P(x) = P(x-1) S(x)/S(x-1)$. Here the Gompertz slope b is assumed to increase over 150 years from $b = 0.07$ to $b = 0.093$ (or 0.08) until the year 1971, and then to stay constant at this maximum value. The characteristic age X , in contrast, is assumed to stay constant at 103 until 1971, and thereafter to increase by 0.15 each year. This change of trends around 1971 was seen in some empirical studies of the last years [8-11].

References

1. Prioux F.: L'évolution démographique récente en France: l'espérance de vie progresse toujours, *Population-F* 63: 437-478, 2008.
2. Stauffer D.: Simple tools for forecasts of population ageing in developed countries based on extrapolations of human mortality, fertility and migration, *Experimental Gerontology* 37: 1131-1136, 2002.
3. Sá Martins J. S., Stauffer D.: Should retirement age be coupled to life expectancy? *Ingenierias (Univ. Nuevo Leon, Mexico)* 7: 35-38, 2004.
4. Zekri L., Stauffer D.: Sociophysics simulations III: retirement demography, *AIP Conference Proceedings* 779: 69-74, 2005.
5. Stauffer D., Moss de Oliveira S., de Oliveira P. M. C., Sá Martins J. S.: *Biology, Sociology, Geology by Computational Physicists*. Elsevier, Amsterdam 2006.
6. Sumour M. A., El-Astal A. H., Shabat M. M., Radwan M. A.: Simulation of demographic change in Palestinian territories, *Int. J. Mod. Phys. C* 18: 1717-1723, 2007.
7. Bomsdorf E.: Life expectancy in Germany until 2050, *Experimental Gerontology* 39: 159-163, 2004.
8. Yashin A. I., Begun A. S., Boiko S. I., Ukraintseva S. V., Oeppen J.: The new trends in survival improvement require a revision of traditional gerontological concepts, *Experimental Gerontology* 37: 157-167, 2001.
9. Wilmoth J. R., Deegan L. J., Lundström H., Horiuchi S.: Increase of maximum life-span in Sweden 1861-1999, *Science* 289: 2366-2368, 2000.
10. Edwards R. D., Tuljapurkar S.: Inequality in life spans and a new perspective on mortality convergence across industrialized countries, *Population and Development Review* 31: 645-674, 2005.
11. Kannisto V., in: *Human longevity, individual life duration, and the growth of the oldest-old population*, edited by Robine J.-M., Crimmins E. M., Horiuchi S., Zheng Y. Springer, Heidelberg 2006, p. 111.
12. Bońkowska K., Szymczak S., Cebat C.: Microscopic modeling the demographic changes, *Int. J. Mod. Phys. C* 17: 1477-1484, 2006.



MAGNETOCARDIOGRAPHY – MEASUREMENT CONDUCTION, DATA FORMATS AND DIAGNOSTIC APPLICATIONS

KAMILA BARON-PĄŁUCKA

*Chair of Automatics
AGH University of Science and Technology, Mickiewicza 30, 30-059 Krakow*

Abstract: Magnetocardiography (MCG) is a noninvasive diagnostic method that builds on properties of a magnetic field generated during cardiac cycle. This paper covers basic rules of measurement conduction, interpretation of recorded data sets, as well as data formats that are commonly used for visualization. MCG diagnostic applications are presented, not only by comparing MCG and ECG, but mainly by emphasizing certain advantages and disadvantages of MCG examination. Diagnostic parameters used for MCG results evaluation are presented – the ones created basing on time runs as well as those originating from maps. Moreover, paper describes content of experimental database, which author plans to use for further research on computer interpretation techniques of MCG data sets in decision support systems for heart disease diagnostics.

Key words: magnetocardiography, MCG, MF maps, PCD maps, heart diseases diagnostics, diagnostic parameters

1. Introduction

Magnetocardiographic examination (MCG) registers intensity of magnetic field generated during cardiac electrical activity and can be considered magnetic equivalent of electrocardiographic examination (ECG). This method arouses interest of scientists for more than 40 years, but thanks to recent technological development it finally became diagnostic method accepted by medical profession as well. This acceptance was granted not only because of well known advantages of MCG, such as non-invasiveness (lack of contact between patient's skin and sensors), ability to diagnose diseases that cannot be discovered with ECG or its suitability for such specialized applications as monitoring fetal heart's activity in last weeks of pregnancy, but mostly because of the fact that technological advancement of MCG devices allowed them to be moved out from magnetically shielded rooms and be placed next to patients' beds.

When MCG devices that allow "next-to-bed" working environment became commercially available, MCG systems installations started in many leading medical centers – both in Europe and USA. This caused a series of publications, which not only reaffirmed high expectations tied in with MCG, but also presented new areas of MCG application and paved the way to implementations.

2. MCG data formats

Magnetocardiographic examination registers intensity of the magnetic field generated during cardiac electrical activity. Electrical impulses, flowing through human heart and causing the contraction and relaxation of atria and chambers, are according to Maxwell equations the source of the magnetic field that is oriented perpendicularly to the electrical field. The values of the intensity of the magnetic field that are registered in course of a magnetocardiographic examination can be collected in one of the following formats.

2.1. Time runs

The values of the intensity of the magnetic field can be registered in form of time runs – each measuring point over patient torso is associated with one time run. Morphological features of MCG and ECG time runs are lot alike – on MCG time runs there are parts similar to P wave, QRS complex and T and U waves from ECG time run – there is also timing correlation between those elements. The significant difference is the fact, that in measuring points placed over lower thorax, in proximity of the midsternal plane, time runs with normal orientation of R and T waves are registered, whereas in measuring points placed over upper left thorax, time runs have reversed orientation (compare in Figure 1: time runs from box 3 and 4 with time runs from box 1) .

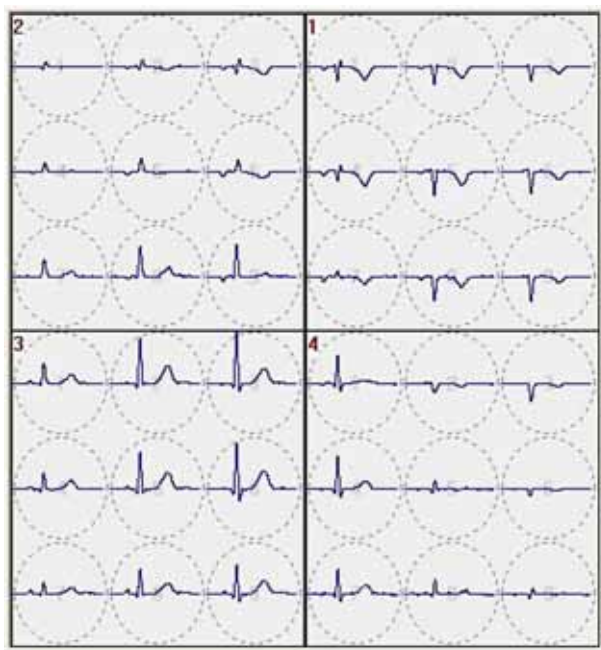


Fig. 1. MCG time runs from 9 channels, collected sequentially in four consecutive measuring positions. In measuring points over lower thorax (3 and 4) in proximity of the midsternal plane, registered signals have normal orientation of R and T waves, whereas in points over upper left thorax (1) R and T waves are reversed. On the basis of MCG, CardioMag Imaging application.

2.2. Magnetic Field Maps (MF maps)

The alternative format of data collected in course of magnetocardiographic examination is the MF map (Magnetic Field Map). This format is created by computing spatial distribu-

tion of the measured magnetic field intensity values for each channel (measuring point) in the same time point, as well as of the interpolated values for points placed between sensors. As a result of this operation, contour map or equivalent map with artificial coloring scheme is developed. Figure 2 demonstrates correlation between electrical vectors of the heart in particular phases of cardiac cycle and MF maps.

The visualization method that is frequently used for presentation of data collected in course of the MCG examination is a development of a sequence of the maps computed for consecutive moments of the cardiac cycle. Such visualization, often in form of animation, allows observer to capture temporal-spatial dynamics of the alterations on MF maps related to heart functioning. The example comparison of MF maps sequences for healthy (A) and sick (B) hearts of patients is presented in Figure 3.

It is worth mentioning that analysis of the pathological alterations on the MF maps sequences requires specialized knowledge due to the fact, that map fragments with the largest values of the magnetic field intensity do not equal the areas of the heart that are the most active at the moment. This means that from medical user point of view MF maps are not intuitively readable, because they do not reflect the sequence of the activation of particular fragments of the heart, and as a result do not directly show pathological functioning of the particular heart areas (compare Figure 5). This disadvantage was a direct reason for the development of the alternative visualization method for MCG data – pseudo-current density maps (PCD maps).

2.3. Pseudo Current Density Maps (PCD maps)

PCD maps (or alternatively Arrow Maps) were introduced by Cohen in 1976 in order to enable such representation of magnetic field intensity values, which would reflect the source of measured values – the distribution of the density of the heart's currents. [17].

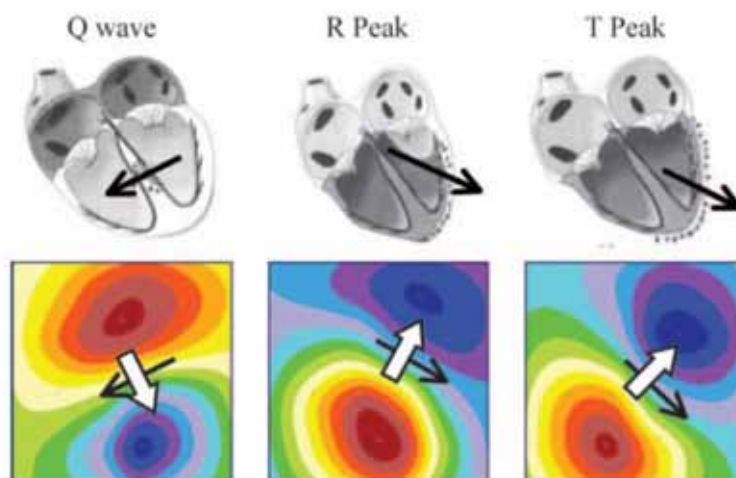


Fig. 2. Correlation between electrical vectors of the heart in particular phases of cardiac cycle and MF maps. Electrical vector is depicted with black arrow whereas vector of the magnetic field is depicted with white arrow. In all phases, as expected, both vectors are mutually orthogonal [9].

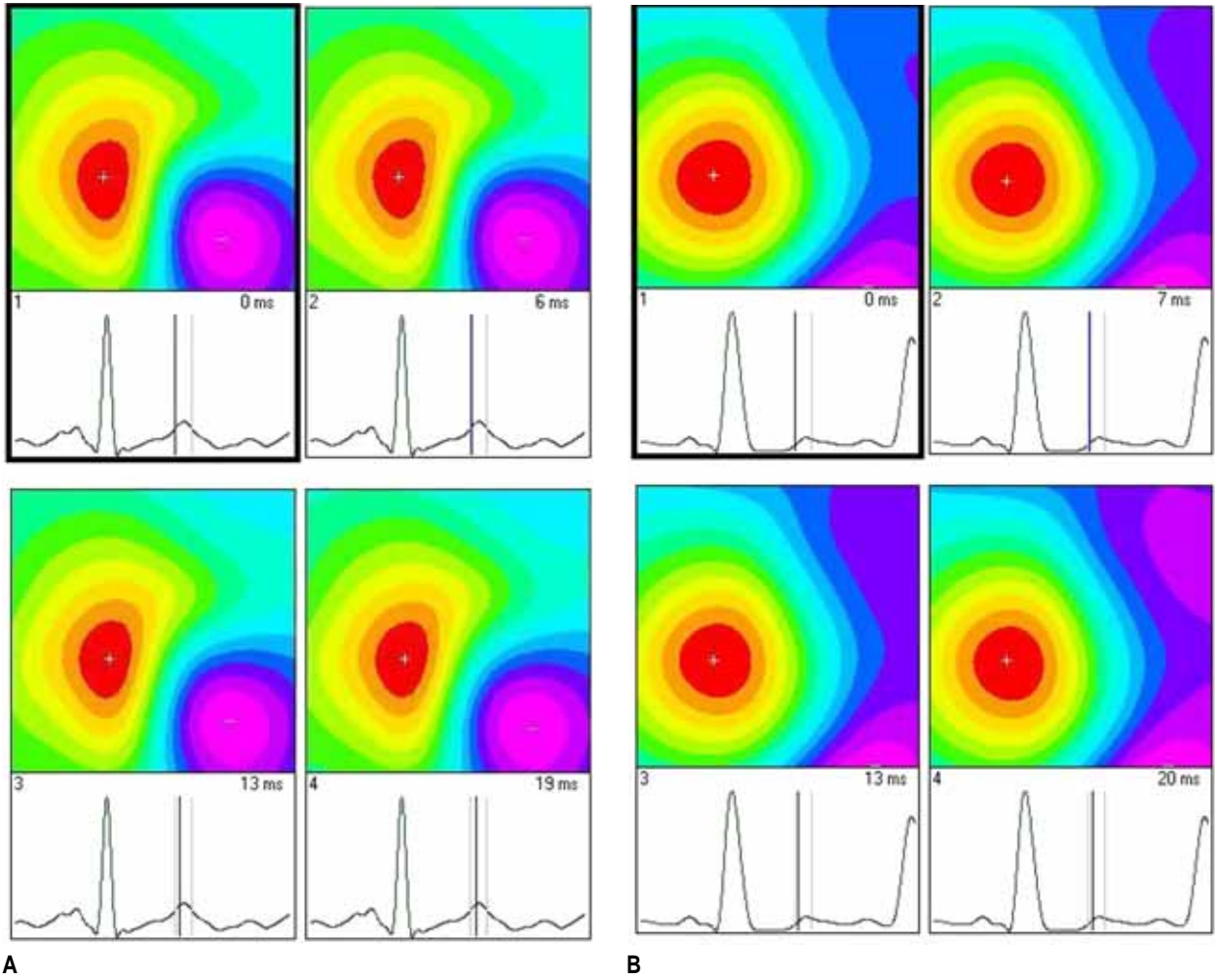


Fig. 3. MF maps sequences in line with the end of T wave of healthy 53 years old male (A) and 54 years old male after stroke (B). On the basis of MCG, CardioMag Imaging application.

The induction of the magnetic field is related to the density of the current that generates this field in accordance with the following equation:

$$\text{rot } \vec{B} = \mu \cdot \vec{j} \quad (1)$$

where:

$\text{rot } \vec{B}$ - rotation of the magnetic field induction

$$\text{rot } \vec{B} = \left(\frac{\partial B_z}{\partial y} - \frac{\partial B_y}{\partial z} \right) \cdot \vec{e}_x + \left(\frac{\partial B_x}{\partial z} - \frac{\partial B_z}{\partial x} \right) \cdot \vec{e}_y + \left(\frac{\partial B_y}{\partial x} - \frac{\partial B_x}{\partial y} \right) \cdot \vec{e}_z$$

$\vec{e}_x, \vec{e}_y, \vec{e}_z$ - versors of the coordinate system

\vec{j} - density of the current

If in course of the MCG examination all three components of magnetic induction vector were registered, it would be possible to obtain distribution of the density of the current that generates this field. Unfortunately, typically only B_z component is registered. Applying to it HC transformation (Hosaka-Cohen transformation) allows to obtain the value of so-called pseudo current density. This transformation is described by following equation:

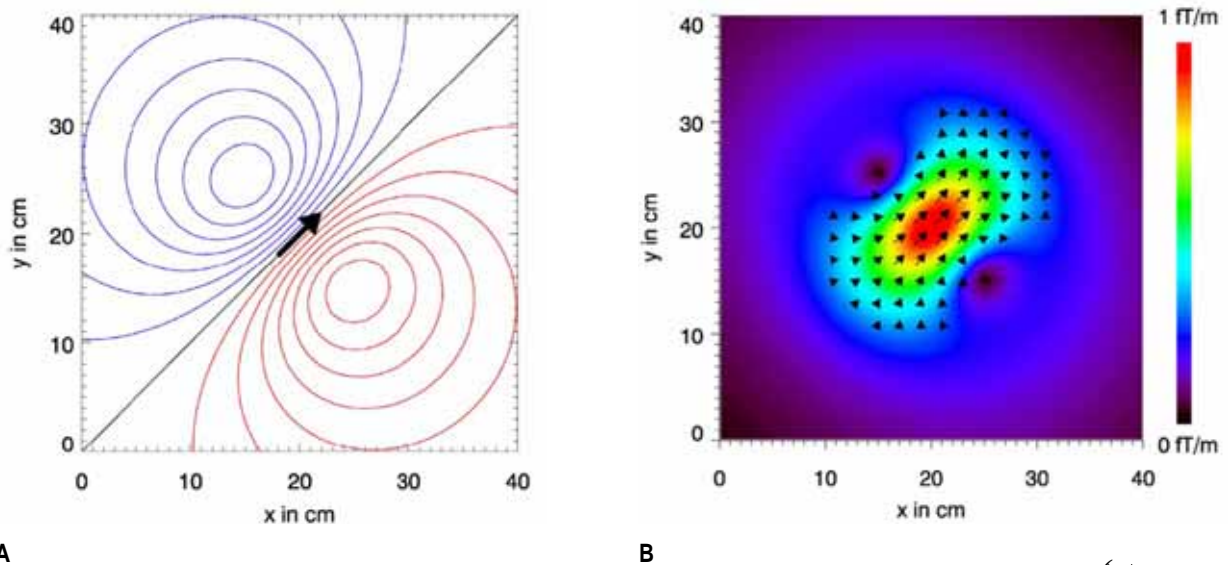
$$\vec{c} = \frac{\partial B_z}{\partial y} \cdot \vec{e}_x - \frac{\partial B_z}{\partial x} \cdot \vec{e}_y \quad (2)$$

where:

\vec{c} - pseudo current density

The map that originates from \vec{c} values calculated for all points of examination area is called PCD map. In its original version of year 1976, PCD map consisted of arrows, which lengths were coding values of the amplitude of \vec{c} in a given point. Nowadays, amplitude of \vec{c} in a given point is depicted by a color from the imposed color scale. The example of the contour MF map and its equivalent PCD map is presented in the Figure 4.

Application of PCD maps in visualization of MCG data results in maps where localization of the point with the largest signal amplitude is equivalent to the localization of the electrical dipole of the heart \vec{p} , and orientation of this point's \vec{c} vector is in accordance with orientation of \vec{p} . Therefore, PCD map is intuitive for doctor's interpretation, since it reflects which areas of the heart are active at the moment. The relation between PCD map and activity of the heart in comparison with analogical relation for MF map is depicted in Figure 5.



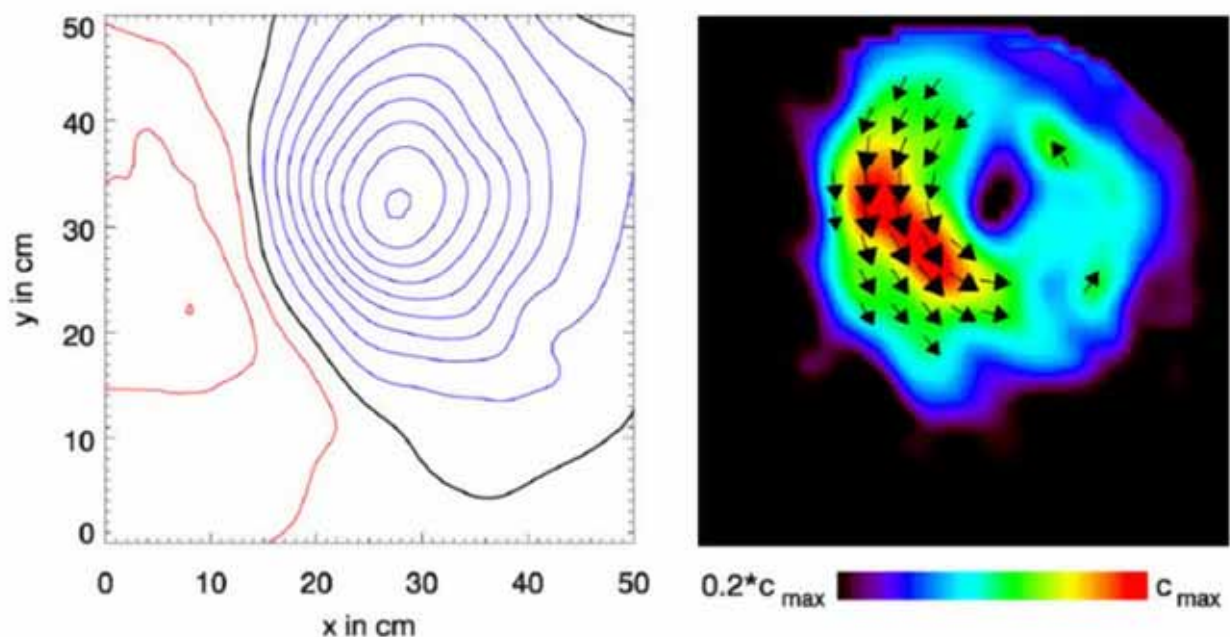
A **B**
Fig. 4. Contour MF map (A) and PCD map (B) for B_z component, calculated basing on Biot-Savart's law for dipole ($|\vec{p}| = 1 \mu Am$) placed 10 cm below map surface [17].

The analysis of the above figures confirms, that PCD map intuitively shows the progress of the right atrium's activation (Fig. 5.B), whereas similar interpretation of the MF map (Fig. 5.A) requires additional knowledge.

The additional advantage of the PCD maps application is the fact, that as contrasted with MF maps, they are independent of the sensor configuration that was used for the registration of the magnetic field (magnetometers, flat gradiometers, SQUIDS). This enables simple comparison of the maps even when they were created on different platforms and in different research centers [17].

3. Forward and inverse problem solutions in magnetocardiography

MCG allows to register the values of the intensity of the heart's magnetic field, but in the limelight remains the question of how, basing on MCG data, can one recreate localization of the source of the electrical activity of the heart. Answering this question is crucial, since observation of the electrical impulses flowing through the heart allows the observer to discover many pathologies such as ischemic disease or infarction scars. In this



A **B**
Fig. 5 **A** – Atrium activation visualized with MF map. The difference between consecutive contour lines is 0.5 pT (red: positive values, blue: negative, black: $B_z=0$); **B** – PCD map equivalent to 5.A map [17]

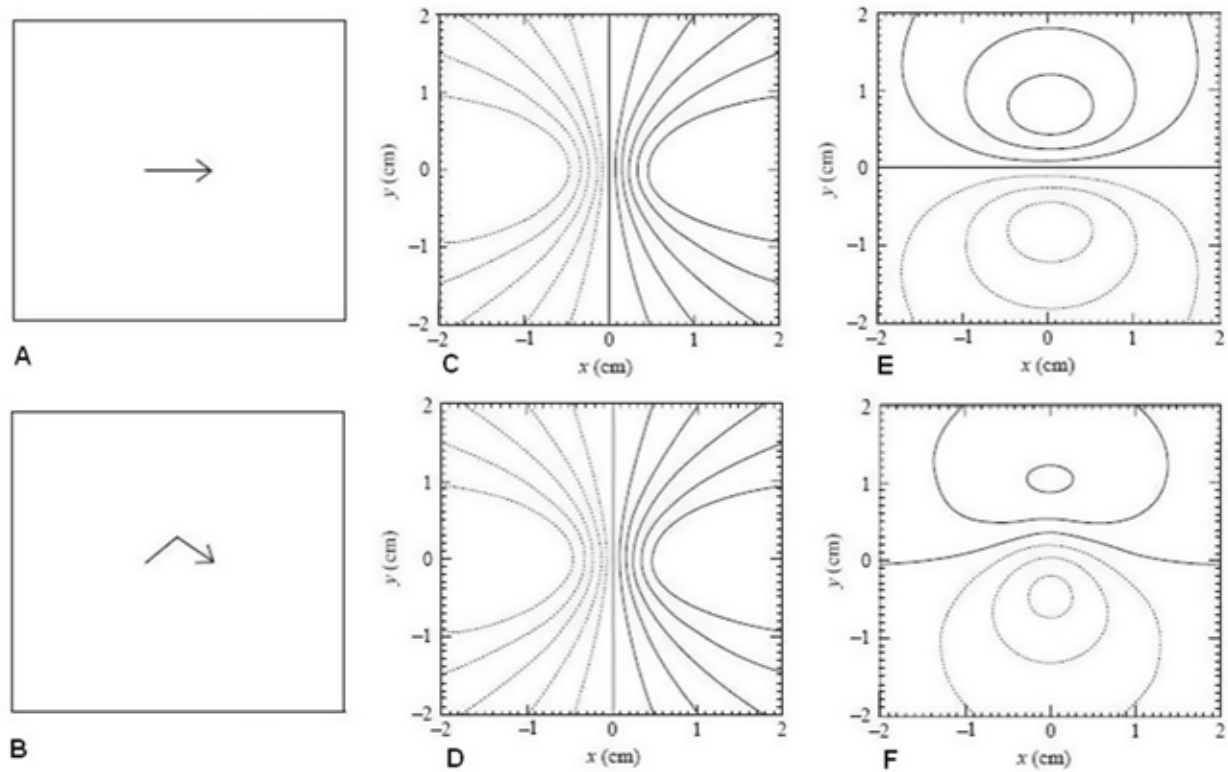


Fig. 6. Straight (A) and curved (B) current paths as the sources generating maps of the electrical field (C and D) and maps of the magnetic field (E and F) registered 1cm above the source and expressed in arbitrary units. [8]

context, the fact that the map of the magnetic field, as opposed to the map of the electrical field, carries the information about the curvature of the path of the current that was the source generating both types of maps [8, 16] becomes a valuable feature of MCG maps. Maps of the magnetic fields generated as a result of the identical currents flowing through straight and curved trajectories are significantly different, whereas analogous maps of the electrical fields do not show any difference at all. This difference is presented in Figure 6, where electrical and magnetic maps created for two different current paths are compared.

MF maps, besides reflecting the differences in the path of the current flow, allow computing the distribution of the currents generated by active cells of the heart muscle. Solution of such analytical task is called the inverse problem solution, but to describe the process of obtaining such solution it is necessary to explain in the first place the process of obtaining forward problem solution.

3.1. Forward problem solution

Computing the intensity of the magnetic field basing on measured distribution of the electrical field is called the forward problem solution. While searching for the solution of such problem, it is necessary to take into the consideration the nature of the physical phenomenon occurring in course of the electrical activity of the heart as well as details of the geometry of the torso. The accuracy with which the intensity of the magnetic field will

be computed depends on the approximations that were made within the “model of the source” articulating the activity of the heart in context of the currents it generates, and within “model of the conductive volume” that describes the conductive properties of the chest. Finally, it has to be decided in which place the magnetic field will be calculated, in relation to the location of the source of the current and conductive volume, as well as the choice of the component of the field to be computed has to be made.

3.2. Inverse problem solution

To solve the inverse problem, especially interesting in context of the magnetocardiography, is to determine the distribution of the currents related to the electrical activity of the heart, on the basis of the measured values of the intensity of the magnetic field. The solution of such problem is called the inverse problem solution. It is worth mentioning, that the inverse problem does not have an unambiguous solution – it is possible that different current distributions give rise to creation of the identical magnetic field intensity maps. In order to determine the localization, orientation and intensity of source of the current, basing on MF maps obtained measurably, it is necessary to solve the forward problem iteratively – the localization, orientation and intensity of the hypothetical source of the current is improved iteratively, so that the map generated by it would be as close to the one obtained measurably as it is only possible.

3.3 Models

There are many different models of the source – from the simplest one which models the whole heart activity with just single electrical dipole, to more complicated models which contain many dipoles, dipole in the movement or even many dipoles in movement that create the layer representing the action potential wavefront.

Similar distinction is observed in case of torso models – the simplest model in use is a homogeneous semi-infinite medium, but there are also more sophisticated models, which not only encompass realistic geometry of human torso but also take into account internal inhomogeneities representing lungs and intraventricular blood masses. It is worth mentioning that advanced models enable obtaining potentially more accurate results, but with the increase of the model's complexity, the risk of potential instability of the solution increases as well.

3.4. Solutions

Depending on the configuration of the chosen models, different types of solutions are obtained – Equivalent Current Dipole (ECD) or Current Density Estimation (CDE).

If a single electrical dipole was chosen as a model of the source, and homogenous semi-infinite medium as a model of a torso, then as a solution of the inverse problem Equivalent Current Dipole will be obtained, which can be considered the first approximation of the parameters of the source of electrical activity of the heart. This solution is accurate enough for many purposes – for example estimation of the location of the initial activation of the ventricle via an accessory pathway in patients with WPW syndrome, or localization of the onset of an ectopic beat originating from an arrhythmogenic region of the heart in patients suffering from periods of sustained ventricular tachycardia. Unfortunately, in case of many cardiac pathologies, this simple solution is not capable of showing complicated electrophysiological processes that underlie the disease.

If electrical activity of the heart cannot be narrowed down to small area, then application of the model of the source in the form of one single dipole does not make sense. In such cases more advanced model, with larger number of dipoles placed in chosen areas of the heart, is applied. Problem to be solved is then defined as of how to choose which dipoles should be active at the moment, so that generated MFM map would be the equivalent of the map measured in course of the MCG examination. Solution of that problem is called Current Density Estimation (CDE) and finding such solution for consecutive MF maps, opens up possibilities of diagnosing cardiac diseases that are otherwise hard to detect. The system of equations that join large amount of dipoles placed on epicardium with measuring points located outside of the volume of the heart, does not have an unambiguous solution, therefore some additional constraints are needed. One of the classes that originate from imposing additional restriction is a group of solutions which assume that the length of the vector that corresponds to the sum of all active dipoles has to be minimal. Such solution is called Minimal Norm Estimation (MNE). Additional knowledge, based on heart physiology, specifies allowed range of the strength and position of dipoles – it helps to stabilize the solution, espe-

cially in cases when dipoles are placed deeply and in cases of data with high level of interference.

4. Diagnostic parameters

The analysis of the magnetocardiographic examination results allows diagnosing many cardiac diseases. Depending on the experience of the performer, the process of making diagnose can be based solely on visual assessment of MF or PCD map sequences, but it can as well comprise of the phase in which auxiliary diagnostic parameters are evaluated. Such parameters can be calculated basing on MCG time runs or MF/PCD maps.

Diagnostic parameters are calculated for the time frames that correspond to the type of the disease being diagnosed – for example in case of ischemic heart diseases (IHD) only ventricular repolarization time runs and maps are taken into consideration. In case of some diseases both exercise and resting tests have to be performed in order to make a diagnose.

Parameters that are most frequently used for diagnose of the ischemic heart diseases include [1, 2, 3, 4, 5]:

1. Parameters calculated based on MF maps:
 - α angle – tilt angle of the vector that joins points of the largest (+) and the smallest (-) amplitude on MF map (for healthy man: $\alpha \in [-110^\circ, 20^\circ]$)
 - rotation of α angle in 30ms (for healthy man: α angle should rotate by less than 45° in 30ms)
 - variation of the distance between (+) and (-) points in 30ms (for healthy man this distance should vary by less than 20mm in 30ms)
 - variation of the ratio between the field strength in points (+) and (-) in 30ms (for healthy man this ratio should vary by less than 0,3 in 30ms)
 - repolarization stabilization interval after exercise (RSI) – time interval between Q wave onset and the stabilization time, which is defined as the moment in which orientation of the vector joining (+) and (-) points reaches within 50° of the orientation at the peak of the T wave (for healthy man normal values depend on gender and age, for instance for men below 50 years old RSI should be within range of 152 ± 35 [ms])
2. Parameters calculated based on MCG time runs, are equivalents of analogical parameters defined for ECG signal:
 - ST amplitude – averaged value of MCG signal within 5ms around point that is situated 60ms after J point of MCG time run (for healthy man normal values depend on gender and age, for instance for men below 40 years old ST amplitude should be within range of 2.2 ± 1.9 [pT])
 - ST slope – the slope of the linear regression line fit to the interval from 20 to 60ms after J point of MCG time run (for healthy man normal values depend on gender and age, for instance for men below 40 years old ST slope should be within range of 16 ± 7 [pT s⁻¹])
 - T wave amplitude – value of the MCG signal at the peak of the T wave (for healthy man normal values depend on gender and age, for instance for healthy men below 40 years old T wave amplitude should be within range of 12 ± 6 [pT])
 - ST-T integral – integrated MCG signal from the J point to the T wave offset (for healthy man normal values depend

on gender and age, for instance for men below 40 years old ST-T integral should be within range of 1170 ± 520 [fT s])

5. Diagnostic applications of MCG

Myocardial Ischemia

One of the most important MCG applications is detection of the Ischemic Heart Diseases (IHD) [4]. Alterations in electrophysiology of the heart that were caused by ischemic disease are often not visible on ECG, thus in order to confirm suspicion of ischemic disease exercise ECG is performed and when it's inconclusive, patient has to be exposed to more invasive tests such as stress-echocardiography or coronary angiography. Therefore MCG non-invasiveness in combination with its high accuracy in diagnosing IHD is one of its greatest advantages.

Similarly to ECG, MCG examination can be preceded by exposing patient to physical or pharmacological stress. In researches carried out so far, both specially designed nonmagnetic ergometers [10] as well as standard ergometers used for exercise ECG [7] were utilized. The exact listing of MCG studies, performed with and without stress, can be found in [12].

Localization of pre-excitation and different sources in the heart

MCG examination enables localization of the accessory pathways which trigger pre-excitation [12], for instance in patients with Wolff-Parkinson-White syndrome [14]. Other similar applications include localization of tachycardia points of origin [19] or localization of premature ectopic complexes [20]. It is also possible to perform three-dimensional localization of amagnetic tip of pacing catheter [15, 21].

Arrhythmia risk stratification

MCG allows to estimate the risk of life-threatening arrhythmia occurrences in patients who in the past suffered from myocardial infarction [12, 4]. Assessment of the risk of sudden death caused by arrhythmia is based on the detection of possible discontinuities in activation of the heart muscle during ventricular depolarization, abnormal inhomogeneity of VR or abnormal heart rate variability. This assessment can be based on analysis of the late fields of MCG map series [22, 23] as well as on magnetocardiographic intra-QRS fragmentation [24] or QT dispersion [25].

Detection of LV hypertrophy

MCG allows to identify patients suffering from left ventricle hypertrophy (LV hypertrophy) [26] as well as to estimate the progression of the disease [27].

Assessment of the fetus heart beat rhythm

MCG examination enables monitoring of the fetus cardiac activity even in the last weeks of the pregnancy. The quality of the registered signal is good enough to capture parameters such as AV conduction, repolarization period or morphological

parameters of the QRS complex [13, 28, 29]. It is also possible to examine fetus in order to detect QT prolongation [30].

Latest applications of MCG that can be found in the literature [4, 18]:

- monitoring of the graft reaction after heart transplantation
- early diagnosis of arrhythmogenic right ventricular dysplasia
- detection of acute myocarditis
- assessment of the risk in patients with Brugada-like ECG patterns
- monitoring of the cardiac activity in animals subject to new drugs testing
- reconstruction of the patient's heart anatomy basing on analysis of 3D map of current density

6. MCG and ECG comparison

Regardless of the fact that the source generating ECG and MCG signals consists of the same currents flowing through the heart, information content carried by both examinations is not identical – moreover, comparison of the value of those information is favorable for MCG examination.

MCG examination is more sensitive in detection of magnetic field generated by tangential currents than ECG is in detection of electrical field generated by the same currents [6, 9, 12]. Furthermore, vortex currents generate magnetic field detected by MCG, but they are not the source of any electrical field that could be detected by ECG. Those features make MCG more suitable for detection of the diseases that are caused by alteration of the direction of the electrical currents flowing through the heart. Since in healthy heart main direction of the activation wavefront is radial, from endocardium to epicardium, then MCG enables more precise detection of the ischemic changes in direction of depolarization and repolarization than ECG does.

It is worth to mention that MCG especially sensitively responds to intra – and extra – cellular currents whereas ECG electrodes placed on patient's thorax measure the difference in the potentials caused by secondary (volume) currents flowing right beneath the skin. This difference is substantial in attempts to measure cardiac activity of the fetus in last weeks of the pregnancy, and was the source of the thrive of fMCG (fetal MCG) which is an examination dedicated to measuring the intensity of the magnetic field generated by fetal heart.

The important advantage of MCG examination is, as previously mentioned, its noninvasiveness. In course of the examination patient's skin remains not only intact but there is also no physical contact between patient's skin and sensors. This can be considered serious ascendance over ECG since it eliminates all problems related to interferences caused by skin-electrode contact. Moreover, thanks to noninvasiveness, MCG can be performed on hyperexcitable patients, allowing to monitor the risk of sudden cardiac death in patients with Rett syndrome [11] or other patients that are hard to enter into communication. Lack of necessity to undress patient or place electrodes on patient's skin shortens the time needed for performing examination. In conjunction with decreased susceptibility to movement artifacts it allows to apply MCG in monitoring of

cardiac activity of small animals in tests of new drug influence on heart – ECG application required animal sedation, therefore introducing additional influence on animal's cardiac activity [18].

In contrary to ECG, configuration of MCG sensors is permanent and is not modified between consecutive examinations. It allows to obtain high level of reproducibility, which is of great significance in case of therapy performed after restenosis or transplantation or in different kinds of clinical tests [8].

Distinction between types of the injury currents is another area of MCG application. Difference between potentials of the ischemic and normal cells at the rest state cause the flow of diastolic injury current, whereas the difference in action potentials between ischemic and normal cells cause the flow of systolic injury current. ECG examination, in course of skin interference filtration filters TQ base line, thus it cannot detect its displacement. As a result, ECG is unable to differentiate between ST segment displacement caused by systolic injury current and the one caused by diastolic injury current. Unlike ECG, MCG can register TQ base line displacement, thus it allows to differentiate between those two types of injury currents [12].

Apart from all of the above advantages, MCG examination does have some weaknesses. The greatest ascendance of ECG over MCG is the existence of numerous publications describing application and clinical suitability of ECG – there is still not enough of literature serving the same purpose for MCG. Even though the number of such publications is increasing, there is still a lack of researches conducted on large group of patients, which could grant for MCG full acceptance of medical profession. Nevertheless, it seems that emergence of such publications is only a matter of time.

7. Experimental database

Available research material in form of MCG data records was acquired in course of diagnostic examinations performed in The John Paul II Hospital in Krakow, with the use of CMI 2409 magnetocardiograph, CardioMag Imaging Inc. Examinations were performed on patients already diagnosed with other techniques and remaining under constant medical consultancy. Database contains results of 466 examinations of which 415 include commentary about patient's health state at the moment of the examination. Following groups can be distinguished:

- patients without a cardiac infarction
- patients without a cardiac infarction but with hypertension
- patients with a cardiac infarction
- patients with a cardiac infarction and hypertension
- ablation patients
- patients after angioplasty

Among available data, four groups were chosen and additionally sorted according to gender and age. Following table presents details of MCG examination data set.

8. The course of planned research

The most common way to analyze diagnostic capabilities of magnetocardiography involves the usage of MCG time runs and computing morphological parameters that base on similarities between MCG and ECG signals. The other way is to attempt to directly utilize MF map sequences.

Instead of using well known parameters, like the alteration in the direction of the magnetic induction vector, it could be interesting to find and use different ones, more related to the flow

Table 1. MCG examination data set

Gender	20-29 years	30-39 years	40-49 years	50-59 years	60-69 years	70-79 years	80-89 years
PATIENTS WITH A CARDIAC INFARCTION							
Women	0	1	0	2	1	1	0
Men	0	0	5	5	5	4	0
PATIENTS WITH A CARDIAC INFARCTION AND HYPERTENSION							
Women	0	2	0	6	3	3	1
Men	0	3	5	15	10	2	0
PATIENTS WITHOUT A CARDIAC INFARCTION							
Women	0	0	10	55	10	3	0
Men	1	1	19	23	7	4	0
PATIENTS WITHOUT A CARDIAC INFARCTION BUT WITH HYPERTENSION							
Women	0	1	8	50	23	11	1
Men	0	1	13	35	14	0	0

of electrical impulses in the heart. For instance, one could try to establish whether it is possible to find on MF or PCD maps trajectories of points with the largest amplitude, which would be characteristic for each of the described test groups. Finding such trajectories on PCD maps would be especially interesting since following points with the largest field intensity values corresponds with monitoring the direction of activation wavefront. The attempt to find and analyze new set of parameters computed based on MF or PCD maps will be the direction of author's research, whereas the main goal will be to develop new methods of medical images interpretation (MF and PCD maps) in the way that could support diagnostics of the chosen heart diseases (infarctions and arterial hypertension).

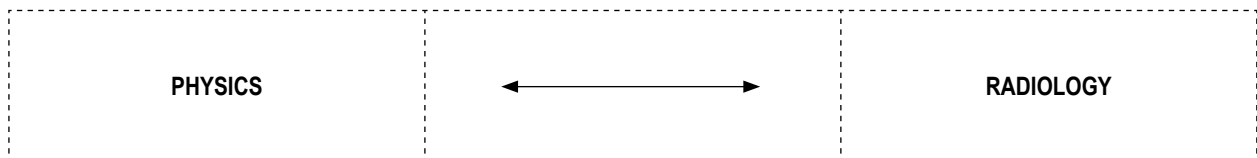
9. Conclusion

This paper describes chosen aspects of new, noninvasive method of heart diseases diagnostics – magnetocardiography. In recent years MCG started to play role of support tool for other diagnostic techniques that are more established in medical profession. Fast technological development suggests that it will gain more importance. MCG data visualized in form of magnetic field map or pseudo-current density map allow to diagnose diseases that could be missed by ECG, moreover non-invasiveness of MCG enables it to be used in situations where ECG could not be used. Indisputably MCG is a promising technique, but rapid development of medical devices was not followed by as dynamical development of computer methods of data analysis. Therefore the main goal of author's research will be to develop new algorithms supporting interpretation of MCG data that could in future assist in advancement of CAD and PACS systems.

Literature

- Makela T., Pham Q. C., Clarysse P.: A 3-D model-based registration approach for the PET, MR and MCG cardiac data fusion. *Medical Image Analysis* 7: 377-389, 2003.
- Chen J., Thomson P., Nolan V.: Age and sex dependent variations in the normal magnetocardiogram compared with changes associated with ischemia. *Annals of Biomedical Engineering*, Vol. 32, No. 8: 1088-1099, August 2004.
- Fenici R., Brisinda D., Nenonen J.: Bedside Multichannel Magnetocardiography in Clinical Practice. *Biomag2002*, VDE Verlag GmbH: 568-570, 13th Int. Conf. on Biomagnetism, Jena 10.-14.8.2002. Berlin 2002.
- Fenici R., Brisinda D., Meloni A.: Clinical application of magnetocardiography. *Expert Review of Molecular Diagnostics*: 291-305, 2005.
- Fenici R., Brisinda D., Meloni A.: Clinical validation of machine learning for automatic analysis of multichannel magnetocardiography. *Lecture Notes on Computer Science*: 143-152, 2005.
- Hanninen H., Takala P., Makijarvi M.: Detection of exercise-induced myocardial ischemia by multichannel magnetocardiography in single vessel coronary artery disease. *A.N. E.* 5 (2): 147-157, 2000.
- Fenici R., Brisinda D., Meloni A.: First 36-channel Magnetocardiographic Study of CAD Patients in an Unshielded Laboratory for Interventional and Intensive Cardiac Care. *Lecture Notes in Computer Science*: 1009-1019, 2003.
- Koch H., Haberkorn W.: Magnetic field mapping of cardiac electrophysiological function. *Phil. Trans. R. Soc. Lond. A* 359: 1287-1298, 2001.
- Steinberg B., Roguin A., Watkins III S.: Magnetocardiogram recordings in a nonshielded environment – reproducibility and ischemia detection. *A. N. E.* 10(2): 152-160, 2005.
- Takala P., Hanninen H., Montonen J.: Magnetocardiographic and electrocardiographic exercise mapping in healthy subjects. *Annals of Biomedical Engineering*, Vol. 29: 501-509, 2001.
- Brisinda D., Meloni A., Hayek G.: Magnetocardiographic imaging of ventricular repolarization in Rett syndrome. *Lecture Notes on Computer Science*: 205-215, 2005.
- Hänninen H.: Multichannel Magnetocardiography And Body Surface Potential Mapping In Exercise-Induced Myocardial Ischemia. *Academic Dissertation*, Helsinki 2002.
- Brisinda D., Comani S., Meloni A.: Multichannel mapping of fetal magnetocardiogram in an unshielded hospital setting. *Prenatal Diagnosis*, Vol. 25: 376-382, 2005.
- Fenici R., Brisinda D., Nenonen J.: Noninvasive Study of Ventricular Preexcitation Using Multichannel Magnetocardiography. *PACE*, Vol. 26: 431-435, 2003.
- Fenici R., Brisinda D., Nenonen J.: Phantom validation of multichannel magnetocardiography source localization. *PACE*, Vol. 26: 426-430, 2003.
- Kosch O., Meindl P., Steinhoff U.: Physical aspects of cardiac magnetic fields and electric potentials. *Biomag 2000. Proceedings of the 12th International Conference on Biomagnetism*: 553-556, 2001.
- Haberkorn W., Steinhoff U., Burghoff M.: Pseudocurrent density maps of electrophysiological heart, nerve or brain function and their physical basis. *BioMagnetic Research and Technology* 4: 5, 2006.
- Koch H.: Recent advances in magnetocardiography. *Journal of Electrocardiology*, Vol. 37, Supplement: 117-122, 2004.
- Moshage W., Achenbach S., Gohl K.: Evaluation of the non-invasive localization accuracy of the cardiac arrhythmias attainable by multichannel magnetocardiography (MCG). *Int J Cardiac Imaging* 12: 47-59, 1996.
- Oeff M., Burghoff M.: Magnetocardiographic localization of the origin of ventricular ectopic beats. *Pacing Clin Electrophysiol* 17: 517-522, 1994.
- Pesola K., Nenonen J., Fenici R.: Bioelectromagnetic localization of a pacing catheter in the heart. *Phys Med Biol* 44: 2565-2578, 1999.
- Mäkijärvi M., Montonen J., Toivonen L.: Identification of patients with ventricular tachycardia after myocardial infarction by high-resolution magnetocardiography and electrocardiography. *J Electrocardiol* 26: 117-124, 1993.
- Korhonen P., Montonen J., Mäkijärvi M.: Late fields of the magnetocardiographic QRS complex as indicators of propensity to sustained ventricular tachycardia after myocardial infarction. *J Cardiovasc Electrophysiol* 11: 413-420, 2000.
- Korhonen P., Montonen J., Endt P.: Magnetocardiographic intra-QRS fragmentation analysis in the identification of patients with sustained ventricular tachycardia after myocardial

- dial infarction. *Pacing Clin Electrophysiol* 24: 1179-1186, 2001.
25. Oikarinen L., Viitasalo M., Korhonen P.: Postmyocardial infarction patients susceptible to ventricular tachycardia show increased T wave dispersion independent of delayed ventricular conduction. *J Cardiovasc Electrophysiol* 12: 1115-1120, 2001.
 26. Fujino K., Sumi M., Saito K.: Magnetocardiograms of patients with left ventricular overloading recorded with a second-derivative SQUID gradiometer. *J Electrocardiol* 17: 219-228, 1984.
 27. Karvonen M., Oikarinen L., Takala P.: Magnetocardiographic indices of left ventricular hypertrophy. *Journal of Hypertension*, Vol. 20, No. 11: 2285-2292, 2002.
 28. Van Leeuwen P., Hailer B., Bader W.: Magnetocardiography in the diagnosis of fetal arrhythmia. *Br J Obstet Gynaecol* 106: 1200-1208, 1999.
 29. Menéndez T., Achenbach S., Beinder E.: Usefulness of magnetocardiography for the investigation of fetal arrhythmias. *Am J Cardiol* 88: 334-336, 2001.
 30. Menéndez T., Achenbach S., Hofbeck M.: Prenatal diagnosis of QT prolongation by magnetocardiography. *Pacing Clin Electrophysiol* 23: 1305-1307, 2000.



AN ALGORITHM FOR DETECTING LESIONS IN CBF AND CBV PERFUSION MAPS

TOMASZ HACHAJ

*Chair of Automatics
AGH University of Science and Technology, Mickiewicza 30, 30-059 Krakow*

Abstract: This paper presents an algorithm that enables detection of lesions in CBF and CBV perfusion maps. There are two steps of the algorithm: at the first step the algorithm detects symmetry axis of an image (between left and right hemisphere), in the second stage the level of asymmetry in cerebral blood flow and cerebral blood volume is measured by detection of regions with different perfusion in both brain hemispheres. Test of the algorithm were performed on a set of 56 different CBF and CBV images showing or not cerebral blood flow and volume anomalies. The paper also describes the method for estimating cerebral blood flow with a non diffusing contrast agent based on the Meier – Zierler convolution model as well as CBF, CBV, MTT and TTP perfusion maps.

Key words: dynamic CT perfusion, perfusion maps, CBF, CBV, lesions detection, symmetry detection, Meier – Zierler convolution model

Introduction

Brain perfusion imaging becomes more and more popular in head injuries, epilepsy, brain vascular disease and especially in stroke diagnosing ([7], [13], [15], [16], [18], [19], [24]). Dynamic CT / MR perfusion treatment is a modern and broadly used neuroradiology technique that enables to evaluate total and regional blood flows in time unit. P-CT treatment enables recognition of structural changes of ischemia and shows the difference between ischemic stroke and hemorrhagic stroke. In the high – industrial countries of Western Europe brain stroke is the third – due to its frequency – reason of death (just after heart attack and cancer) and the most frequent cause of death in elderly age ([10]). There are different methods of treatment of ischemic and hemorrhagic stroke and there is a short period of time when treatment can be used, so it is important to early find the cause of illness. Analyzing the perfusion maps can do it.

There are few algorithms for detecting lesions on CT images (i.e. e. [5]) but there are no common methods for analyzing series of dynamic perfusion images like brain perfusion maps. Commercial software for perfusion imaging that is broadly used in hospitals (i.e. Syngo Neuro Perfusion CT by Siemens) doesn't contain a mechanism that enables automatic detection of perfusion anomalies that can be seen on that kind of maps. This paper presents a method designed by the author which enables detection of potential lesions that can be visualized

of cerebral blood flow (CBF) and cerebral blood volume maps (CBV). Despite the fact that the norm for each of the perfusion parameter has been computed, the diagnosis is based on comparison of relative values of symmetric regions of interest (ROI) of blood perfusion between left and right hemisphere. ([7]).

The algorithm presented in the following paper is mainly based on mathematical morphology which is commonly used as reliable tool for image analysis ([1]). Mathematical morphology is successfully used not only in medical image analysis but also in materials engineering ([2]) and on many other fields of science ([3]). The algorithm derived by the author has been implemented in Matlab environment with using Imaging processing toolbox ([25]) package and mathematical libraries ([26]). The test set for the algorithm consisted of 28 CBF perfusion images and 28 CBV perfusion images that are results of researches on 8 patients. Maps were generated with Syngo Neuro Perfusion CT software by Siemens ([23]).

2. The Meier – Zierler model

There are four types of basic perfusion maps: cerebral blood flow perfusion map (CBF), cerebral blood volume (CBV), mean time transit (MTT) and time to peak (TTP). In order to generate dynamic CT / MR perfusion maps the Paul Meier and Kenneth

L. Zierler model is commonly used ([7]). In this radiology treatment the contrasting material is injected in to the cardiovascular system relatively quickly (impulse injection). CT scanner measures the contrast material that remains in the capillary network. As a result the time density curve (TDC, also time intensity curve TIC) for brain arteries and tissues is obtained. In Meier – Zierler model the impulse residue function (IRF, $R(t)$) is also defined. This function indicates the amount of contrast in the brain tissues as the function of time. The value of pixels in TTP perfusion map is measured as maximal value of TDC curves. This map doesn't need any further calculation. It is not possible to calculate $R(t)$ directly, because there is no possibility to identify in non – invasion way the arteries that transmit blood to separate regions of the brain. Instead of that contrast material is injected that remains in the capillary network and can be measured by CT scanner (the mass of the contrast in tissues $Q(t)$). If the blood flow is constant and contrast enhancement is linear dependent to contrast concentration the Meier – Zierler model can be used:

$$Q(t) = CBF \cdot [C_A(t) \otimes R(t)] \quad (1)$$

Where $Q(t)$ and $C_A(t)$ are the contrast enhancement of brain tissues and arteries (values can be obtained from CT / MR scans), \otimes is a convolution operator. According to Axel [12] blood volume that flows through capillary network (CBV) can be obtained as:

$$CBV = \frac{\int_0^{\infty} Q(t) dt}{\int_0^{\infty} C_A(t) dt} \quad (2)$$

If impulse residuum function ($R(t)$) is known one can calculate MTT as follows:

$$MTT = \frac{\int_0^{\infty} R(t) dt}{R_{\max}} \quad (3)$$

Where R_{\max} is the maximal value of $R(t)$ curves. Cerebral blood flow (CBF):

$$CBF = \frac{CBV}{MTT} = \frac{R_{\max} \cdot \int_0^{\infty} Q(t) dt}{\int_0^{\infty} R(t) dt \cdot \int_0^{\infty} C_A(t) dt} \quad (4)$$

Concentration of contrast in tissues $Q(t)$ is correlated with concentration of contrast in arteries $C_A(t)$ and impulse residuum function $R(t)$ as it states in equation (1) so $R(t)$ can be calculated as a product of deconvolution. The most common way of solving that problem is to change it into the matrix equation and after it solves it with singular value decomposition method (SVD) ([13], [14], [20], [21], [22]).

The values obtained this way are used for construction proper perfusion maps (separate map for TTP, CBF, CBV and

MTT). Each pixel corresponds to the value of perfusion map in the given point. Usually a map has a resolution of 512 x 512 pixels in the gray scale (because of DICOM format there can be more than 256 gray shades). The symbols used in the following algorithm are presented in Table 1.

Table 1. Notation used in the description of the algorithms (based on notation from [1]).

Notation in algorithm	Description
$A := B$	Assignment A to B.
I	The binary image.
$I(x, y)$	Value (color) of pixel of binary image with coordinates (x, y) .
i	Gray shades image.
$i(x, y)$	Value of pixel of gray shades with coordinates (x, y) .
a	Asymmetry map (CBF / CBV).
$a(x, y)$	Value of pixel of asymmetry map with coordinates (x, y) .
Floor	Returns the largest integral value that is not greater than number given.
Fill	„Filling the holes” in the binary image.
Label	Labels all the components in the binary image.
Bin_X	Binarization with bottom threshold X.
$I \ominus E_X$	Erosion with semi – circular structural element with diameter X.
$I \oplus E_X$	Dilation with semi – circular structural element with diameter X.
$I \circ E_X$	Opening with semi – circular structural element with diameter X.
$I \bullet E_X$	Closing with semi – circular structural element with diameter X.
$Med_{Y \times Y}$	Median filter sized YxY.
$A \cap B$	Logical multiplication of images A and B.
$A \cup B$	Logical sum of image.
\bar{I}	Mirror image of image I towards vertical symmetry axis.

3. Detecting the symmetry axis on CBF and CBV images

In order to do further perfusion image analysis it is necessary to find lines that separate left brain hemisphere from right (in the following text it is called "symmetry axis"). In many CBF and CBV image the head of the patient is slightly rotated on small angle towards bed of tomograph (the symmetry axis isn't orthogonal towards OX axis). The symmetry axis of the image isn't always the same line that separates the brain hemispheres, what makes problem more complicated. In commercial software the symmetry axis selection is made manually (i.e. [23]). It is difficult to propose the certain algorithm for automatic determination of symmetry axis because CT scans are made in many different plains and because of that any assumption about the shape of the image cannot be stated. Those facts also obstruct the structural-based image analysis algorithms (algorithms of that kind often find good solutions in medical images describing [4]).

The author's method of symmetry axis detection for CBF and CBV maps is based on basic observation: "For a uniform body it's center of mass is also its center of volume [6]. If a body has got a symmetry axis, that symmetry axis come through the center of volume, so for a uniform body the center of mass lays on a symmetry axis if fit exists. So assuming uniformity and symmetry of a body we can determine the symmetry axis finding its center of volume. The algorithm of symmetry axis derivation comes as follow:

- Find the square window in the area of image (ROI) in which pixels corresponding to brain are located:

$$\begin{aligned} x_{\min} &= \min_x : I(x, y) > 0 \\ x_{\max} &= \max_x : I(x, y) > 0 \\ y_{\min} &= \min_y : I(x, y) > 0 \\ y_{\max} &= \max_y : I(x, y) > 0 \end{aligned} \quad (5)$$

- Compute number of rows of ROI ($y_{\max} - y_{\min}$), separate the ROI on identical number of horizontal "slices" of the same width as basic ROI (best results very obtained for 20 regions). For each of the regions compute coordinates of the center of mass as follows:

$$\begin{aligned} x_m &= \frac{\int \rho \cdot x \cdot dV}{m} \\ y_m &= \frac{\int \rho \cdot y \cdot dV}{m} \end{aligned} \quad (6)$$

Where:

$$\rho = \begin{cases} 0 & \text{ gdy } I(x, y) = 0 \\ 1 & \text{ gdy } I(x, y) > 0 \end{cases}$$

White circles on Fig 1.a mark centers of mass of the example image.

- Centers of mass obtained in the previous step were used for calculation of the symmetry axis of the figure. The angular coefficient and the translation coefficient were both estimated with least square method. In order to improve

detection of symmetry axis several first and last centers of mass should be omitted (empirically tested, that it should be 3 first and 3 last centers). This is because the irregularity of borders of brain image of CBF and CBV maps. The symmetry axis found by the algorithm is marked on Fig 1 by the white straight line. The improvement in the final calculation of symmetry axis can be obtained by performing on each of the "stripes" of image morphological closing with structural semi-circular element with relatively large size (best results was for 25 pixels diameter).

The image is rotated around point that lays in the arithmetical center of mass of brain so that the symmetry axis is now orthogonal to OX axis. The constant point of the rotation is calculated as:

$$\begin{aligned} x_c &= \frac{x_2 + x_1}{2} \\ y_c &= \frac{y_2 + y_1}{2} \end{aligned} \quad (7)$$

Points (x_1, y_1) and (x_2, y_2) on Fig 1.a are the first (when looking from the top of the picture) and the last points that is common for the symmetry axis and the image of the brain.

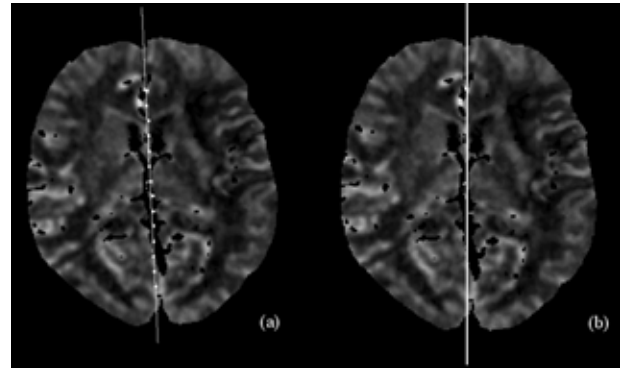


Fig 1. (a) A CBF image with centers of mass marked (white circles). A white line towards them is a potential symmetry axis of the brain (the line was approximated with least square method). (b) The same image after rotating the image around arithmetical center of brain. Potential symmetry axis (white line) is now orthogonal to OX axis.

4. The algorithm for lesions detection in CBF and CBV perfusion maps

The same algorithm for detection potential lesions (asymmetries with the sufficient size) was used for processing both kinds of maps. The values of the factors used as the parameters in the algorithm were empirically determined. The algorithm goes as follows:

- Loading the image from the DICOM file. In order to make analysis of the algorithm easier each image was colored with color palette that can be seen on Fig 2. Black color corresponds to smallest values of CBF / CBV, red color corresponds to the highest ones.

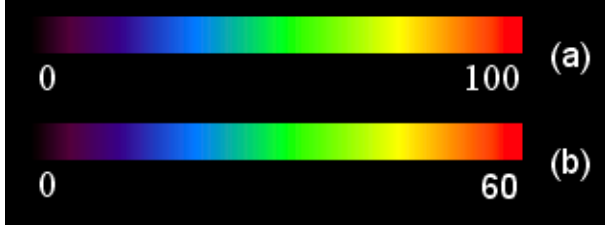


Fig 2. Color palates that were used for coloring the CBF (a) and CBV (b) perfusion maps.

- Detection of the symmetry axis with this algorithm that was described in paragraph 3. The image is also rotated around constant point calculated according to equation (7). After that operation the symmetry axis should be orthogonal to OX axis.
- Reduction of number of colors (gray shades) on CBF and CBV map. Reduction is necessary because it improves results of median filtration (see (d)). After this operation the homogeneous areas on both sides of brain map are obtained.

$$i(x, y) := \begin{cases} 0 & \text{when } i(x, y) \geq 0, \quad i(x, y) < 15 \\ 1 & \text{when } i(x, y) \geq 15, \quad i(x, y) < 30 \\ 2 & \text{when } i(x, y) \geq 30, \quad i(x, y) < 45 \\ & \dots \end{cases}$$

In another words:

$$i(x, y) := \text{Floor}((i(x, y) / 15) * 15)$$

- Median filtration with the window size of 15x15 pixels. Median average filter doesn't generate new values of pixels, thanks to that homogeneous areas on both sides of brain map are obtained. The result image lacks some details (the presence of them would make further analysis of image harder because they generate large number of asymmetry regions). If there are too much small asymmetry regions the proper classification turns to be impossible.

$$i := \text{Med}_{15 \times 15}(i)$$

- Compare the left and the right sides of the image. As the result the asymmetry map is obtained. The asymmetry map generation goes as follows:

For each pixel on $i(x, y)$ that belongs to the left part of the image, check $i(x, y) > 0$ or for the symmetrical pixel towards symmetry axis detected in (b)) $\bar{i}(x, y) > 0$.

If $i(x, y) = 0$ and $\bar{i}(x, y) = 0$, the background of the image is found.

In the other case one of the following condition is satisfied:

If $i(x, y) > 0$ and $\bar{i}(x, y) = 0$ or $i(x, y) = 0$ and $\bar{i}(x, y) > 0$ then one of the pixels belongs to the brain region and the other can belong to the background (if the symmetry axis wasn't set properly, the region of CBF / CBV map is asymmetric) or both of pixels belong to the brain region, but in one of the cases CBF / CBV value is very small.

If $i(x, y) > 0$ and $\bar{i}(x, y) > 0$ both regions belong to the brain.

Relative asymmetry of regions is computed:

If $i(x, y) > \bar{i}(x, y)$

$$a(x, y) := \text{Floor}\left(10 \cdot \left(\frac{i(x, y)}{\bar{i}(x, y)}\right)\right)$$

In other cases:

$$a(x, y) := \text{Floor}\left(10 \cdot \left(\frac{\bar{i}(x, y)}{i(x, y)}\right)\right)$$

If one of the pixels $i(x, y)$ or $\bar{i}(x, y)$ has 0 value then 1 is assigned.

- Detection of potential asymmetry. The binarization with bottom threshold 60 is performed.

$$A := \text{Bin}_{60}(a)$$

- The symmetry axis obtained in (b) does not necessarily separate brain into symmetry regions. On the asymmetry map A the order of the brain region can be detected as potential asymmetry. In order to eliminate this effect the binary mask of "potentially biggest brain region" P is created. The mask is the same size as mask A and it is consisted of pixels for which $i(x, y) > 0$ or $\bar{i}(x, y) > 0$. All the "holes" in the interior region of map are removed. The border of the mask is also removed by morphological opening with semi-circular structural element of diameter 5.

$$P(x, y) := \text{Bin}_1(i \cup \bar{i})$$

$$P := \text{Fill}(P)$$

$$P := P \ominus E_5$$

- Calculation of logical multiplication of the asymmetry mask A and the brain mask P.

$$A := A \cap P$$

- Elimination of narrow links between regions. Morphological opening with semi-circular structural element of diameter 3 performs that operation.

$$A := A \circ E_3$$

- The last step of the algorithm is eliminating all the small regions. Performing morphological erosion of semi-circular structural element of diameter 10 accomplishes this level. On the result image there are only regions that contain some pixels that „survived“ the above operation.

$$l := \text{Label}(A)$$

$$A' := A \ominus E_{10}$$

If $A'(x, y) > 0$ add the whole region with label $l(x, y)$ to the result image A.

- The asymmetry map A is combined with CBF / CBV map (from point (b) of this algorithm). On the left side of the image region with fractional decreasing of CBF / CBV can be seen (the left side of the patient is on the right side of the image).

The results of above algorithm is presented step by step on Fig 3 for CBV map (in case of CBF maps results are similar). Fig 4 shows four pairs of CBF / CBV perfusion maps and the same pairs (after processing them by the algorithm) with lesions marked.

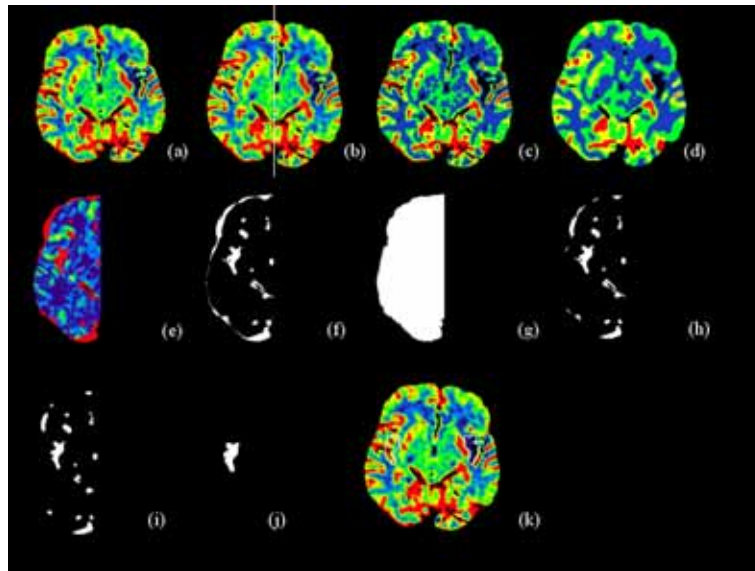


Fig 3. The steps of asymmetry – detection algorithm in CBV maps. This figure is described in the text.

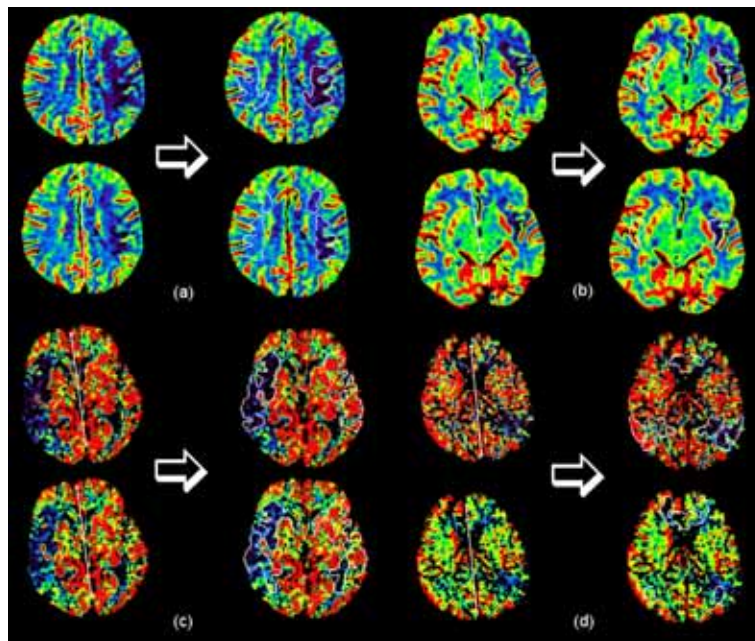


Fig 4. Four pairs of CBF (top left) and CBV (bottom left) perfusion maps. Right from the arrow the same pair after processing it by the algorithm. Detected borders of potential lesions regions are marked with white line. Description of the images: (a), (b) CBF and CBV is slightly decreased on the left on the level of the top sides of lateral ventricle frontally and parietally (c) CBF and CBV is decreased in the region of right middle cerebral artery, brain stroke was diagnosed (d) CBF and CBV is slightly decreased on the left on the level of the top sides of lateral ventricle frontally, parietally and temporally.

Results and discussion

The algorithm for detection asymmetry on perfusion maps has been tested on 28 CBF and 28 CBV perfusion maps from 8 different patients. That test set consisted of 24 cases where abnormal perfusion was diagnosed. The symmetry axis was rightly detected in 42 cases (21 for CBF and 21 CBV maps, because CBF and corresponding to it CBV map have identical

pixels positions). In other cases deviation wasn't greater than 5 degrees from proper symmetry axis. In three cases for CBF maps and four cases for CBV maps improper symmetry axis causes overestimation of asymmetry regions (Fig 4.d, the improper region can be seen in the central part of the brain near confluence of the sinuses [8], [9]). The errors of that kind could be caused by insufficient symmetry of the binary mask applied on the brain. There are two reasons of this: asymmetry of CBF

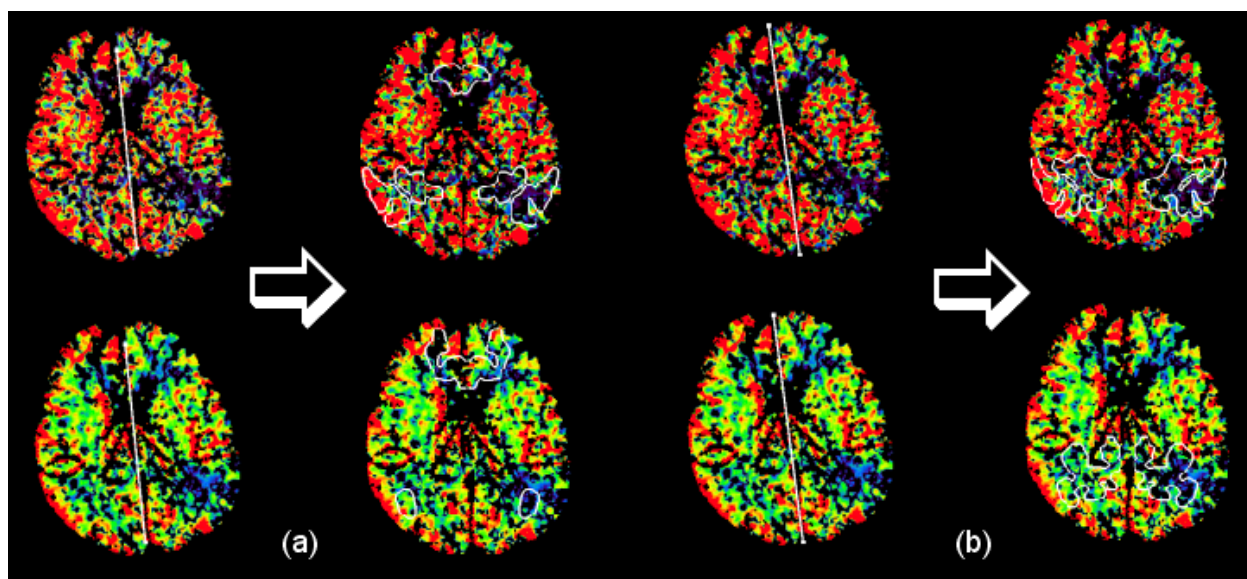


Fig 5. The accuracy improvement of algorithm after manually choosing symmetry axis that can be seen in some cases (more details in paragraph 5). Pair of CBF / CBV asymmetry map with detected borders of potential lesions regions marked with white line (the same case as in Fig 4.d)). (a) Symmetry axis was detected automatically (overestimation of asymmetry regions), (b) After setting symmetry axis manually overestimated region disappeared.

/ CBV perfusion maps (lack or very small perfusion in some regions) or natural brain asymmetry.

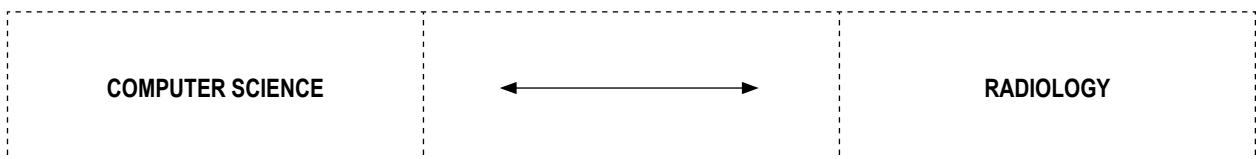
The detection of asymmetry was tested on the same set of images. All of the maps that don't have diagnosed asymmetry were rightly classified (no asymmetry detected). On one of the images of CBF that consisted lesions no changes were detected (on the level of the top sides of lateral ventricle in the left hemisphere; in medical documentation lesions was described as fractional). On three CBF and CBV maps small excessive regions of asymmetry were detected that were situated close to automatically detected symmetry axis (for this maps symmetry axis wasn't rightly detected and it was slightly rotated towards the true axis that separate brain hemispheres). In one case in CBV map algorithm detected a large asymmetry region (it was enlarged by region near automatically detected symmetry axis).

The algorithm presented in this publication has achieved satisfactory results. 85,7% maps were properly diagnosed (85,7% for CBF and 85,7% CBV). 75% errors in CBF maps and 100% errors in CBV maps were caused by over – detection of asymmetry regions. Errors were eliminated in cases when symmetry axis was manually selected (Fig 5). After that 96,4% CBF maps and 100% CBV maps were rightly diagnosed. In order to eliminate that kind of errors new algorithm for symmetry axis detection should be developed. Only in one case for CBF maps fractional lesions were not detected (that is 3,6% of error diagnosis for population of CBF maps and 1,8 for population of all map that was tested). Important remark is that the same algorithm can produce proper asymmetry maps for both CBF and CBV perfusion maps. Further researches by the author will be directed on improving the algorithm shown, adapting it to other perfusion maps (TTP and MTT) and proposing methods for automatic creation of diagnosis prognoses based on information derived by the detection algorithms.

References:

- [1] John Goutsias, Sinan Batman, *Morphological Methods for Biomedical Image Analysis, Medical Imaging, Volume 2. Medical Image Processing and Analysis*, Washington USA, 2000
- [2] Krzysztof J. Kurzydłowski, Leszek Wonjnar, Janusz Szala, *Praktyka analizy obrazu, Polskie Towarzystwo Stereologiczne*, Kraków 2002
- [3] Zygmunt Wróbel, Robert Koprowski, *Praktyka przetwarzania obrazów w programie Matlab, Akademicka Oficyna Wydawnicza Exit*, Warszawa 2004
- [4] Marek R. Ogiela, *Strukturalne metody rozpoznawania obrazów w kognitywnej analizie obrazów medycznych*, Uczelniane Wydawnictwa Naukowo-Dydaktyczne, Kraków 2004
- [5] Adam Sędziwy, *Automatyczne wykrywanie i analiza zmian patologicznych w obrazach MR i CT struktur mózgowych*, rozprawa doktorska, Kraków 2003
- [6] *Encyklopedia fizyki*, PWN, Warszawa 1972
- [7] Jerzy Walecki, Tomasz Bułski, Katarzyna Sklinda, *Choroby naczyniopochodne ośrodkowego układu nerwowego, Postępy neuroradiologii*, Warszawa 2007, 472-512
- [8] Jolanta Sikorska, Katarzyna Sklinda, Tomasz Ochrynik, *Anatomia radiologiczna OUN, Postępy neuroradiologii*, Warszawa 2007, 151-166
- [9] Jerzy Gielecki, Anna Żurada, Grzegorz Gajda, Wiesław Cybulski, *Ośrodkowy i obwodowy układ nerwowy*, Górnicki Wydawnictwo Medyczne 2008, CD-R
- [10] Hans – Christopher Diener, Michael Forsting, *Udar mózgu. Podręczny atlas*, Wydawnictwo Medyczne, Wrocław 2004
- [11] K.L. Zierler, *Equations for measuring blood flow by external monitoring of radioisotopes*, *Circ Res* 1965; 16: 309-21

- [12] L. Axel, Cerebral blood flow determination by rapid-sequence computed tomography: a theoretical analysis, *Radiology* 1980; 137: 679-686
- [13] Makoto Sasaki, Kohsuke Kudo, Hirobumi Oikawa, CT perfusion for acute stroke: Current concepts on technical aspects and clinical applications, *International Congress Series* 1290 (2006), 30-36
- [14] R. Wirestam, E. Ryding, A. Lindgren, B. Geijer, S. Holtås, F. Ståhlberg, Absolute cerebral blood flow measured by dynamic susceptibility contrast MRI: a direct comparison with Xe-133 SPECT, *Magnetic Resonance Materials in Physics, Biology and Medicine* 11 (2000), 96-103
- [15] Michael H. Lev, Alan Z. Segal, Jeffery Farkas, Syeda T. Hossain, Christopher Putman, George J. Hunter, Ronald Budzik, Gordon J. Harris, Ferdinando S. Buonanno, Mustapha A. Ezzeddine, Yuchiao Chang, Walter J. Koroshetz, R. Gilberto Gonzalez, Lee H. Schwamm, Utility of perfusion-weighted CT imaging in acute middle cerebral artery stroke treated with intra-arterial thrombolysis: prediction of final infarct volume and clinical outcome, *Stroke* 32 (2001), 2021-2028
- [16] James D. Eastwood, Michael H. Lev, Tarek Azhari, Ting-Yim Lee, Daniel P. Barboriak, David M. Delong, Clemens Fitzek, Michael Herzau, Max Wintermark, Reto Meuli, David Brazier, James M. Provenzale, CT Perfusion Scanning with Deconvolution Analysis: Pilot Study in Patients with Acute Middle Cerebral Artery Stroke, *Radiology* 2002; 222: 227-236
- [17] Matthias Koenig, Michael Kraus, Carmen Theek, Ernst Klotz, Walter Gehlen, Lothar Heuser, Quantitative assessment of the ischemic brain by means of perfusion-related parameters derived from perfusion CT, *Stroke* 32 (2001), 431-437
- [18] Richard E. Latchaw, Howard Yonas, George J. Hunter, William T.C. Yuh, Toshihiro Ueda, A. Gregory Sorensen, Jeffrey L. Sunshine, Jose Biller, Lawrence Wechsler, Randall Higashida, George Hademenos, Guidelines and recommendations for perfusion imaging in cerebral ischemia, *Stroke* 34 (2003), 1084-1104
- [19] James D. Eastwood, Michael H. Lev, Max Wintermark, Clemens Fitzek, Daniel P. Barboriak, David M. Delong, Ting-Yim Lee, Tarek Azhari, Michael Herzau, Vani R. Chilukuri, James M. Provenzale, Correlation of early dynamic CT perfusion imaging with whole-brain MR diffusion and perfusion imaging in acute hemispheric stroke, *AJNR* 24 (2003), 1869-1875.
- [20] XingFeng Lia, Jie Tiana, EnZhong Lia, XiaoXiang Wanga, JianPing Daib, Lin Aib, Adaptive total linear least square method for quantification of mean transit time in brain perfusion MRI, *Medical Image Processing Group, Institute of Automation, Chinese Academy of Sciences, Beijing, China, Department of Radiology, Tian Tan Hospital, Beijing, China*. Received 27 September 2002; accepted 24 January 2003
- [21] H.-J. Witsack, A.M. Wohlschläger, E.K. Ritzl, R. Kleiser, M. Cohnena, R.J. Seitz, U. Mödder, CT-perfusion imaging of the human brain: Advanced deconvolution analysis using circulant singular value decomposition, *Computerized Medical Imaging and Graphics* 32 (2008), 67-77
- [22] T.S. Koh, C.K. Markus Tan, L.H. Dennis Cheong, C.C. Tchoyoson Limc, Cerebral perfusion mapping using a robust and efficient method for deconvolution analysis of dynamic contrast-enhanced images, *NeuroImage* 32 (2006), 643-653
- [23] Siemens AG, Clinical Applications. Application Guide. Software Version syngo CT 2007A, Siemens Medical, 06/2006
- [24] Kohsuke Kudo, Perfusion Mismatch Analyzer (PMA), Acute Stroke Imaging Standardization Group (Online only), <http://asist.umin.jp>
- [25] Matlab 6 – Imaging processing toolbox, User's Guide, The MathWorks, Inc., March 2008 (Online only), http://www.mathworks.com/access/helpdesk/help/pdf_doc/images/images_tb.pdf
- [26] Matlab 7 – Mathematics, The MathWorks, Inc., March 2008 (Online only), http://www.mathworks.com/access/helpdesk/help/pdf_doc/matlab/math.pdf



THE REGISTRATION AND ATLAS CONSTRUCTION OF NOISY BRAIN COMPUTER TOMOGRAPHY IMAGES BASED ON FREE FORM DEFORMATION TECHNIQUE

TOMASZ HACHAJ

*Chair of Automatics
AGH University of Science and Technology, Mickiewicza 30, 30-059 Krakow*

Abstract: This article presents the algorithm for nonlinear registration images of brain computer tomography. The registration process is performed by affine transformation optimized by Nelder – Mead simplex method and non-rigid free form deformation model based on B – splines. That algorithm is also used for creation of simple intensity driven deformable brain atlas that can be used for indexing different parts of patient's brain. Algorithm was tested on 28 CT images, with resolution 512 x 512 pixels, obtained for 8 different patients.

1. The registration of image

Registration is the process of finding a transformation T that best matches two images according to a criterion of similarity [7]. One image is the reference, which remains fixed during the registration process, while the other is deformed in the geometric space of the reference. The reference image is also called "fixed or target image" and the transformed image is called the "moving image". After registration of the image ("making it similar to other known images – so called cases") there is an opportunity to use it in system of automatic image understanding ([11], [12]) and describe them more successfully without registration. The researches described in this paper were performed on the set of brain computer tomography (CT) images. The main goal was to register that set of images in order to enable atlas-based description of image's content. Deformable brain atlases are adaptable brain templates that can be individualized to reflect the anatomy of new subjects ([9]). This allows an automated labeling of structures in new patients' scans. Nonlinear registration approaches are commonly classified into two major types, intensity-based and model-based, depending on the type of information that drives them. Model-driven algorithms first build explicit geometric models, representing separate, identifiable anatomic elements in each of the scans to be matched. Model-driven approaches contrast with intensity-driven approaches. Intensity driven approaches aim to match regional intensity patterns in each scan based on mathematical or statistical criteria. Typically, they

define a mathematical measure of intensity similarity between the deforming scan and the target. The second approach was adopted by the author because it does not require the segmentation or preprocessing of registered images.

Many brain images registration algorithms are developed and tested for magnetic resonance (MR) and require prior segmentation of the image ([20], [21], [22]). There are some cases when there are only brain CT images (i.e. during dynamic brain perfusion CT ([13], [14])) that can be used for proper diagnosis statement. Dynamic brain perfusion CT generates set of blood perfusion maps where due to detecting asymmetries important brain lesions can be detected ([15]). It is important to find the size of this lesions and to describe their position in the image. As perfusion maps are product of set of CT scans there is a possibility to use one of these CT scans (often the first or one of the first images where the injected contrast agent is still not visible) as the "fixed or target image" and the brain atlas image as "moving image". After a registration a brain atlas image on the new CT scan the map describing the individual parts of brain is created.

Global spatial transformation

One of the simplest methods of registration images is affine transformation ([19]). The affine transformation captures only the global motion of the image.

The basic affine transformation in R^3 is:

$$\begin{bmatrix} x' \\ y' \\ z' \end{bmatrix} = A \cdot \begin{bmatrix} x \\ y \\ z \end{bmatrix} + \bar{b} \quad (2.1)$$

Where:

$$A = \begin{bmatrix} a_{11} & a_{12} & a_{13} \\ a_{21} & a_{22} & a_{23} \\ a_{31} & a_{32} & a_{33} \end{bmatrix}, \bar{b} = \begin{bmatrix} b_1 \\ b_2 \\ b_3 \end{bmatrix} \quad (2.2)$$

If $\bar{b} = \bar{0}$ we simply get the equation of linear transformation.

Several common spatial transformations applied to images can be expressed in terms of an affine equation. In R^2 the matrix responsible for scaling will be:

$$A_s = \begin{bmatrix} s_{11} & 0 \\ 0 & s_{22} \end{bmatrix}, \bar{b} = \bar{0} \quad (2.3)$$

$$x' = s_{11} \cdot x$$

$$y' = s_{22} \cdot y$$

Rotation:

$$A_R = \begin{bmatrix} \cos\theta & \sin\theta \\ -\sin\theta & \cos\theta \end{bmatrix}, \bar{b} = \bar{0} \quad (2.4)$$

$$x' = x \cdot \cos\theta - y \cdot \sin\theta$$

$$y' = x \cdot \sin\theta + y \cdot \cos\theta$$

Translation:

$$A_t = \begin{bmatrix} 1 & 0 \\ 0 & 1 \end{bmatrix}, \bar{b}_t = (t_1, t_2) \quad (2.5)$$

$$x' = x + t_1$$

$$y' = y + t_2$$

All of these transformations can be simply combined by multiplying transformation matrixes, in example if we want to perform scaling rotation translation:

$$\begin{bmatrix} x' \\ y' \end{bmatrix} = A_R \cdot A_t \cdot A_s \cdot \begin{bmatrix} x \\ y \end{bmatrix} + \bar{b}_t \quad (2.6)$$

Those three transformations in R^2 have all together five degrees of freedom:

$$\bar{d} = [s_{11}, s_{22}, \theta, t_1, t_2] \quad (2.7)$$

Let $I' = \text{Aff}(\bar{d}, I)$ be an affine transformation of image I . In order to find optimal affine transform with parameters \bar{d} the function to minimized was defined as:

$$f(\bar{d}) = -|r(I', I_{ref})| \quad (2.8)$$

Where:

$r(A, B)$ – correlation coefficient between A and B , where A and B are matrices or vectors of the same size given by equation:

$$r = \frac{\sum_m \sum_n (A_{mn} - \bar{A})(B_{mn} - \bar{B})}{\sqrt{\left(\sum_m \sum_n (A_{mn} - \bar{A})^2\right) \cdot \left(\sum_m \sum_n (B_{mn} - \bar{B})^2\right)}} \quad (2.9)$$

Correlation coefficient can be used for measurement the quality of the registration images (i. e. [4]).

\bar{A}, \bar{B} – mean value of all elements of A or B

I_{ref} – reference image of registration.

In the author's researches the Nelder – Mead simplex method was used ([1], [2]) that was proposed as a good solution ([3]) for finding optimal vector (2.7). The initial vector for the process of optimization was $\bar{d} = [1, 1, 0, 0, 0]$ (void transformation).

3. Local spatial transform, non – rigid free form deformation transformation

The affine transformation captures only the global motion of the brain. An additional transformation is required, which models the local deformation of it. The nature of the local deformation of the brain can vary significantly across patients and with age. Therefore, it is difficult to describe the local deformation via parameterized transformations. Instead, the free form deformation (FFD) model, based on B – splines, which was successively used i.e. in registration breast MR images [4], CT liver images [5] or tracking and motion analysis in cardiac images [6]. The basic idea of FFD's is to deform an object by manipulating an underlying mesh of control points. The resulting deformation controls the shape of the 3 – D or 2 – D object and produces a smooth and continuous transformation.

One familiar technique to represent a nonrigid transformation is to employ spline functions such as B – splines, because B – splines are locally controlled, they are computationally efficient compared to the other globally controlled splines [5].

B – spline free form deformation is a non-rigid registration algorithm that has been widely used in the past few years ([7]). The transformation model is a free-form deformation (FFD) that is described by a cubic B-spline. For any point of image x, y , the B – spline transformation is computed from the positions of the surrounding 4x4 control points. The mesh of control points controls the deformation of the whole image. The basic idea of FFD in image registration process is to manipulate the position of points in mesh grid in order to minimize the “difference” (error function) between new and reference images.

The transformation model of a free-form deformation that is performed by a cubic B – spline can be described by the equation below:

$$T(x, y) = \sum_{l=0}^3 \sum_{m=0}^3 \beta_l(u) \cdot \beta_m(v) \cdot \phi_{i+l, j+m} \quad (3.1)$$

Where:

i, j – the indices of the control points,

$$i = \left\lfloor \frac{x}{\delta_x} \right\rfloor - 1, \quad j = \left\lfloor \frac{y}{\delta_y} \right\rfloor - 1 \quad (3.2)$$

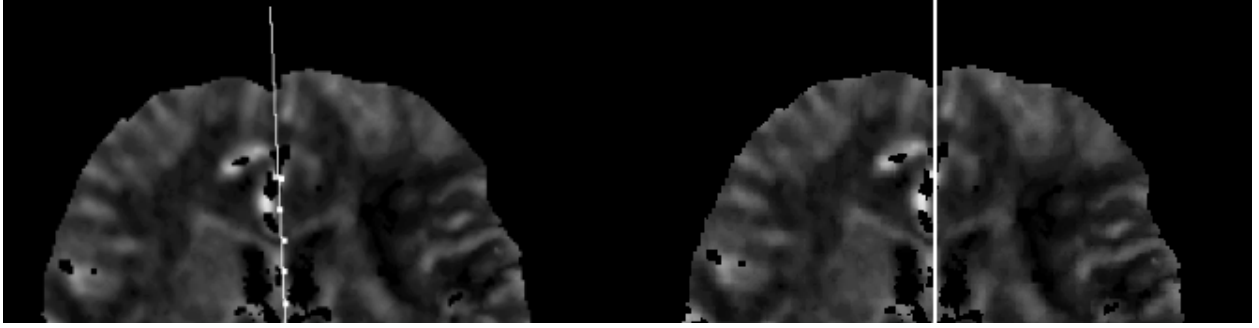


Fig 1. Adaptive mesh refinement during iterations of algorithm. New point of mesh is placed between two old points. At the beginning mesh with size 3x 3 (black points), in the next step 5 x 5 (new points are gray) and the final 9 x 9 mesh (white points).

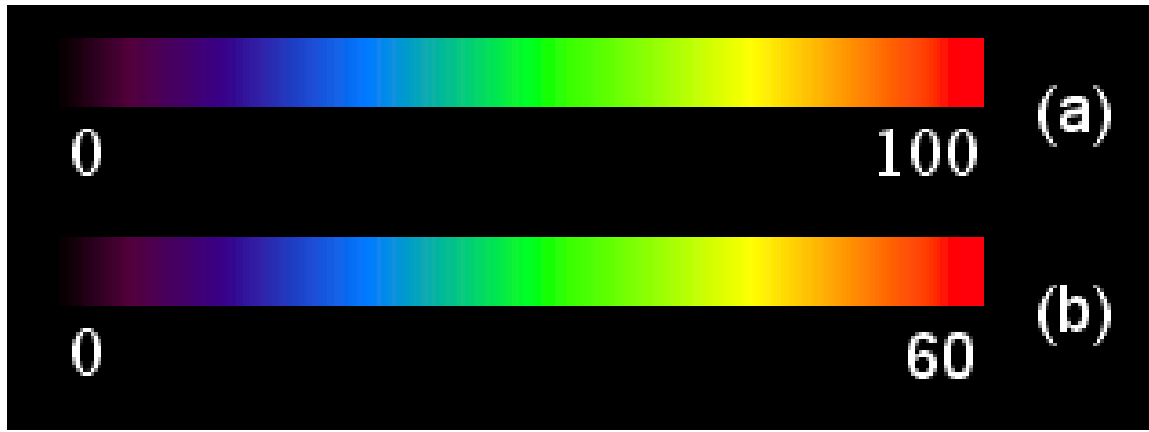


Fig 2. (a) The image of the brain with mesh of control points size 6 x 6. The distance between nearest points ϕ in the row / column is δ . (b) Control point $\phi_{i,j}$ affects points only inside the $4 \cdot \delta \times 4 \cdot \delta$ neighborhood domain (the error computation during the optimization process of the position of each of the control points is performed only inside this region).

δ_x, δ_y – the spacing between the control points (in mesh grid).

u, v – the relative positions of (x, y) inside that cell in the 2D space,

$$u = \frac{x}{\delta_x} - \left\lfloor \frac{x}{\delta_x} \right\rfloor, \quad v = \frac{y}{\delta_y} - \left\lfloor \frac{y}{\delta_y} \right\rfloor \quad (3.3)$$

$\phi_{i,j}$ – set of deformation coefficients that is defined on a sparse, regular grid of control points placed over the moving image.

The functions β_0 through β_3 are the third – order spline polynomials:

$$\beta_0(t) = \frac{(-t^3 + 3 \cdot t^2 - 3 \cdot t + 1)}{6} \quad (3.4)$$

$$\beta_1(t) = \frac{(3 \cdot t^3 - 6 \cdot t^2 + 4)}{6} \quad (3.5)$$

$$\beta_2(t) = \frac{(-3 \cdot t^3 + 3 \cdot t^2 + 3 \cdot t + 1)}{6} \quad (3.6)$$

$$\beta_3(t) = \frac{t^3}{6} \quad (3.7)$$

In the discrete case the return coordinates must be changed in to integer values. After calculation the coordinates of the pixel $(x_{new}, y_{new}) = T(x, y)$ that will be transformed to the current x, y pixel the value of color (gray level) in the pixel must be computed. In the author's algorithm the shown below method of computation of gray level is used:

$$(x_{local}, y_{local}) := T(x, y) - \lfloor T(x, y) \rfloor \quad (3.8)$$

$$perc(0) = (1 - x_{local}) \cdot (1 - y_{local})$$

$$perc(1) = (1 - x_{local}) \cdot y_{local}$$

$$perc(2) = x_{local} \cdot (1 - y_{local})$$

$$perc(3) = x_{local} \cdot y_{local}$$

$$color(0) = I(\lfloor x \rfloor, \lfloor y \rfloor)$$

$$color(1) = I(\lfloor x \rfloor, \lfloor y \rfloor + 1)$$

$$color(2) = I(\lfloor x \rfloor + 1, \lfloor y \rfloor)$$

$$color(3) = I(\lfloor x \rfloor + 1, \lfloor y \rfloor + 1)$$

Where $I(x, y)$ is the value of color (gray level) of the input image I .

$$I_{out}(x, y) = \sum_{i=0}^3 color(i) * perc(i) \quad (3.9)$$

The registration error value based on pixel distance (log) between two images used by the author in the algorithm:

$$C(A, B) = \frac{\sum_{i=1}^n \sum_{j=1}^m \log(|A_{ij} - B_{ij}| + 1)}{n \cdot m} \quad (3.10)$$

The registration error can be also computed in image domain: $([k, k + o], [l, l + p]) \supset ([1, n], [1, m])$

$$C(A, B) = \frac{\sum_{i=k}^{k+o} \sum_{j=l}^{l+p} \log(|A_{ij} - B_{ij}| + 1)}{k \cdot l} \quad (3.11)$$

The algorithm is a modified version of the B – spline registration algorithm in [4]. It does not include the control grid smooth optimization, instead the grid refinement was used. The local transformation is represented as a combination of B – spline FFD's at increasing resolutions of the control point mesh. The control point mesh at level l is progressively refined by inserting new control points between the existing ones to create the control point mesh at level $l + 1$ (Fig 1.).

The new image to register is I , the reference image is I_{ref} . The “de – scalping” (partitioning brain from the non-brain tissues [23]) is computed on I and I_{ref} brain images. In order to perform “de – scalping” the following fast three – step algorithm designed by author was used:

- Find bones (skull) in CT image (simple threshold operation)
- Find tissues other than bones (simple threshold operation)
- Take as the result image only those tissues that are inside closed region defined by bones.

The result of this algorithm can be seen in Fig. 3.

The complete registration algorithm goes as follows:

1. Calculate the optimal affine transformation with using Nelder – Mead algorithm
2. Set the input mesh nodes number ($nRows, nColumns$)
 $nRows := 8$
 $nColumns := 8$
3. Initialize the grid nodes of deformation mesh with size $nRows \times nColumns$.
4. Set the number of grid refine operation to 2 and gradient recalculation operation to 6
 $refine := 2$
 $recalculation := 6$
5. For $r = 1$ to $refine + 1$
Set the resize factor
 $resize_factor := \frac{r}{refine + 1}$

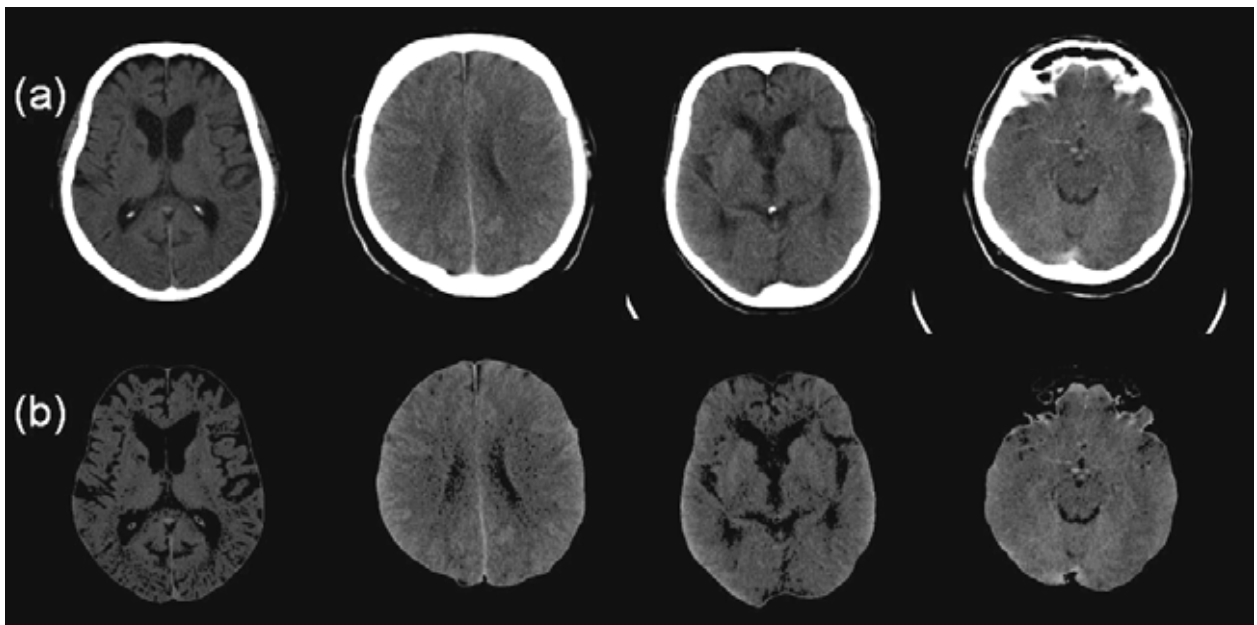


Fig 3. The example results of “de – scalping” algorithm ((a) before (b) after “de – scalping”)

- Resize image according to *resize_factor*, use gaussian smoothing on new created images in order to make optimization process faster
- Compute the value of gradient movement constant:

$$\mu = 0.2 \cdot \left(\frac{I_{rows} - 1}{nRows - 1} + \frac{I_{columns} - 1}{nColumns - 1} \right)$$

Where:

$I_{rows}, I_{columns}$ is number of rows and columns in input matrix I .

- For $z := 1$ to recalculation
- Compute the gradient of cost function (3.11)

$$\nabla C = \left[\frac{\partial C(I, I_{ref}, \Phi_1)}{\partial \Phi_1}, \frac{\partial C(I, I_{ref}, \Phi_2)}{\partial \Phi_2}, \dots, \frac{\partial C(I, I_{ref}, \Phi_n)}{\partial \Phi_n} \right]$$

(using the central differential quotient method), each control point affects points only inside its $4 \cdot \delta \times 4 \cdot \delta$ neighborhood domain (Figure 4).

- Recalculate the control points of mesh grid

$$\Phi := \Phi + \mu \cdot \frac{\nabla C}{|\nabla C|}$$

$$\mu := \mu \cdot 0.85$$

- Recalculate nodes of deformation mesh.

$$nRows := 2 \cdot nRows + 1$$

$$nColumns := 2 \cdot nColumns + 1$$

- Recalculate nodes of deformation mesh with size $nRows \times nColumns$. Each new node appears between two old one and its position is interpolated with spline interpolation (Fig. 1).
- Compute deformation on new image according to deformation mesh

$$I := \text{splineTransform}(I, \Phi)$$

4. Experiment and discussion

The experiment was performed on 28 CT images, with 512×512 pixels resolution, from 8 different patients. Each image was acquired from a series of dynamic brain perfusion CT scans (often the first or one of the first images where the injected contrast agent is still not visible). The aim of registration was to generate the brain maps that will be accurate enough to name some of the “main parts” of brain in new images. In order to do that, the “reference image” of the algorithm described above is now the new image, and the “image to registrate” is one of the set of “brain atlas reference image”. This algorithm was implemented in the Matlab environment and the C programming language (compiled mex functions for faster performance).

The atlas consists of 12 brain CT images (the “reference images” for the registration process) and 12 images with labeled regions that describe some parts of brain (Fig 4, brain region labels based on [18]). The template images were created from a set of CT images acquired from one healthy patient (similarly to original Talariach atlas templates that was based on orthogonal sections acquired post mortem from only one 60-year-old female subject [9]).

Images from dynamic brain perfusion CT treatment have more noises and movement artifact in them then “typical” brain CT images (Fig 5.) that makes process of registration even harder.

The example results of registration of three brain images are shown in Fig 6. The brain regions detected in images (Fig 6. e) are marked with a white line. The final mesh of control points (size 29×29) for the same three cases can be see in Fig 7. In Fig 8. The differences between atlas images and the new images are presented before (Fig 8. a) and after the registration (Fig 8. b).

Table 1. presents the summary results of the image registration process. The error (computed with (3.10) between new image and atlas image before and after registration) decreases in all cases.

Table 1. Error before and after registration – error function (3.10)

Number	Error before registration	Error after registration
1	0.9205	0.72356
2	0.9826	0.79034
3	0.9922	0.82229
4	0.9091	0.75868
5	1.2056	1.0558
6	1.2028	1.0506
7	1.2454	1.1302
8	1.0754	0.97403
9	0.9874	0.80488
10	0.8958	0.74321
11	0.9196	0.77166
12	0.7982	0.68605
13	0.7228	0.71876
14	0.6822	0.5947
15	0.7531	0.65938
16	0.6308	0.58591
17	0.7750	0.67902
18	0.6528	0.57475
19	0.6397	0.60927
20	0.5617	0.44583
21	0.8419	0.79936
22	0.7263	0.67874
23	0.7795	0.72103
24	0.6470	0.6006
25	1.0059	0.77045
26	0.9757	0.75389
27	0.9507	0.81015
28	0.8895	0.77162

The algorithm presented in this publication can be used as a reliable tool for registration not only medical images but also any type of time-series or similar in shape image classes. After creating a set of atlas images and altering role of reference image with “moving image” the deformable brain atlas system

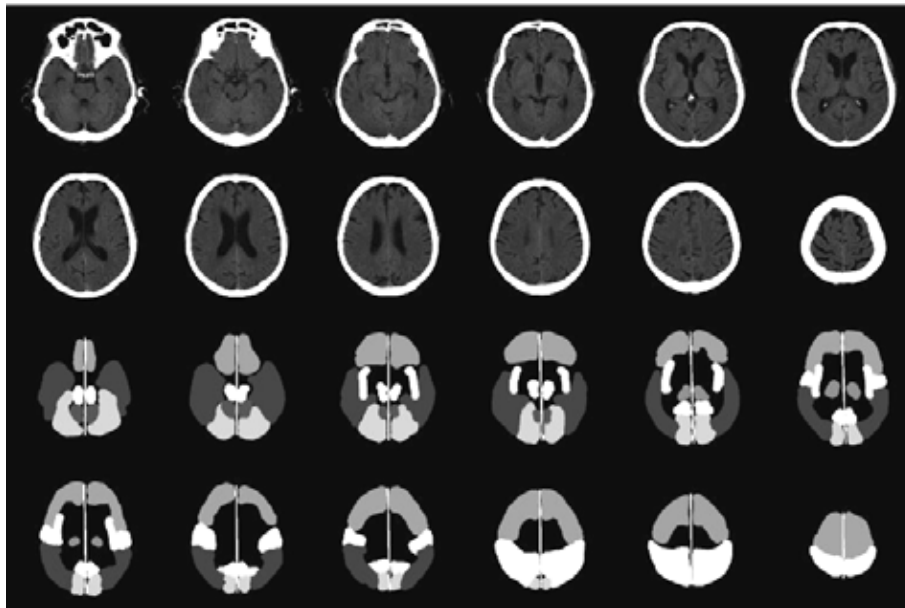


Fig 4. Images form atlas, top two rows – raw CT images, bottom two rows – map of the brain parts, each color (gray level) symbolize different brain area: symmetry axis (229), Frontal lobe (77), parietal lobe (153), temporal lobe (29), occipital lobe (102), diencephalon (67), insula, insular lobe (135), mesence phalon; midbrain (188), anterior lobe of cerebellum (37)

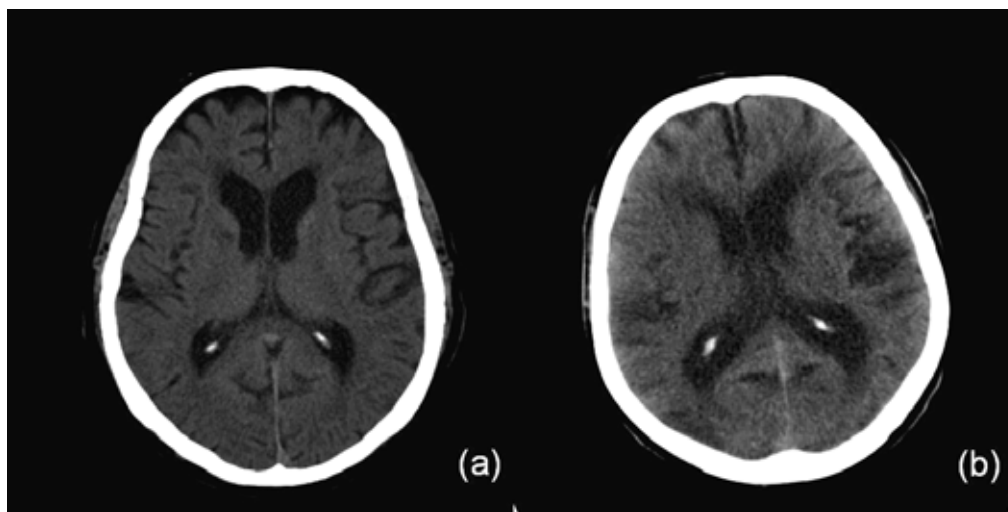


Fig 5. (a) "Plain" CT image, (b) CT images registrated during dynamic CT perfusion treatment. Noises and movement artifacts are clearly visible.

can be obtained. Images used in process do not need any prior preprocessing (in the case of brain optionally "de-scalping").

The main reason of the errors that appear even after the registration process is that images are acquired from different patients and from different modalities (there is no possibility to create 2D brain atlas images in all possible axial slices), besides between patient difference there are also different radius in which patients lays they heads so different regions of the brain can be see in the "same" axial slices. Another reason of errors that can be clearly seen in Fig 6. d is that affine transform often finds local minimum of error function not performing rotation of image correctly (see the twisted "symmetry axis" be-

tween brain hemispheres). There is also a difference between atlas- and "new images" because atlas images are "plain CT" images and "new images" came from perfusion CT treatment and has more noises and movement artifact in them. These problems can be solved by creating some kind of "eigenbrains" like those in [10].

The further research of the author will be focused on testing different similarity measures (i.e. based on Shanon information theory [8]) that can improve the accuracy of registration during rigid and non – rigid algorithm level. The second goal will be testing the deformable atlas in diagnosing the set of perfusion CT brain maps and comparing it with medical docu-

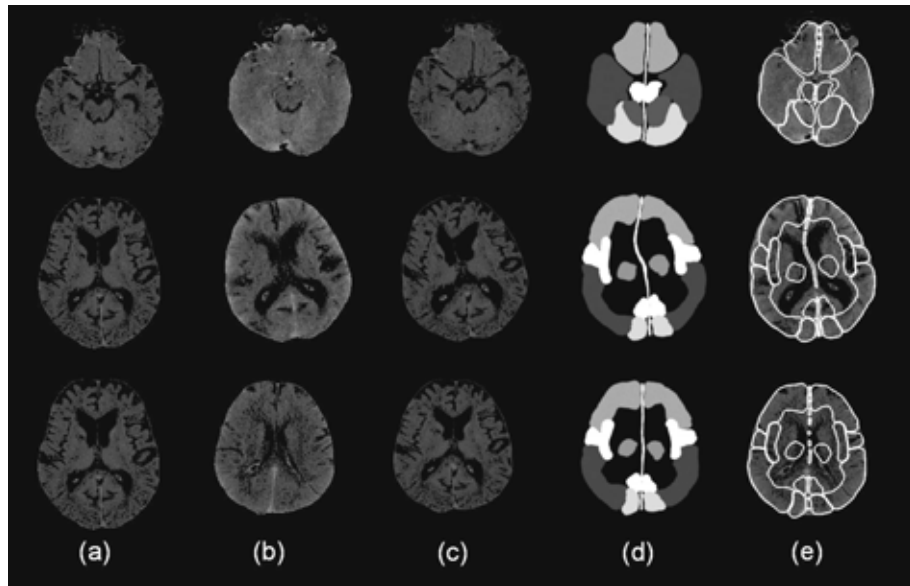


Fig 6. The example results of the algorithm: (a) reference images of brain atlas (b) new images (c) adapted (registered) brain atlas image (d) adapted (registered) brain atlases labeled maps (e) adapted (registered) brain atlases labeled maps combined with input images.

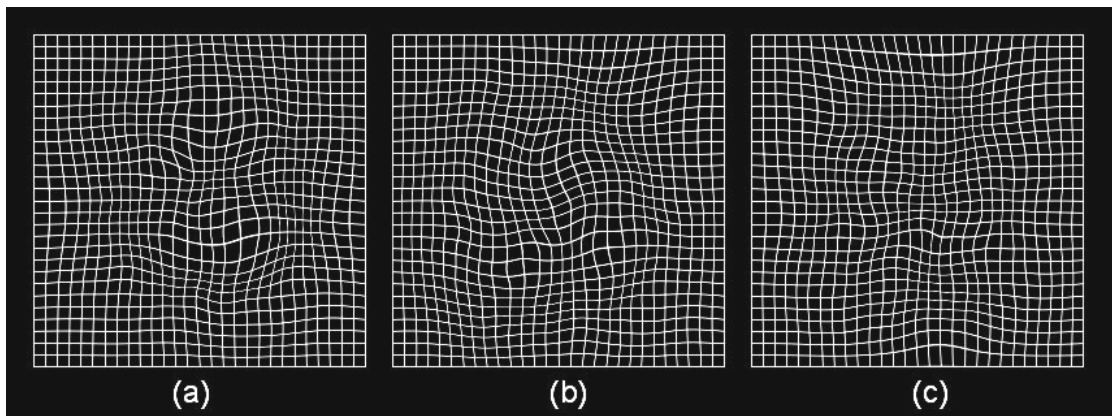


Fig 7. The final mesh grid (size 29 x 29) that was used for deformation brain atlases in Fig 6 c) and d).

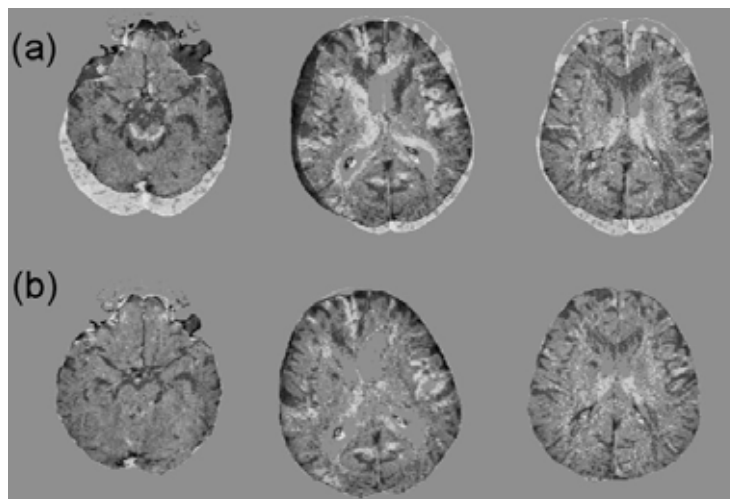


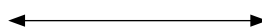
Fig. 8 Difference (a) before and (b) after the registration between images from Fig 6 a) and b).

mentation of each case in order to propose algorithms proper for automatic image understanding ([16], [17]).

References:

- [1] Jeffrey C. Lagarias, James A. Reeds, Margaret H. Wright, Paul E. Wright, Convergence properties of the Nelder – Mead simplex method in low dimensions, SIAM Journal of Optimization, Vol. 9, No. 1, pp. 112-147, 1997
- [2] William H. Press, Brian P. Flannery, Saul A. Teukolsky, William T. Vetterling, Downhill Simplex Method in Multidimensions, Numerical Recipes in C, Second Edition (1992), pp. 408-412
- [3] John L. Semmlow, Biosignal and Biomedical Image Processing. MATLAB – Based Applications, CRC Press 2004
- [4] D. Rueckert, L. I. Sonoda, C. Hayes, D. L. G. Hill, M. O. Leach, D. J. Hawkes, Nonrigid Registration Using Free-Form Deformations: Application to Breast MR Images, IEEE Transaction on Medical Imaging, Vol. 18, No. 8, August 1999
- [5] Fumihiko Ino, Kanrou Ooyama, Kenichi Hagihara, A data distributed parallel algorithm for nonrigid image registration, Parallel Computing, 2005
- [6] E. Bardinet, L. D. Cohen, N. Ayache, Tracking and motion analysis of the left ventricle with deformable superquadrics, Med. Image Anal., Vol. 1, No. 2, pp. 129-149, 1996
- [7] Adriane Parraga, Johanna Pettersson, Altamiro Susin, Mathieu De Craene, Benoit Macq, Non-rigid registration methods assessment of 3D CT images for head-neck radiotherapy, Medical Imaging 2007: Image Processing, 2007 Macq
- [8] Julia A. Schnabel, Daniel Rueckert, Marcel Quist, Jane M. Blackall, Andy D. Castellano-Smith, Thomas Hartkens, Graeme P. Penney, Walter A. Hall, Haiying Liu, Charles L. Truwit, Frans A. Gerritsen, Derek L. G. Hill, David J. Hawkes, A Generic Framework for Non-Rigid Registration Based on Non-Uniform Multi-Level Free-Form Deformations, Medical Image Computing and Computer-Assisted Intervention (MICCAI) 2001
- [9] P. Thompson, M. Mega, K. Narr, E. Sowell, R. Blanton, A. Toga, Brain image analysis and atlas construction, Handbook of Medical Imaging, chapter 17. Pages 1066-1119, SPIE. 2000
- [10] Usha Sinha, Hooshang Kangarloo, Principal Component Analysis for Contentbased Image Retrieval, RadioGraphics 2002; 22: 1271-1289
- [11] M. R. Ogiela, R. Tadeusiewicz, Modern Computational Intelligence Methods for the Interpretation of Medical Images, Springer-Verlag, Berlin-Heidelberg, 2008
- [12] R. Tadeusiewicz, M. R. Ogiela, Medical Image Understanding Technology, Springer Verlag, Berlin-Heidelberg, 2004
- [13] Makoto Sasaki, Kohsuke Kudo, Hirobumi Oikawa, CT perfusion for acute stroke: Current concepts on technical aspects and clinical applications, International Congress Series 1290 (2006) 30-36
- [14] Aleksa Cenic, Darius G. Nabavi, Rosemary A. Craen, Adrian W. Gelb, and Ting-Yim Lee, Dynamic CT Measurement of Cerebral Blood Flow: A Validation Study, January 1999
- [15] Richard E. Latchaw, Howard Yonas, George J. Hunter, William T.C. Yuh, Toshihiro Ueda, A. Gregory Sorensen, Jeffrey L. Sunshine, Jose Biller, Lawrence Wechsler, Randall Higashida, George Hademenos, Guidelines and recommendations for perfusion imaging in cerebral ischemia, Stroke 34, (2003) 1084-1104
- [16] Ryszard Tadeusiewicz, Marek R. Ogiela, Automatic Image Understanding – A New Paradigm for Intelligent Medical Image Analysis (opening article), BIO-ALGORITHMS AND MED-SYSTEMS, Vol. 2, No. 3, 2006, pp. 5-11
- [17] Ryszard Tadeusiewicz, Marek R. Ogiela, Structural Approach to Medical Image Understanding, Bulletin of the Polish Academy of Sciences – Technical Sciences, Vol. 52, No. 2, 2004, pp. 131-139
- [18] Antoine Micheau, Denis Hoa, Atlas of brain MRI cross-sectional anatomy, Anatomy of the whole human body: medical imaging and pictures, 2008, <http://www.imaio.com/en/e-Anatomy>
- [19] L. Ramirez, N. G. Durdle, V. J. Raso, Medical image registration in computational intelligence framework: a review, Electrical and Computer Engineering, 2003. IEEE CCECE 2003. Canadian Conference on Volume 2, 4-7 May 2003, Vol. 2, pp. 1021-1024
- [20] P.J. Phillips, Y. Vardi, S.M. Dunn, M.S. Buchsbaum, J.L. Spiegel-Cohen, An automatic MR-PET registration algorithm, Pattern Recognition, 1996, Proceedings of the 13th International Conference on Volume 3, 25-29 Aug. 1996, Vol. 3, pp. 533-537
- [21] Guorong Wu, Feihu Qi, Dinggang Shen, Learning-based deformable registration of MR brain images, Medical Imaging, IEEE Transactions on Volume 25, Issue 9, Sept. 2006, pp. 1145-115
- [22] Simon K. Warfield, Jan Rexilius, Petra S. Huppi, Terrie E. Inder, Erik G. Miller, William M. Wells III, Gary P. Zientara, Ferenc A. Jolesz, Ron Kikinis, A Binary Entropy Measure to Assess Nonrigid Registration Algorithms, Fourth International Conference on Medical Image Computing and Computer-Assisted Intervention, 2001 Oct 14-17, Utrecht, The Netherlands, pp. 266-274
- [23] A. Purwar, R. Gupta, M. K. Sarma, G. Bayu, A. Singh, D. K. Rathore, S. Saksena, R. Trivedi, A. Mishra, M. Haris, P. Mohan, R. Rathore, De-scalping of the brain in echo planar DT-MRI, Proceedings of International Society of Magnetic Resonance in Medicine 14, 2006

COMPUTER SCIENCE



RADIOLOGY

IMAGE PROCESSING APPLICATION FOR ENHANCEMENT OF MEDICAL DIAGNOSTIC FEATURES

JOANNA JAWOREK, ELIASZ KAŃTOCH

*Students' Scientific Society „Implant”
Faculty of Electrical Engineering, Automatics, IT and Electronics
AGH University of Science and Technology*

Abstract: Automatic analysis of medical imaging is the permanently developed discipline requiring the interdisciplinary collaboration linking medicine and computer science. The technique oriented on the increasing the resolution of the medical images is presented.

Introduction

Nowadays medical images are a very important and very popular source of information, used by medical doctors for disease detection and location. Medical imaging refers to the techniques and processes that present the human body in two and three dimensions[1]. Recently, a great advancement has been made in the field of medical imaging. New techniques and processes are used to create images of the human body for clinical purposes, e.g. for visible range imaging better cameras and new microscopy techniques have been developed. Although the amount of medical images produced in the world increases each year, their quality for diagnosis and therapy remains suboptimal [1],[2]. In our application we propose the application of the latest medical imaging technologies and algorithms to increase the quality of the images.

This paper is arranged as follows. In section 2 we described the software application, image processing operations and presented the algorithm on a flowchart. Section 3 shows an example result of tomography. In Section 4 we described a function dedicated for mammograms. Implementation and statistical conclusion are presented in Section 5. Finally, Section 6 summarizes the conclusions and presents our plans for the future.

Image processing and the specification of the software application

The aim of our research was to develop a software application that will help doctors to diagnose a disease more efficiently,

through the improvement of the image quality. The program's interface can be seen in Figure 1 and contains the most common image processing operations such as: binarization, filtration and histogram equalization but also morphological operations (erosion, dilation, closing and opening) [3],[4]. A special button “mammography” launching a set of dedicated image transformations simplifies the interpretation of the mammography images (Section 4). We can compose the operation chain and change every single parameter of each operation.

A properly chosen sequence of operation is very helpful in eliminating the majority of noise that always appears in the image (compare Figure 1 and Figure 2). It also helps in image stabilization, by the extraction of the most important and significant features (e.g. sharpening of the organ edges, separating interesting organs from the rest of the image) [2]. All these transformations can be important for the location of tumors or other pathologies, study of the anatomical structures before the surgery, and planning of the treatment.

In Figure 3 a simplified flowchart [5] has been presented including only the main steps. In every single moment while using the application, the operator can also use functions like:

- save image, open image, delete image
- execute the list of operations, remove all chosen operations, remove a single operation
- compose the operation chain and change every single parameter of each operation
- import operation chain from an XML file (default list)
- export the list of operation to an XML file

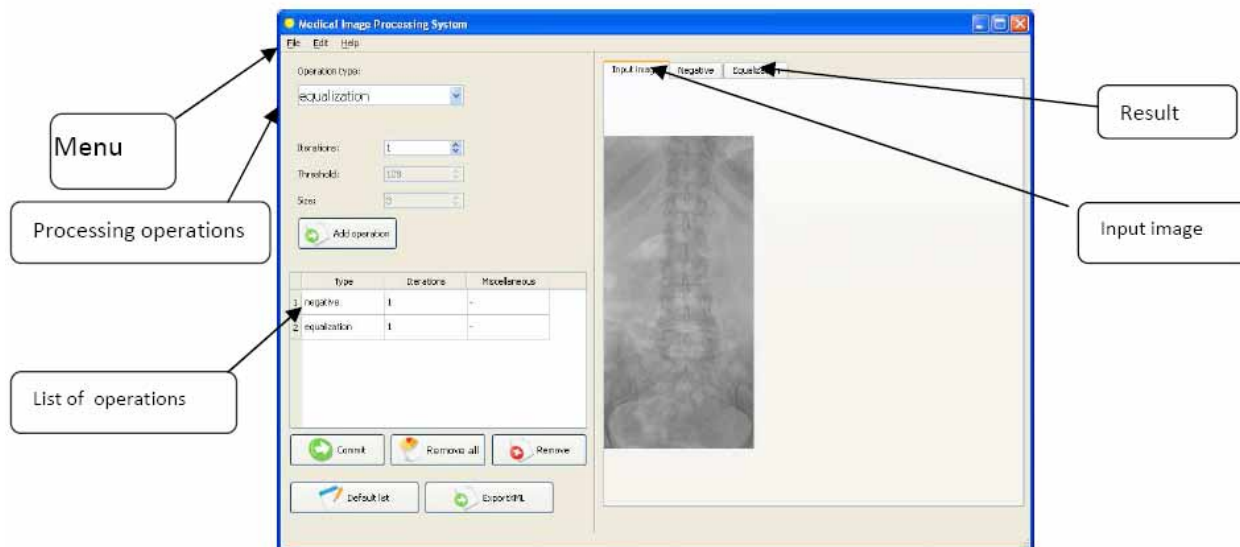


Fig. 1. Interface of the application with the input medical image of the backbone

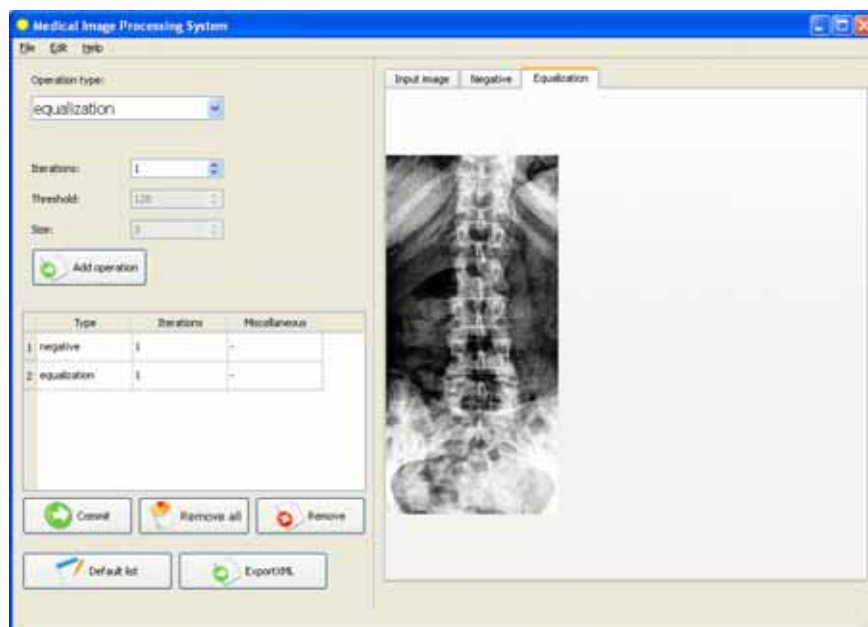


Fig. 2. Output image of the backbone after negation and histogram equalization operation

An acceptable result

Computer tomography was introduced in the 1970s and since that time it has become a very important tool in medical imaging [1]. It is currently commonly used to detect many different diseases like: cancer, acute and chronic changes in the lung and polyps, so it is very important to have a acceptable quality of the images [6]. For the input image let us take as an example abdomen tomography image (Figure 4), which is very unclear. After applying a sequence of operations including: negation and filtration, our output image (Figure 5) has changed dramatically.

Mammography image

Mammography is a low-power X-ray technique (about 0.7 mSv) that examines the human breast and gives a picture of the internal structure (Figure 6) [12]. These particular special pictures may help radiologists in the diagnosis of breast problems including cancer, milk ducts or small abnormal tissue [7]. Interpretations of mammograms can be problematic firstly because a normal breast can appear differently for each woman and secondly because of the quality and gray scale representation of the tissue that makes the decision much more difficult.

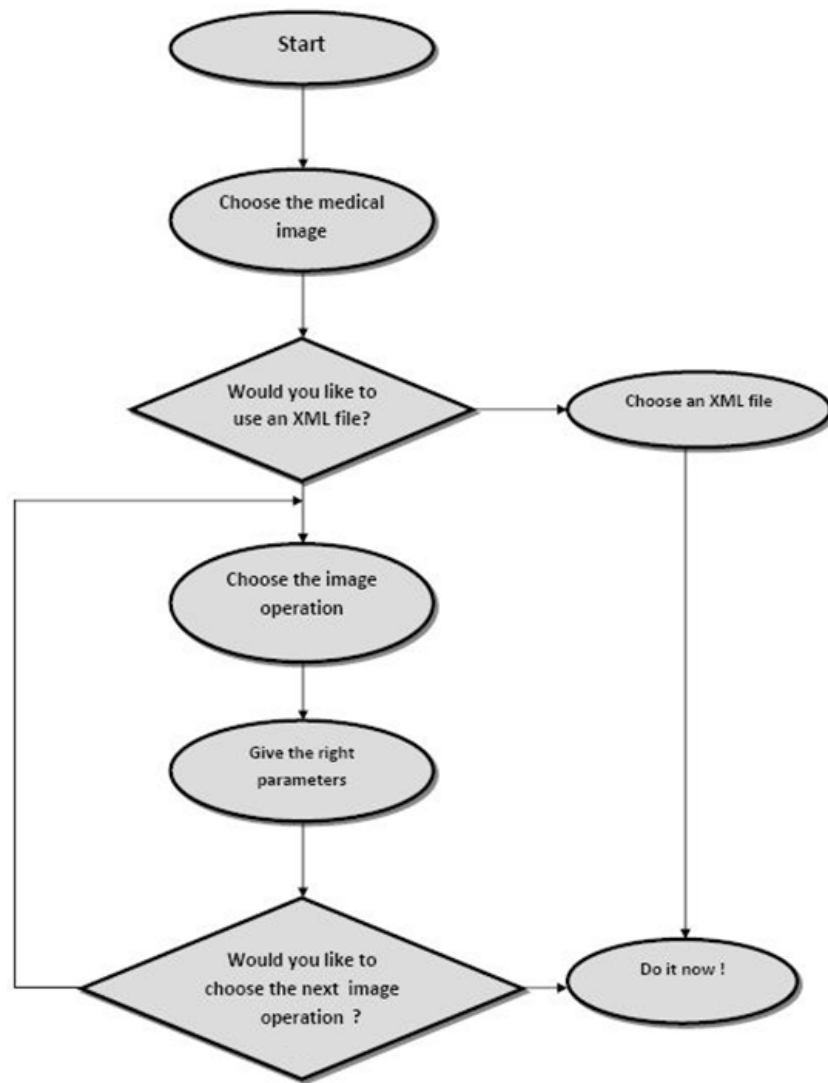


Fig. 3. Main diagram of the application

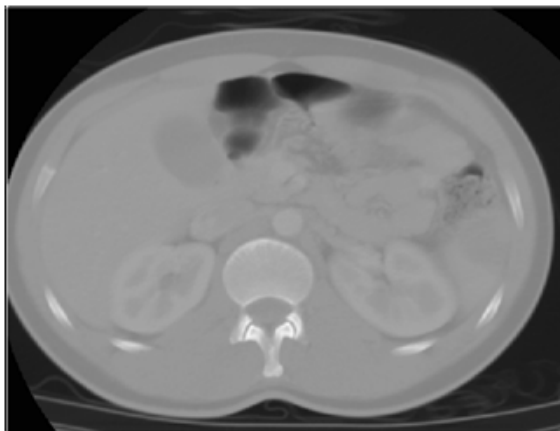


Fig. 4. Input image of the Computed Tomography (CT) scan of cross section of the human abdomen. It is impossible to study the anatomical structure



Fig. 5. Output image of the tomography usable to locate pathologies and study the structure thanks to the processing performed

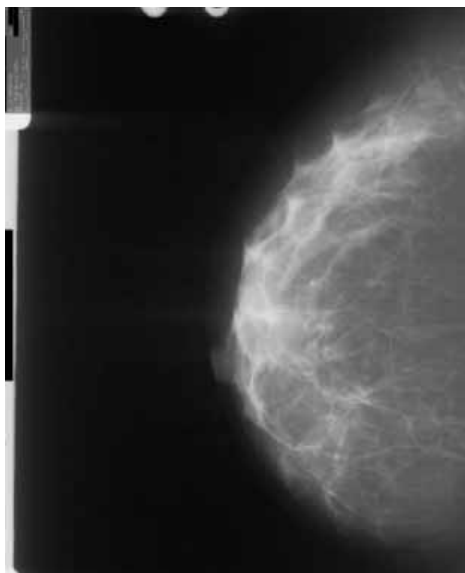


Fig. 6. Regular mammography which shows the internal structure of the breast

Our proposal of the function chain dedicated for the interpretation of the mammography images contains the following steps:

- Reading the input image
- Converting the image to a grayscale
- Filtration (reducing the noise)
- High-pass filtering
- Binarization
- Converting from intensity format to RGB
- Segmentation
- Displaying the output image

The colors in the image make objects easier to distinguish for doctors while diagnosing. In the new GUI we provide a button to enlarge the places which can contain abnormal tissue (Figure 7). It is helpful for us by measuring the object and to assess whether the tissue is abnormal or not.

Implementation and testing

Keeping in mind that the application was developed for doctors and not for computer scientists, we provided a special button for automatic selection of a file in the XML format [8] where the most common sets of operations for the medical images are stored, for example: computer tomography, MRI, ultrasonography.

The application has been developed in the C++ language with QT, OpenCV (Open Source Computer Vision Library) [9],[10],[11] and Matlab. It is cross-platform and can be compiled for the operating systems from Windows and Linux families.

Testing of correct modification for each kind of image was carried on several images (about 50). It is surely insufficient to draw or write any statistical conclusion, however our input and output images were judged by doctors, which marked the quality of the output image as promising and helpful during the diagnostic of the diseases (Figure 8).

Conclusion and perspectives

Image processing offers many advantages increasing the quality of the image. It should never be forgotten that it is only a computer application and the last decision should always belong to the doctor. In this paper, we propose an image process-

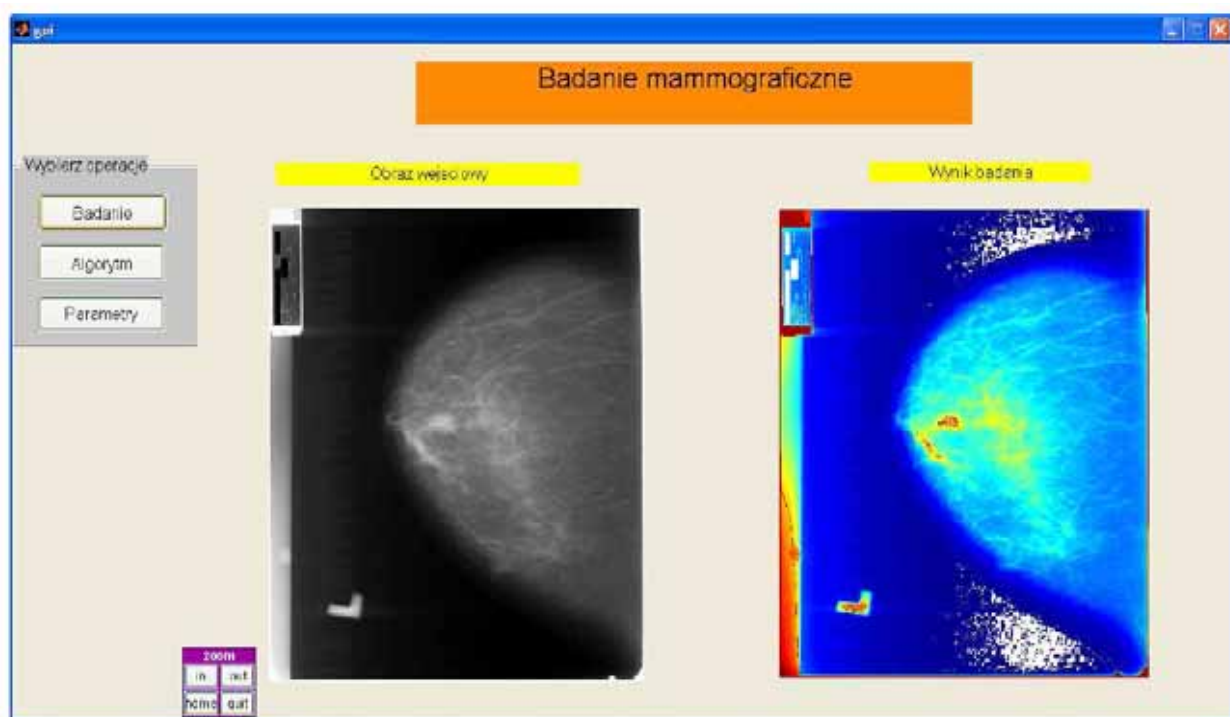


Fig 7. Interface of the application for mammography images. We can see the input and output image and the zoom function.

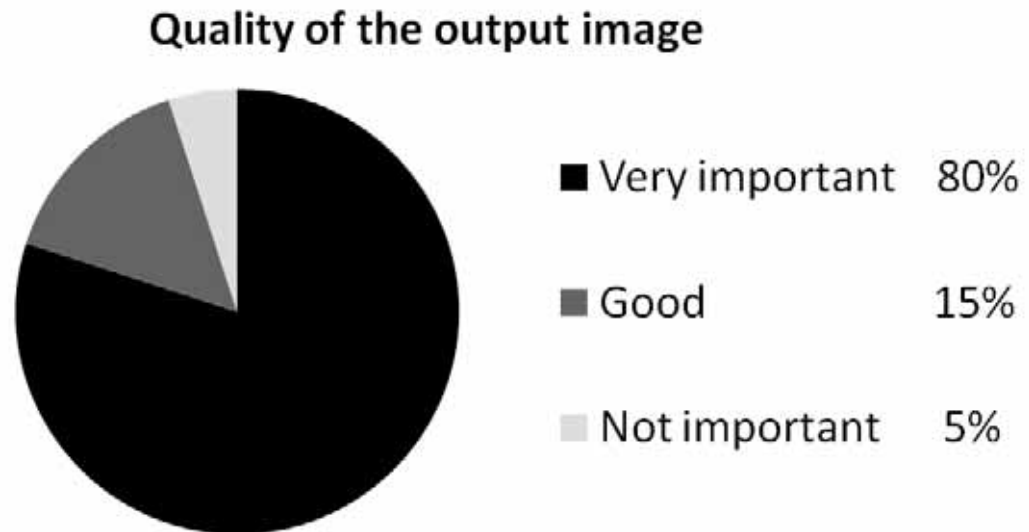


Fig. 8. The quality of 50 output images judged by 20 doctors.

ing application that supports doctors in diagnosing. The authors hope that it will be useful not only for clinical purposes but also for young doctors and students, for which it is not always easy to determine the diagnosis correctly. A second promising perspective is to broaden the amount of functions and the use of new methods to automatically detect and mark small tumors or pathological images.

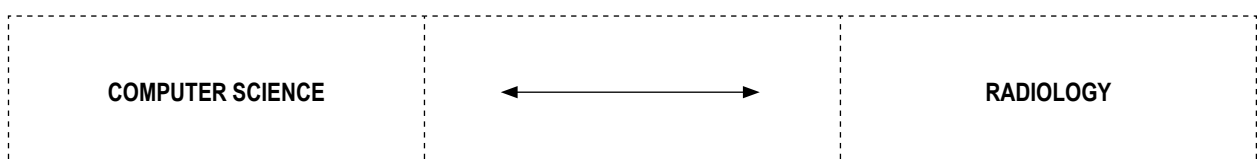
Acknowledgements

We would like to thank our research tutor dr hab. inż. Piotr Augustyniak for inspiring discussions and scientific guidance and the Department of Bioinformatics and Telemedicine Medical College Jagiellonian University for supplying the images. We are also grateful to Tomasz Knap for helping us with the implementation of the software.

References

1. Cytowski J., Gielecki J., Gola A.: *Cyfrowe przetwarzanie obrazów medycznych. Algorytmy technologie zastosowania*, Warszawa 2008
2. Tadeusiewicz R., Ogiela M.: *Automatic Image Understanding New Paradigm for Intelligent Medical Image Analysis*, Bio-Algorithms and Med-Systems, 2006
3. Tadeusiewicz R., Flasiński M.: *Rozpoznawanie obrazów*, Warszawa 1991
4. Malina W.: *Metody cyfrowego przetwarzania obrazów*, Warszawa 2005
5. Wirth N.: *Algorytmy + struktury danych = programy*, Warszawa 2002
6. http://en.wikipedia.org/wiki/Computed_tomography
7. <http://www.nlm.nih.gov/medlineplus/ency/imagepages/1105.htm>
8. McLaughlin B., Edelson J.: *Java i XML. Wydanie III*, 2007
9. Zieliński T.P.: *Cyfrowe przetwarzanie sygnałów*, Warszawa 2007
10. <http://opencvlibrary.sourceforge.net/> (OpenCV library)
11. Ezust A., Ezust P.: *Introduction to design patterns in C++ with Qt4*, <http://cartan.cas.suffolk.edu/oopdocbook/open-source/>
12. Chmielewski L., Kulikowski J.L., Nowakowski A.: *Obrazowanie biomedyczne*, 2004

Research tutor
dr hab. inż. Piotr Augustyniak



DIGITAL SKELETONIZATION AS A PROBE OF CORRELATION BETWEEN SUTURAL BONES AND DIFFUSION LIMITED AGREGGATION CLUSTERS

JANUSZ SKRZAT, JERZY WALOCHA

*Department of Anatomy
Jagiellonian University, Medical College, Kopernika 12, 31-034 Kraków, Poland*

Abstract: Skeletonization of the digital images of the sutural bones and computer generated clusters formed by diffusion limited aggregation process (DLA) revealed branch-like patterns underlying the shape of these objects. Density of DLA cluster is determined by the ratio of particle size to distance a particle moves in one step. Skeletons of DLA clusters aggregated from particles whose size was 20 pixels show the most similar fractal dimension to the skeletons of sutural bones. The skeletons obtained from DLA clusters formed by lesser (5, 10 pixels) or bigger (30, 40, 50 pixels) particles are less accurate to model basic pattern underlying shape of the sutural bones because of divergences in their fractal dimension.

Key words: Diffusion limited aggregation, Wormian bones, Cranial sutures

Introduction

A digital skeleton is a compact representation that allows mathematical analysis of the object. This is homotopic, thin and median in relation to the object it represents. Skeletonization is a technique, which allows to obtain basic structure of the object and to preserve most topological information [7, 8, 12]. This technique is a convenient tool to get a simplified representation of shapes and therefore can help to understand framework of composite objects like biological patterns.

Small bones found in human cranial sutures, particularly in the lambdoid suture are example of intricate, irregular objects. Sutural bones also termed wormian bones are ossicles, which develop from accessory ossification centers within cranial suture and fontanelles. These inconstant bones vary in size and number, which is generally limited to few or several entities, though they may exist as singular isolated bones [2, 3, 10]. Sutural bones have usually irregular shape, which often resembles stellate or branch patterns (fig. 1).



Fig. 1. Close up view on sutural bones

Morphological appearance of sutural bones resembles clusters that are obtained by the diffusion-limited aggregation algorithm. Diffusion-limited aggregation (DLA) is the process whereby particles undergoing a random walk due to Brownian motion cluster together to form aggregates of a branch-like structures of fractal nature (fig. 2). As the cluster grows, there is a greater probability for particles to stick to the ends than to penetrate the interior. The shape of the DLA cluster is controlled by the possibility of particles to reach the cluster. Some

variations are also observed depending on the geometry of the growth, whether it is from a single point radially outward or from a plane or line for example [4, 11]. Diffusion-limited aggregation as a model of pattern formation has attracted considerable attention since it was introduced by Witten and Sander in 1981. It was used not only to physical systems in the Laplacian growth class but it has been also applied to biological systems [1, 9].

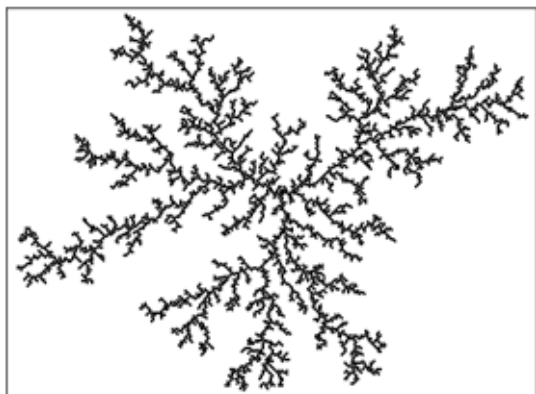


Fig. 2. A typical cluster generated by diffusion-limited aggregation algorithm containing 5000 particles.

Up till now, neither skeletonization nor diffusion-limited aggregation procedures have been applied to investigate geometrical properties of the sutural bones. Therefore purpose of this study is to determine whether skeletonization of the images of the sutural bones lead to similar patterns, which can be obtained from clusters formed by diffusion limited aggregation process. The second goal was to find out how far these structures present similar complexity expressed by the value of fractal dimension.

Material and methods

Sutural bones were found in the adult human skulls that are housed in the Department of Anatomy of the Medical College of the Jagiellonian University. Morphometric analysis of the 14 sutural bones located within lambdoid suture was performed in a following way: first, the posterior aspect of the skull was photographed using digital camera (Canon EOS D30), zooming on the sutural bones. Further their contours were traced as a 1 pixel line (0,35 mm) using the Graphire tablet (Wacom). Resolution of each image was 72 ppi. Enclosed contour of each sutural bone was filled with black colour, saved as a grayscale bitmap file and skeletonized using ImageJ software. This technique extracted a region-based shape feature representing the general form of an object, according to the algorithm that erodes repeatedly the image until only the skeleton remains (fig. 3).

Digital skeletonization was also performed on images of DLA clusters, which were generated on the computer with implemented ImageJ software, including Diffusion Limited Aggregate Models plugin (by A. Karperien and W. Rasband, Charles Sturt University, Australia) [7]. As a reference, we generated DLA clusters, which vary in size of initial particle measured

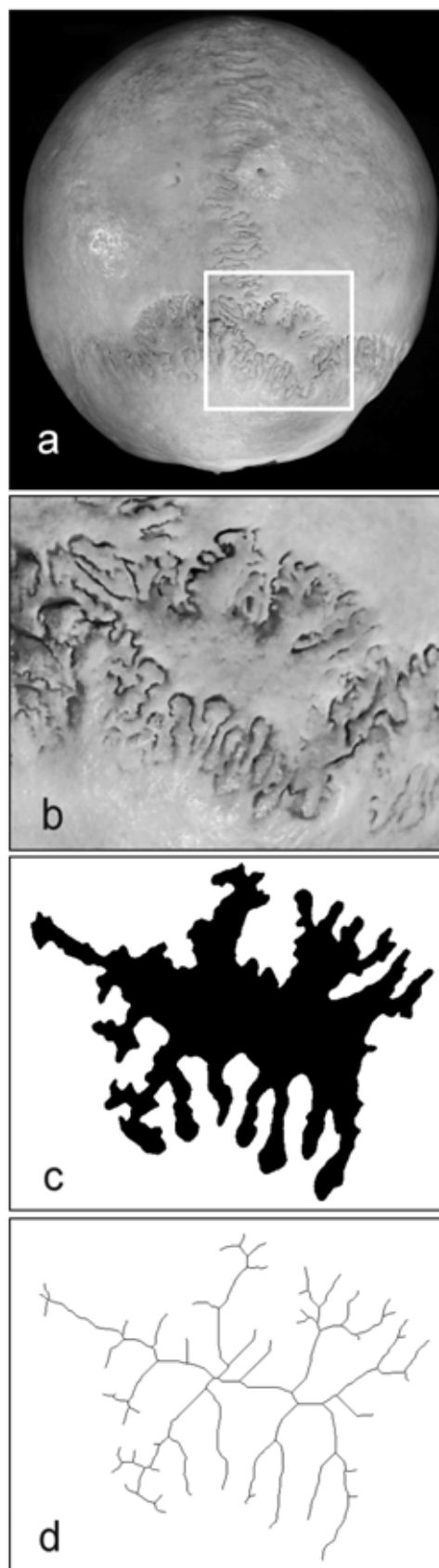


Fig. 3. Subsequent steps leading to the digital skeleton of the sutural bone; a – posterior view of the skull, sutural bone demarcated by the rectangle, b – magnified image of the sutural bone, c – isolated shape of the sutural bone, d – digital skeleton of the sutural bone.

by the number of pixels (px). The size of initial particles was following: 5, 10, 20, 30, 40, and 50 pixels. Thus we obtained 6 sets of DLA clusters, each included 14 aggregates. All aggregates were composed of round shaped particles, whose number was arbitrary selected as 5000. The example of such cluster and its digital skeleton shows fig. 4.

Next images (black skeleton, white background) obtained from sutural bones and DLA clusters were subjected to the fractal analysis using FracLac plugin for ImageJ software (developed by A. Karperien, Charles Sturt University, Australia) [6]. Fractal dimension was calculated as box-dimension. The equation for finding a fractal dimension (D_f) approximates scale and details of the object:

$$D_f = \lim_{\epsilon \rightarrow 0} \left[\frac{\log N(\epsilon)}{\log \epsilon} \right]$$

where the limit is found as the slope of the regression line for the data, and N denotes number of pieces that compose the object at scale ϵ .

To assess if the fractal dimensions of digital skeletons obtained from DLA clusters and sutural bones have the same shape of distribution, Kruskal-Wallis test was applied and followed by multivariate comparison test to find out statistically significant differences among samples.



Fig. 4. Computer generated DLA cluster (size of aggregated particles – 20 pixels, number of particles – 5000) and its digital skeleton presented as 1 pixel thick segmented lines.

Results

Digital skeletons of the sutural bones and DLA clusters show similar branch-like pattern but of various complexity expressed by fractal dimension (fig. 5). Estimated fractal dimension of the digital skeletons of the 14 sutural bones range from 1,09 – 1,32 with median 1,16 and mean equal to 1,18. Skeletons obtained from generated DLA clusters deliver bigger span of fractal dimension (1,03 – 1,50) than those of the sutural bones. However, in each group of the DLA clusters fractal dimension is less variable than in the case of sutural bones (table 1).

In the light of the Kruskal-Wallis test ($H = 88, 30; p < 0,05$) analyzed samples do not come from the same distribution (fig. 6). The result of multiple comparison test (table 2) indicates statistically significant difference between fractal dimensions of skeletons of the sutural bones and skeletons of the DLA clusters aggregated from the particles, which size was 5, 40 and 50 pixels.

Although the distributions of fractal dimensions of the skeletons of DLA clusters generated from particles, whose size is

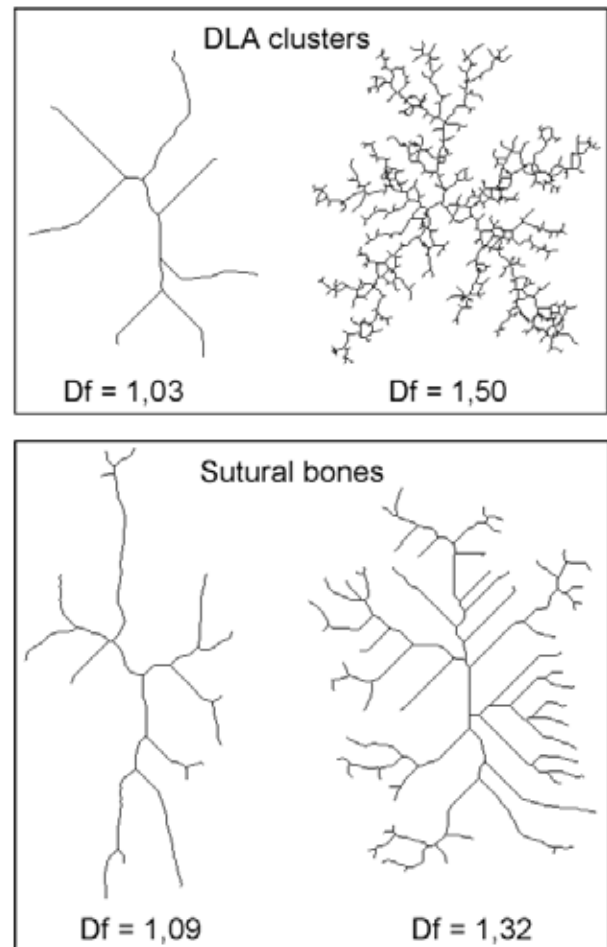


Fig. 5. The less and the most complicated skeletons of the DLA clusters and the sutural bones, scored by fractal dimension (D_f).

10, 20 and 30 pixels do not differ significantly from the distribution of fractal dimension of the skeletons of the sutural bones (table 2), the most adequate to simulate skeletons of the sutural bones seems to be DLA clusters aggregated from particles of size 20 pixels. The skeletons of these clusters yield fractal dimensions (1,16 – 1,25), which completely fits within the range of variation of fractal dimension (1,09 – 1,32) estimated for skeletons of the sutural bones. In this case, the difference between mean fractal dimension (1,20 for skeletons of DLA clusters and 1,18 for skeletons of the sutural bones) is the smallest ($\Delta = 0,02$).

Skeletons of DLA clusters made of particles, whose size is 30 pixels, yield lower mean fractal dimensions ($D_f = 1,12$) than skeletons of the sutural bones ($D_f = 1,20$) and thus bigger difference ($\Delta = 0,08$). Hence, range of variation of fractal dimensions estimated for the skeletons of these clusters (1,07 – 1,18) correspond partially only to the variation of the fractal dimension presented by the skeletons of sutural bones (1,09 – 1,32).

On the other hand, skeletons of DLA clusters obtained from smaller particles (10 pixels) show higher mean fractal dimension ($D_f = 1,33$) than skeletons of the sutural bones ($D_f = 1,18$) what makes the biggest difference between means ($\Delta = 0,15$). Hence, the range of variation of fractal dimension of

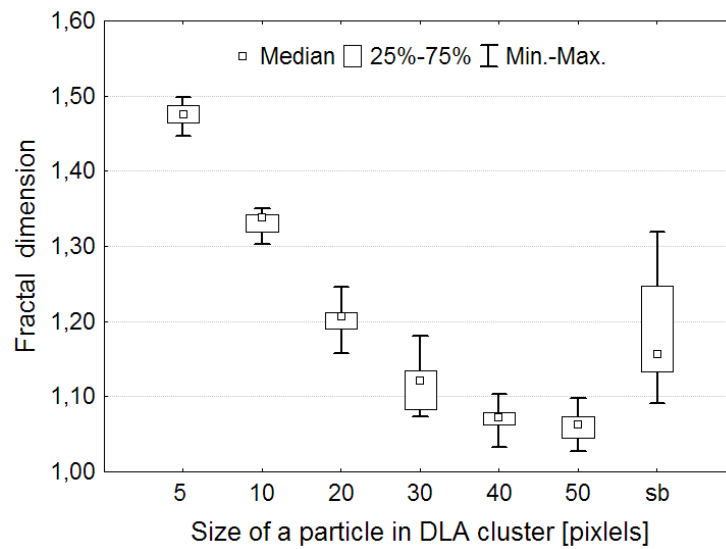


Fig. 6. Medians and variation of the fractal dimensions of the digital skeletons – DLA clusters versus sutural bones (sb).

Table 1. Statistics for fractal dimensions of the digital skeletons of the DLA clusters and the sutural bones (sb).

Cluster	Sample	Median	Mean	SD	Min	Max
5 px	14	1,48	1,47	0,015	1,45	1,50
10 px	14	1,34	1,33	0,015	1,30	1,35
20 px	14	1,21	1,20	0,024	1,16	1,25
30 px	14	1,12	1,12	0,033	1,07	1,18
40 px	14	1,07	1,07	0,018	1,03	1,10
50 px	14	1,06	1,06	0,021	1,03	1,10
sb	14	1,16	1,18	0,070	1,09	1,32

Table 2. Results of multiple comparison test for fractal dimensions of the digital skeletons of DLA clusters and sutural bones (sb). Statistically significant $p < 0,05$.

Cluster	5 px	10 px	20 px	30 px	40 px	50 px	sb
5 px	–	1,0000	0,0469	0,0000	0,0000	0,0000	0,0047
10 px	1,0000	–	1,0000	0,0024	0,0000	0,0000	0,3844
20 px	0,0469	1,0000	–	0,6906	0,0039	0,0005	1,0000
30 px	0,0000	0,0024	0,6906	–	1,0000	0,7377	1,0000
40 px	0,0000	0,0000	0,0039	1,0000	–	1,0000	0,0401
50 px	0,0000	0,0000	0,0005	0,7377	1,0000	–	0,0065
sb	0,0047	0,3844	1,0000	1,0000	0,0401	0,0065	–

these clusters (1,30 – 1,35) overlap only higher values of fractal dimensions estimated for skeletons of sutural bones (1,09 – 1,32).

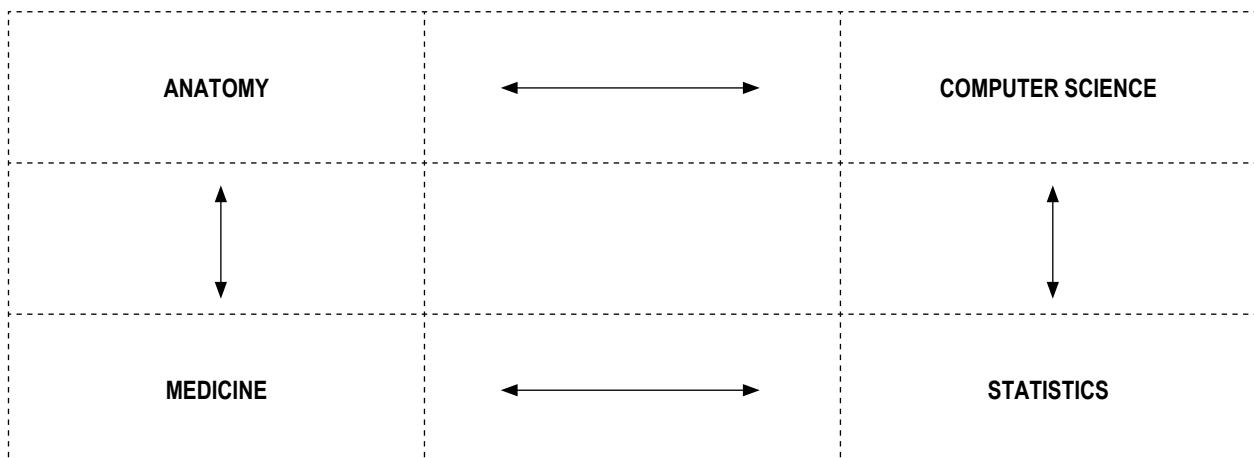
DLA clusters composed of particles which size was 5, 40 and 50 pixels yield fractal dimensions, which are different statistically from fractal dimensions of the skeletons of the sutural bones. Therefore these clusters do not properly model basic pattern of the examined sutural bones.

Conclusions

Diffusion-limited aggregation is a fractal algorithm that can produce similar patterns, which can be found among the sutural bones. Digital skeletons of the sutural bones and computer generated DLA clusters present branch-like shapes but of various fractal dimension. Complexity of the DLA cluster skeletons changes according to the initial size of the aggregating particles. Cluster composed of small particles shows higher fractal dimension than clusters aggregated from bigger particles. Size of particles 20 pixels found as the most adequate to simulate skeletons of the sutural bones corresponds to the diameter of distal finger-like processes that are peripheral elements of the sutural bones. This could imply that random process may underlie sutural bone formation and similarities in the digital skeletons may suggest common mechanism of their formation based on fractal algorithm. Branch-like shapes of the sutural bones supports an idea of application of fractal geometry in description of their morphology. Hence, relationship between skeletons of the sutural bones and DLA cluster may shed new light on the style of pattern formation during cranial morphogenesis.

References

1. Barra F., Davidovitch B., Levermann A., Procaccia I., Laplacian growth and diffusion limited aggregation: different universality classes. *Phys Rev Lett* 87: 134501-134504, 2001.
2. Bennett K.A., The etiology and genetics of wormian bones. *Am. J. Phys. Anthropol.* 23: 255-260, 1965.
3. Berry A.C., Berry R.J., Epigenetic variation in the human cranium. *J. Anat.* 101: 361-379, 1967.
4. Halsey T.C., Diffusion-limited aggregation: A model for pattern formation, *Physics Today* 53: 36, 2001.
5. Karperien A., Fractal dimension and Lacunarity. *FracLac* plugin for ImageJ: <http://rsb.info.nih.gov/ij/plugins/fracLac/fracLac.html>, 2007.
6. Karperien A., Rasband W., Diffusion Limited Aggregated Models: <http://rsb.info.nih.gov/ij/plugins/DLA.html>, 2006.
7. Lee S.W., Lam L., Suen C.Y., A systematic evaluation of skeletonization algorithms. *Int. J. Pattern Recognition Artificial Intelligence* 7: 1203-1225, 1993.
8. Murthy I.S.N., Udupa K.J., A search algorithm for skeletonization of thick patterns. *Computer Graphics Image Processing* 3: 247-259, 1974.
9. Noeim F., Moatamed F., Sahimi M., Morphogenesis of the bone marrow: fractal structures and diffusion limited growth. *Blood* 87: 5027-5031, 1996.
10. Pal G.P., Routal R.V., A study of sutural bones in different morphological forms of skulls. *Anthrop. Anz.* 44: 169-73, 1986.
11. Witten T.A., Sander L.M., Diffusion-limited aggregation. *Phys. Rev. B* 27: 5686-5697, 1983.
12. Wright M.W., Cipolla R., Giblin P.J., Skeletonization using an extended Euclidean distance transform. *Image Vision Computing* 13: 367-375, 1995.



LEARNING-BY-E-TEACHING: EXPERIENCE FROM INVOLVING STUDENTS IN PREPARATION OF E-LEARNING MATERIALS

ANDRZEJ A. KONONOWICZ, ALEKSANDRA J. STACHOŃ,

ANNA ROMANOWSKA-PAWLICZEK, PIOTR OBTUŁOWICZ, WIESŁAW PYRCZAK

*Department of Bioinformatics and Telemedicine, Medical College, Jagiellonian University,
31-530 Krakow, Św. Łazarza 16, Poland, www.bit.cm-uj.krakow.pl*

Abstract: Creation of e-learning materials is considered as a time consuming and costly process. Involving students in preparation of educational content may be beneficial in many ways. Firstly, it motivates students to self-study following a similar pattern as it is the case in learning-by-teaching sessions. Secondly, some of the students' projects may be reused in development of more advanced e-learning resources. The aim of this paper is to summarize three-year experiences gained in two elective courses on e-learning technologies offered to students of medicine and applied computer science. The spectrum of topics taken up by students is outlined. Possibilities of applying the outcomes of these courses in practice are discussed.

Introduction

Courses on e-learning technologies are still quite rare in academic curricula. Considering the fact that the demand on e-learning resources worldwide has increased significantly over the past few years it becomes obvious that this situation requires a change. In this context it seems to be worthwhile to make an attempt to involve students not only in passive usage of e-learning materials but also in creation of their content.

Background

The idea to involve students in preparation of didactic resources derives from the long-established tradition of Learning-by-Teaching (LbT). Various studies have already reported outcomes of including senior students (4-6 year) in teaching activities organized for junior students (1-3 year). Effects of peer-assisted learning (PAL) have been tested among others in Physiotherapy [6], Diversity Issues in Healthcare [7], Clinical Examination [1] and Early Patient Contact [2] programmes. J. Secomb [5] presents in her work a systematic review of peer teaching and learning in clinical education. The cited work, focusing mainly on the nursery discipline, summarizes the key benefits of learning-by-teaching – e.g. increase in cognitive development, improvement in students' motivation for learning and building up confidence in clinical practice. In almost all cases the polled students were satisfied with their experiences gained in peer teaching and learning sessions.

Method

The Department of Bioinformatics and Telemedicine at Jagiellonian University Medical College offers its students two elective courses on creating e-learning resources. These courses are geared toward two different target groups: students of medicine and students of applied computer science.

The elective course on e-learning technologies offered to medical students is organized around elementary IT technologies useful for creation of electronic educational materials. Within this course, students of the fourth year learn principles of web languages (HTML), authoring environments (Macromedia¹ Dreamweaver) and computer graphics (Corel Paint Shop Pro). Outcomes of this activity are e-learning web-pages on selected medical topics created single-handedly by groups of students (consisting of 1-4 students). Our e-learning tutors are encouraged to search for information concerning a self-chosen medical topic, transform and integrate it into a web-adjusted form, which is destined for a previously selected target group (e.g. lay person, patients, students of medicine, specialists).

The course offered to fourth year students of applied computer science is more technical-oriented. In this course an overview of e-learning tools and standards is made. One of the most interesting, due to its multidisciplinary character, tasks assigned to students of computer science is to prepare animations in Flash technology on a selected biological process or medical procedures.

¹ Currently Adobe

Additionally, students might participate in a students' scientific workgroup as an extracurricular activity. Discussing there many telemedicine related subjects, some of them took also the opportunity to create new e-learning sites or refine existing ones which were prepared within e-learning courses.

Significant differences between a classical Learning-by-Teaching method and the approach selected for our study can be noticed. E-learning does not require a direct link between the teacher and students. Educational resources in electronic form replace usually the personal contact with a tutor. In consequence senior students taking part in our activities were not brought in direct contact with their target groups but created their work "off-line" for future use.

This study reports on the content obtained as a result of students' e-learning activities in the Department of Bioinformatics and Telemedicine. Unlike many previous studies, this paper does not concentrate on quantitative or qualitative aspects proving effectiveness of Learning-by-Teaching or examining students' satisfaction with peer teaching. Instead, the aim of this paper is to outline the spectrum of topics taken up by students and to discuss the possibilities of applying the outcomes of these courses in practice.

Results

In the years 2005-2008, forty-five students completed the elective course destined for medical student delivering nineteen

e-learning projects. The course for students of computer science took place for the first time last year (2007) and was completed by twelve students. Fourteen Flash animations have been created within the course. The student's scientific workgroup delivered four additional web projects. Fig.1 presents an overview of graphical layouts taken from selected web pages and animations created by students within these e-learning courses.

Students took up many interesting and actual subjects from the field of healthcare. Among these were e.g. physiology and pathology of cardiovascular system, digestive system, nervous system and vertebral column. Projects concerning treatment methods of heart related problems were present, as well as materials about resuscitation methods (e.g. heart massage). Students took a keen interest in topics of fertility, contraception and HIV/AIDS (fig. 2). Some of the students' web-pages and presentations explain basic biological structures and processes as urine production, circulation of iron in human and protein's synthesis. Also such noteworthy topics as carbon monoxide poisoning, drugs addiction and history of medicine were described by students.

Tab. 1 summarizes the branches of medicine covered by students in their works. From a large set of projects prepared by students within LbT sessions a few examples has been chosen and described below.

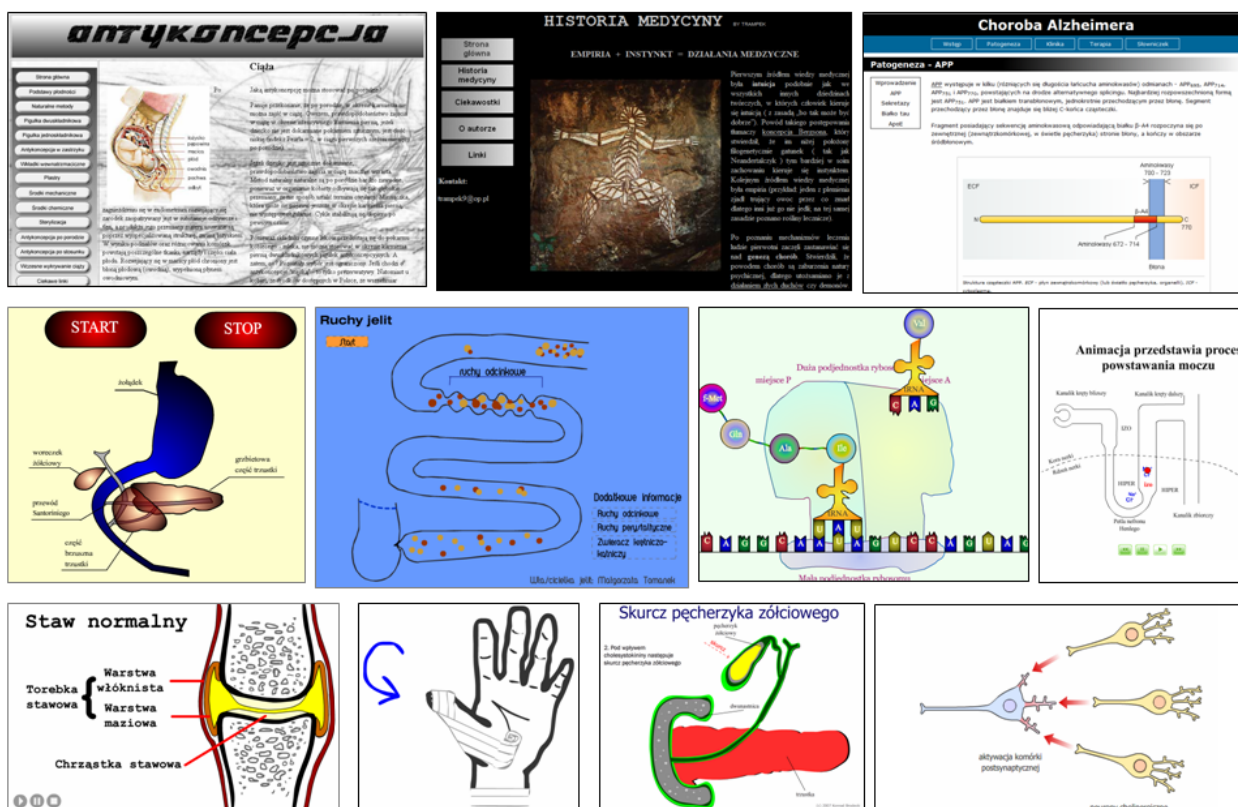


Fig. 1. Overview of graphical layouts taken from selected web pages and animations created by students within our e-learning courses [13-22].

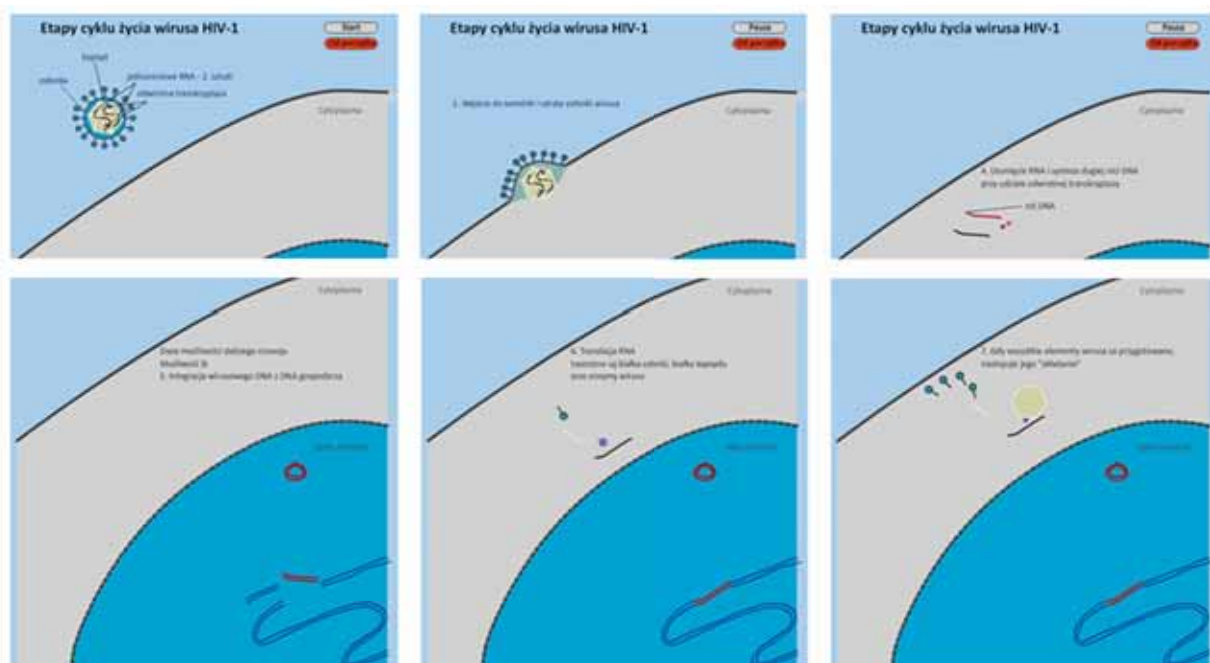


Fig. 2. HIV's lifecycle in Flash animation [23].

Tab. 1. Specification of selected topics in e-learning courses.

Branch of medicine	No. of web pages	No. of animations
Cardiology	2	1
Gynaecology	2	-
Neurology	2	-
Oncology	1	-
Infectious Diseases	1	1
Dermatology	1	-
Internal Medicine	6	1
Surgery	1	-
Paediatrics	1	-
Emergency medicine	-	5
Toxicology	3	-
Basic Sciences	1	7
Others	1	-

Cardiovascular diseases are the number one cause of death worldwide. High rates of morbidity are observed both in industrialized and developing countries. WHO experts estimate that in the course of the next few years 20 millions people will die yearly due to cardiovascular diseases [8]. In Poland cardiovascular diseases cause half of all deaths [9,10]. Because

of this global pandemic it is crucial to make people aware of causes of cardiovascular illness, develop methods enabling their early diagnosis and effective treatment as well as promote healthy lifestyle.

The most frequent among various cardiovascular disorders is the ischemic heart disease. This medical condition often leads to heart attack and death. Prophylaxis and treatment of atheroembolism is therefore an interesting topic for future doctors. Coronary angioplasty, a common treatment method of myocardial ischemia, has been described by students in form of a web-page entitled **miE-PTCA** (nicE-PTCA). PTCA – an acronym of *Percutaneous Transluminal Coronary Angioplasty* – is a medical procedure consisting in recanalization of stenotic artery with use of small balloon and stent. This method is currently very common and is regarded as an alternative method to various kinds of myocardial ischemia therapy [4].

Authors of the above described a web-page which combined in an interesting way specialist knowledge with information for lay readers. Their major goal was to familiarize patients waiting for PTCA with concepts related to this procedure. Content of the miE-PTCA has been logically and comprehensible prepared. It includes basic knowledge (e.g. anatomy of coronary vessels), subject related information (e.g. definition of PTCA, recommendations and contradictions) and practical advices useful for patients (e.g. preoperative preparation, postoperative recommendations). Web page visitors may learn that angioplasties undergo annually several thousands people in Poland, and about half million worldwide. Mortality rate in this kind of operation is less than 1%, whereas effectiveness reaches even 90% [11].

Other heart related problems discussed by students are congenital heart diseases, prepared in the form of a web-page: **E-Wady Serca** (E-heart defects, fig. 3). This site is destined for

medical students and to parents/carers of children with heart disorders. Pictures of cardiovascular system illustrate mechanisms leading to pathological symptoms of such disorders as: atrial septal defect (ASD), ventricular septal defect (VSD), patent ductus arteriosus – Botall's duct (PDA), tetralogy of Fallot (TOF) and hypoplastic left heart syndrome (HLHS). The reviewed web presentation has a clear educational character. In the introductory part normal physiological blood circulation is outlined. Characteristics of the above mentioned congenital heart disorders include information on their spread, typical symptoms and various treatment methods. A closer look at the web-page will give the opportunity to discover many interesting facts like that the frequency of some cardiac abnormalities is higher in females than males (ASD, VSD, PDA), or a detailed explanation of the Norwood procedure (i.e. a series of operations in HLHS) [3].

The presented page is also a practical example on that how projects of students from different background may complement each other. A static diagram proposed by medical students showing blood circulation in physiological and various pathological states (fig. 3) has been extended into an animated version by a student of computer science (fig. 4).

Some of the students attending courses on e-learning technologies went into the subject of first aid techniques (animations fig. 5, fig. 6). This topic is always of great importance and up-to-date, but knowledge in this subject still not enough widespread. Life-saving techniques should be taught not only to medical students but also be addressed to larger parts of the society.

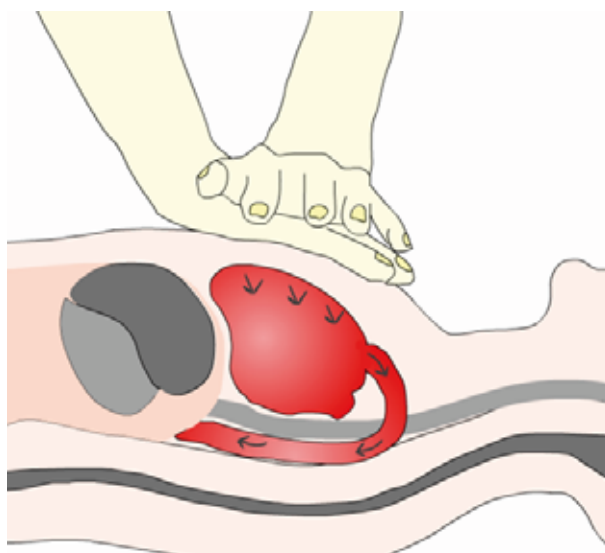


Fig. 6. Examples of students' projects: Resuscitation [27].

Discussion

Students' involvement in preparation of educational e-learning materials (medical web-pages and Flash animations) motivates to self-directed information search, logical reasoning and concept association. The proposed activities gave students possibility to present both their knowledge and artistic skills. An excellent example of that is a web-page on neurophysiology which includes original illustrations of high quality drawn single-handedly by a student (fig. 7).

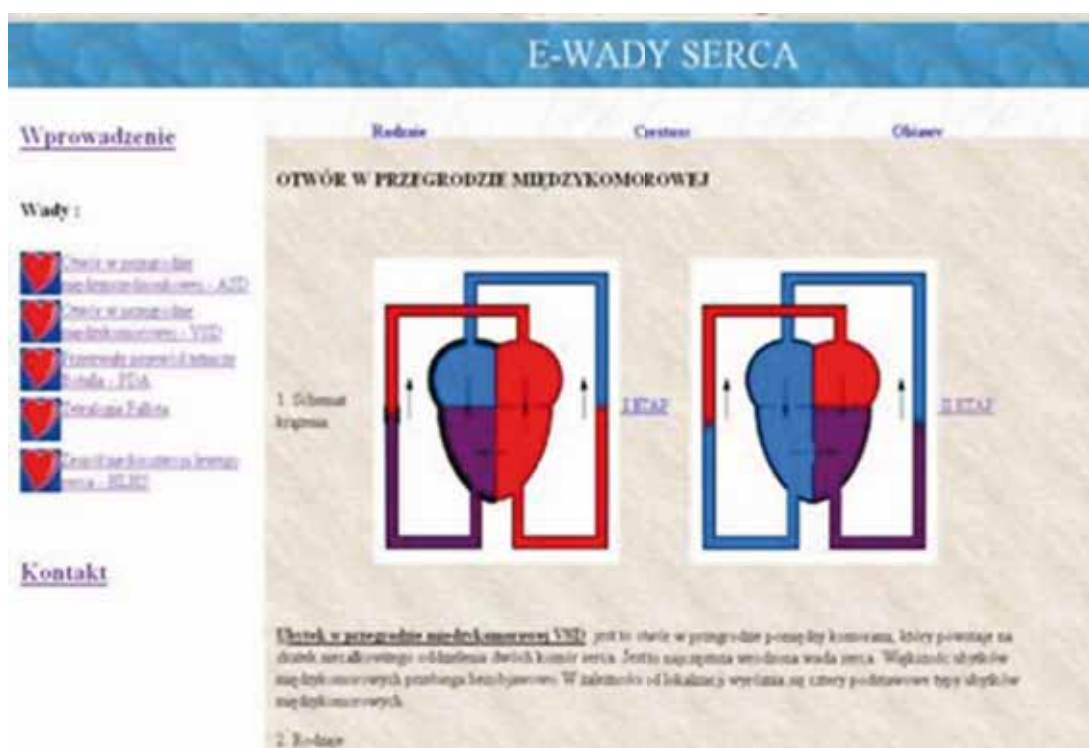


Fig. 3. A web-page within an e-LbT session discussing the subject of congenital heart disorders [24].

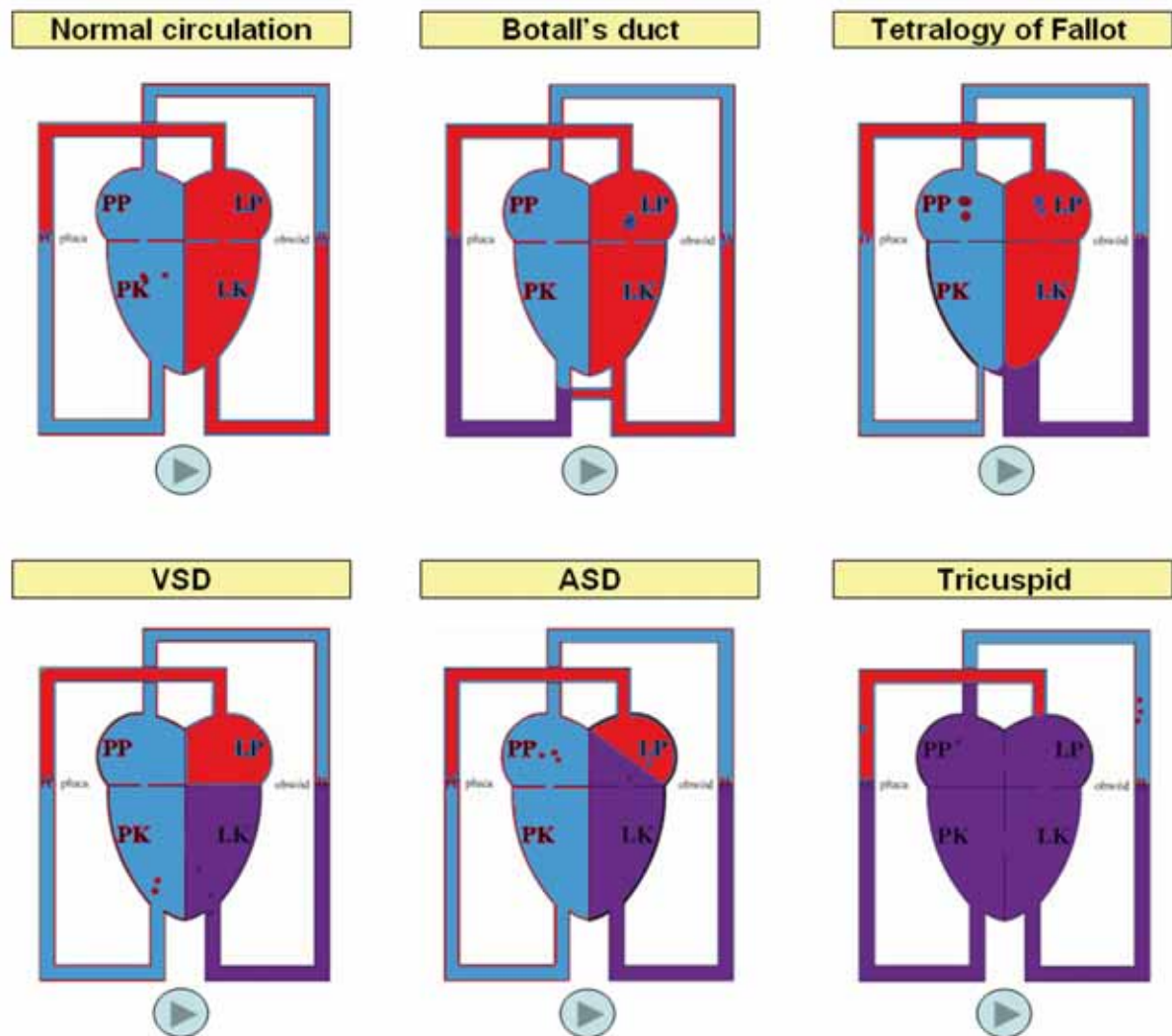


Fig. 4. Enrichment of medical e-learning pages by students of computer science [25].

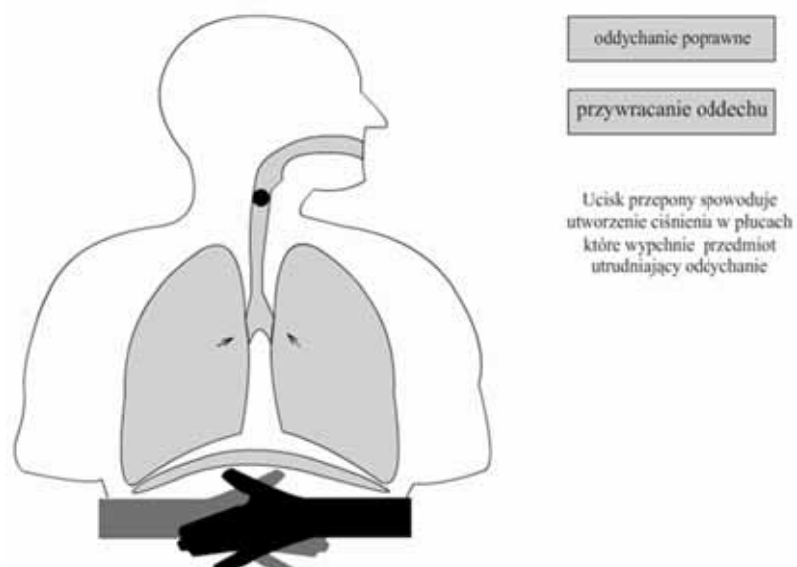


Fig. 5. Examples of students' projects: First aid tutorial [26].

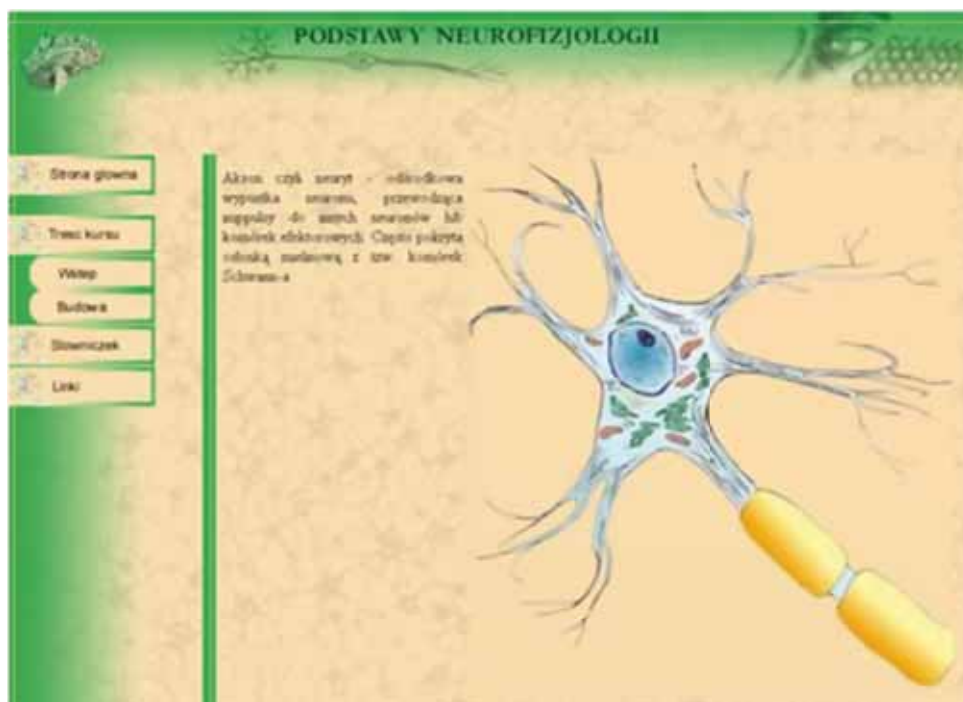


Fig 7. Web-page in neurophysiology [28].

Students creating their own educational materials are believed to memorize better the presented information. The strong IT character of this class may be perceived as an inspiring change for medical students not used to this form of learning. We believe that it has the potential to increase positive attitude to science and foster the ability of life-long learning. Students seemed to be keen on taking up this kind of activity and in most cases they performed well in preparing e-learning materials. A few of them presented their projects at students' scientific conferences. Among them were two consecutive International Scientific Conferences of Medical Students held in Krakow (2007, 2008). The students' web-pages have been presented within Telemedicine & Biocybernetics sessions. Some of the projects are presented on [12].

Students' activity during e-learning courses and later on the presentation of their work at conferences gave them the chance to consolidate and broaden their bio-medical knowledge. These activities constitute also great opportunity to interchange ideas and experiences achieved as a result of self-preparing educational materials as well as writing and presenting scientific dissertations. Students had also a chance to present their work to medical specialists, who evaluated their activities. Some of the e-learning courses prepared by students at the Department of Bioinformatics and Telemedicine JUMC are regularly updated and expanded. They seem to have the potential to be an interesting extension to traditional learning activities.

The obtained results are good examples of practical connection of technology and medicine. E-learning materials prepared by medical students were taken in many cases as a knowledge base for computer science students while preparing their animations. The ready animations enrich the existing pages ensuring their constant evolution.

Well prepared animations and web-pages taken from students' projects may be re-used by peer students and also by

the faculty in many different ways. One of the possibilities is to present these materials on students' portals or e-learning platforms as a source for self-directed learning. A further option is to apply this content for creation and enrichment of more advanced e-learning resources like virtual patients. Indexed learning objects could be gathered in specialized repositories and reused by the faculty as extension of traditional lectures or textbooks. After profound review it is also thinkable to offer these materials as informational material for patients or their families. Before publishing, it is of course necessary to obtain authors' consent and clarify the intellectual property rights (IPR) of all content available in these educational materials.

Inclusion of best projects in teaching practice at the university raises also some concerns. Faculty teachers in charge of the e-learning classes have technical background and assisted the students mainly in technology related questions. Therefore, all students' projects should undergo before publishing a detailed review by the clinical teachers. With the increased number of projects, providing additional incentives for the clinical faculty staff to do the review could be very helpful.

When looking at the courses from the technical perspective it can be noticed, that they were organized on the basis of professional authoring tools like Dreamweaver or Flash. This software is on the one hand very powerful and flexible, but on the other also expensive and (for some students) difficult to learn. Working on the level of HTML editors, even of WYSIWYG² type, may seem nowadays to be a too deep-level approach. However, relying solely on the authoring tools available in Learning Content Management Systems (LCMS), like Blackboard or Moodle, may create portability problems.

² WYSIWYG Editor (What-You-See-Is-What-You-Get) is an editor class enabling visual authoring of web pages without the need to deal directly with HTML code.

E-learning interoperability standards (like SCORM or IMS) are in the authors' belief not yet the perfect remedy for this problem. More technically apt students may in addition find the technical constraints of LCMS limiting. The huge differences in IT-knowledge among medical students make it additionally difficult to target the classes.

Further work

All web-pages and animations created within the course have been gathered on one single e-learning portal, which is currently waiting for a faculty review. Projects which have been accepted are intended to be published on-line. A next study will concentrate on examination of the educational impact of these web-pages on junior students.

Immense progress in e-learning technologies makes it necessary to update the course annually. A modification of the programme to include more user-friendly, free-of-charge software should definitely be considered.

Summary

The study presented outcomes of two elective courses on e-learning technologies destined for students of medicine and applied computer science. Senior medical students created their own e-learning web sites from various medical fields (e.g. cardiology, internal medicine or neurology) geared towards different target groups. Students of computer science extended the web sites by creating Flash animations. Taking the role of content authors, students practiced how to structure knowledge for learning. Examples of future application of the gathered resources were given (e.g. self-directed study, virtual patients, extension of lectures). The authors would welcome to collaborate with medical teachers in the review of the educational content created by students and their later application in didactic practice.

References

- [1] Field M., Burke J., McAllister D., Lloyd D.: Peer-assisted learning: a novel approach to clinical skills learning for medical students, 41(4), 411-418, 2007.
- [2] Glynn L., MacFarlane, Kelly M., Cantillon P., Murphy A.: Helping each other to learn – a process evaluation of peer assisted learning, 6(18), <http://www.biomedcentral.com/1472-6920/6/18>.
- [3] Moszura T. i in.: Zastosowanie stentów wewnątrznaczyniowych w wieloetapowym leczeniu dzieci z zespołem niedorozwoju lewego serca – doświadczenia własne, Kardiochirurgia i Torakochirurgia Polska, 4(2), 148-154, 2007.
- [4] Pawłowska-Jenerowicz W., Lechowicz W., Dąbrowski M.: Korzystny wpływ leczenia angioplastyką wieńcową ostrej fazy zawału mięśnia sercowego na wydolność układu krą-

żenia w rocznej obserwacji, Postępy w Kardiologii Interwencyjnej, 2/3(5), 199-206, 2006.

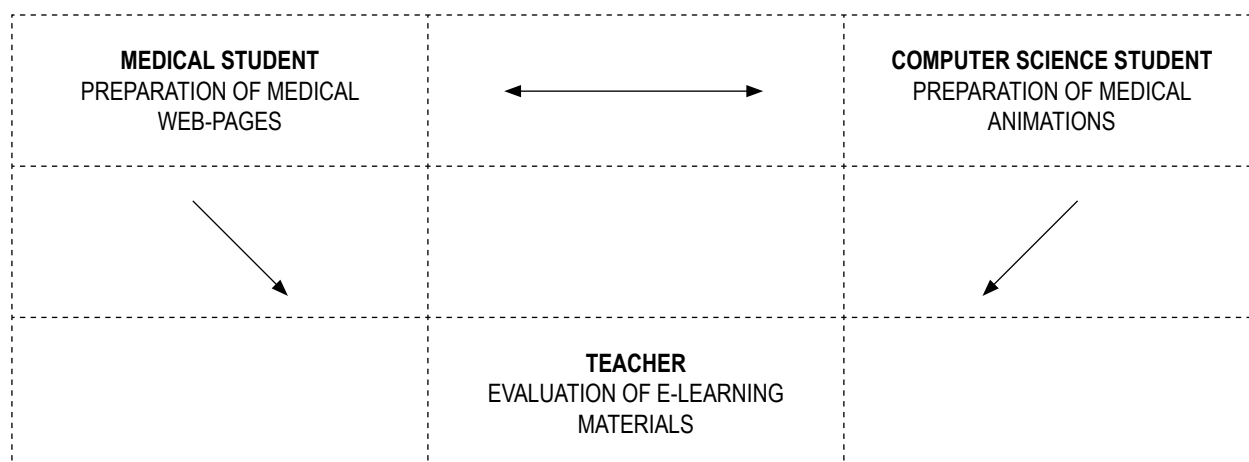
- [5] Secomb J.: A systematic review of peer teaching and learning in clinical education, 17(6), 703-716, 2008.
- [6] Solomon P., Crowe J.: Perceptions of student peer tutors in a problem-based learning programme, Medical Teacher, 23(2), 181-186, 2001.
- [7] Tang T., Hernandez E., Adams B.: „Learning by Teaching”: A Peer-Teaching Model for Diversity Training in Medical School, Teaching and Learning in Medicine, 16(1), 60-63, 2004.

Web pages

- [8] WHO Homepage, Cardiovascular diseases – http://www.who.int/topics/cardiovascular_diseases/en/ (last visited 9.05.2008)
- [9] Polskie Towarzystwo Kardiologiczne, Epidemiologia chorób układu krążenia – <http://www.ptkardio.pl/pl/archiwum/213.html>, In Polish (last visited 9.05.2008)
- [10] Poradnik Medyczny, Choroby układu krążenia w Polsce – <http://www.poradnikmedyczny.pl/mod/archiwum/4779.html>, in Polish (last visited 9.05.2008)
- [11] Resmedica, Angioplastyka w leczeniu choroby wieńcowej – <http://www.resmedica.pl/zdart3991.html>, in Polish (last visited 9.05.2008)
- [12] Koło Telemedycyny i Biocybernetyki – <http://www.telemedycyna.cm-uj.krakow.pl>, In Polish (last visited 9.05.2008)

Authors of described projects

- [13] Liszka M., Pastuszek M., Sporek M., 2006. Web page Antykoncepcja.
- [14] Wolak P., 2006. Web page Historia medycyny.
- [15] Opalka M., Gontkiewicz Ł., Nawrot M., 2008. Web page Choroba Alzheimera.
- [16] Godyń P., 2007. Animation Endogeneza trzustki.
- [17] Tomanek M., 2007. Animation Ruchy jelit.
- [18] Paluch J., 2007. Animation Synteza białka – translacja.
- [19] Kuśmierski P., 2007. Animation Proces powstawania moczku.
- [20] Walas M., 2007. Animation Reumatoidalne zapalenie stawów.
- [21] Opoczyński P., 2007. Animation Bandażowanie ręki.
- [22] Brodecki K., 2007. Animation Skurcz pęcherzyka żółciowego.
- [23] Tomanek M., 2007. Animation Etapy cyklu życia wirusa HIV-1.
- [24] Mirek A., Czajka M., Popławski M., 2006. Web page E-Wady Serca.
- [25] Pękała I., 2007. Animation Wady serca.
- [26] Godyń P., 2007. Animation Przywracanie oddechu.
- [27] Opoczyński P., 2007. Animation Masaż serca.
- [28] Potocki P., 2006. Web page Neurofizjologia.
- [29] Lubojemska P., Zajac T., Samecki B., Polańska E., 2006. Web page miE-PTCA.



INSTRUCTION FOR AUTHORS

1. The original and one Photostat copy of the manuscript should be mailed to: Managing Editor Zdzisław Wisniowski. Authors are strongly urged to submit a CD containing the manuscript in Word for PCs format along with the hard copies. Articles already published or those under consideration for publication in other journals or periodicals should not be submitted.
2. Manuscripts should be in English. Usage of correct language is the responsibility of the author.
3. Submission of manuscripts to us implies that the copyright of the entire material except those already copyrighted by other publications like tables, figures etc and those permission the author(s) have already obtained, belongs to the publisher.

PRESENTATION

4. The text may be prepared from a good quality laser printer or electronic typewriter. It is to be typed (one side only) on a regular sheet of paper A4 size preferred with single line spacing. New Times Roman font of 12 point size is recommended. Authors are requested to paste figures and tables (if possible) at appropriate places in the text. If this is not possible, they may be given separately, in which case their exact locations in the text may be marked by pencil.
5. The article should begin with a short ABSTRACT followed by a short INTRODUCTION. The rest of the article may be titled and arranged as per the wishes of the author.
6. REFERENCES should continue the last section of the article. In the text, references to other papers or books should be cited using consecutive numbers in parenthesis (e.g. [1,2]) and they should be listed numerically in the last section.

Examples:

I. Pyrczak W., Sarapata K.: Instructions for authors: references. Bio-Algorithms and Med-Systems, 1, 386, 2005

II. Tadeusiewicz R., Ogiela M.R.: Medical Image Understanding Technology. Springer Verlag, Heidelberg 2004

Authors are to make sure that each reference appearing in the text appears in the list of references at the end and vice versa.

7. TITLE PAGE AND FIRST PAGE – The title page of the manuscript, the name(s) of author(s) and institution(s) where the work has been carried out should be typed out on a separate sheet of paper.
8. Section headings (ABSTRACT, INTRODUCTION etc.) are to be typed in upper case letters and placed on a separate line
1. Scientific names should be typed in italics or underlined
2. Tables should be numbered consecutively using Arabic numerals.
3. Illustrations should be limited to materials essential for the text. All figures should be numbered consecutively and should be submitted as sharp, high-quality prints. Figures that are to appear as a group should be photographed and mounted together. All figures and groups of figures should be trimmed at right angles and pasted directly on the typescript in the appropriate places. They should be of a size permitting photographic reduction by 25% together with text (not more than 15 cm across for page width and not higher than 20 cm). Legends to figures should appear directly below the respective figures.
4. In line drawings, all lines should be of uniform thickness; letters and numbers should be of professional quality and proper dimensions, approximately 1mm high when reproduced.
5. RUNNING TITLE – Please make sure to mention the running title (short title) of the article separately in the first page where the title, names of authors, their affiliations, etc. are given.
6. PREFERRED LENGTH – The length of the manuscript may be limited to 20-25 A4 size pages (20 cm width – 26 cms height) through this is not binding.
7. PERMISSION – Authors must obtain permission from other publishers if they use already published and copyrighted materials.
8. COLOUR FIGURES – Cost of printing color figures will be charged to the author at the rate of U.S. \$ 125 per plate of four color pages.
9. REPRINTS – The order for reprints should be placed at the time of submission of the article itself, so that it may be out for printing without loss of time, if found suitable for order for not less than 100 reprints is to be made.

MANUSCRIPT SUBMISSION:

1. Electronic – the www.bams.cm-uj.krakow.pl address is available for all authors to submit manuscript. The instruction is available at each step of submission process.
2. The pdf or doc file with figures and tables incorporated into the manuscript body can be sent by email – address: bams@cm-uj.krakow.pl